Self Assembled Materials for Solar Cell Application

Dissertation

Zur Erlangung des Grades

„Doktor der Naturwissenschaften”

Im Promotionsfach physikalische Chemie

Maria Carmen Lechmann-Dorn

Geb. am 13.12.1981 in Aachen

Mainz, 2010

Die vorliegende Arbeit wurde am Institut für Physikalische Chemie der Johannes-Gutenberg Universität Mainz, am Max-Planck-Institut für Polymerforschung in Mainz und der Soul National University in Korea in der Zeit von März 2007 bis Februar 2010 angefertigt.

Abgabedatum: 3.2.2010

Pfürungstermin: 13.4.2010

Abstract:

In der vorliegenden Arbeit wurden Materialien und Aufbauten für Hybrid Solarzellen entwickelt und erforscht.

Der Vergleich zweier bekannter Lochleitermaterialien für Solarzellen in einfachen Blend-Systemen brachte sowohl Einsicht zur unterschiedlichen Eignung der Materialien für optoelektronische Bauelemente als auch neue Erkenntnisse in Bereichen der Langzeitstabilität und Luftempfindlichkeit beider Materialien.

Weiterhin wurde eine Methode entwickelt, um Hybrid Solarzelle auf möglichst unkomplizierte Weise aus kostengünstigen Materialien darzustellen. Die „Eintopf“-Synthese ermöglicht die unkomplizierte Darstellung eines funktionalen Hybridmaterials für die optoelektronische Anwendung. Mithilfe eines neu entwickelten amphiphilen Blockcopolymers, das als funktionelles Templat eingesetzt wurde, konnten mit einem TiO_2-Precursor in einem Sol-Gel Ansatz verschiedene selbstorganisierte Morphologien des Hybridmaterials erhalten werden. Verschiedene Morphologien wurden auf ihre Eignung in Hybrid Solarzellen untersucht. Ob und warum die Morphologie des Hybridsystems die Effizienz der Solarzelle beeinflusst, konnte verdeutlicht werden. Mit der Weiterentwicklung der „Eintopf“-Synthese, durch den Austausch des TiO_2-Precursors, konnte die Solarzelleneffizienz von 0.15 auf 0.4 % gesteigert werden. Weiterhin konnte die Übertragbarkeit des Systems durch den erfolgreichen Austausch des Halbleiters TiO_2 mit ZnO bewiesen werden.

Abstract:

New materials and assemblies were designed and tested for hybrid solar cell application. A simple blending approach was used to prepare hybrid solar cells in a convenient, cheap and fast method. Nano crystalline TiO_2 rods were blended with different hole conducting materials and tested in solar cell devices. Comparing their performance in photovoltaic devices, while experimental conditions are kept identical, showed that the choice of solvent and photovoltaic characterization conducted in inert atmosphere is of different influence for different hole conducting materials. External influences as long term stability were investigated.

In comparison to the blend approach a new one-pot approach was invented to prepare a nanostructured, multi-functional material with orthogonal properties. It consists of TiO_2 as a functional metal oxide and a new amphiphilic block-copolymer poly(ethyleneoxide)-*b*-poly(triphenylamine) (PEO-*b*-PTPA) that was synthesized. The hybrid material was obtained within a single step via self assembly in solution. Therefore a method had to be found to obtain crystalline TiO_2 under mild conditions. Within the materials synthesis the block-copolymer not only acts as a templating agent but also adds an electronic functionality to the resulting hybrid material. During the synthesis a variety of self assembled morphologies ranging from spheres to wires were created in a controlled fashion. The obtained morphology depends on the weight fraction of the polymer, solvent, TiO_2 precursor and acid. Studying films on silicon wafers with scanning electron microscopy (SEM) and transmission electron microscopy (TEM) a ternary phase diagram could be mapped whereas the crystallinity of TiO_2 could be proved by high resolution-TEM. Different morphologies of this self assembled hybrid material were tested for solar cell application. Even for devices with layer thicknesses of the active material below 10 nm power conversion efficiencies up to 0.15 % at 1 sun and 1.5 AM were observed. The solar cell efficiency was increased with further development of the one-pot approach by changing the precursor. A polyethyleneglycole modified titanate was used as precursor in combination with the functional block copolymer PEO-*b*-PTPA. Again self-assembled network morphologies were obtained and tested in solar cell devices. While the formation of percolating networks is of general importance the solar cell performance was found to depend on the morphological design of the hybrid material. With the aid of conductive scanning force microscopy, it was proven to preserve a percolating network despite an increase of the active layer thickness. In combination with a special functionalized Ti-precursor hybrid bulk heterojunction solar cells having a maximum power conversion efficiency of 0.4 % at 1 sun and 1.5 AM were obtained.

초록:

혼성 태양전지 응용에 도입하기 위한 새로운 물질과 자가조립을 고안하여 적용하였다. 혼성 태양전지를 제작은 쉽고 싸며 빠르게 준비할 수 있는 간편한 블렌딩 방법을 사용하였다. 나노 결정질인 TiO_2 막대와 다양한 정공 전도물질을 블렌드하여 태양전지 디바이스를 테스트하였다. 광전지 디바이스 성능을 비교하기 위하여 다른 실험조건을 동일하게 유지하였고, 용매의 선택은 안정한 환경에서 광전지 특성을 측정할 때에 다른 정공 전도물질에서 다른 영향을 보였다. 또한 외부환경에 의한 긴 시간 안정성도 살펴보았다.

단순한 블렌드 방법과 달리, 새로운 one-pot 방법을 통해 나노 구조를 가지며 수직 성질을 비롯한 여러 기능을 가지는 물질을 만들 수 있었다. 이는 금속산화물인 TiO_2 와 새롭게 합성한 양쪽성 블록 공중합체인 폴리에틸렌옥사이드-*b*-폴리트라이페닐아민 (PEO-*b*-PTPA)을 사용하였다. 용액 속에서 자가 조립하는 특성을 이용하여 한 단계로 혼성물질을 만들었다. 따라서 온건한 조건에서 TiO_2 결정을 만드는 방법을 고안해야 했다. 물질을 합성하는 동안 블록공중합체는 템플레이트 역할 뿐만이 아니라 혼성물질에 전기적 성질이 띄도록 하는 역할을 해준다. 합성 조건에 따라서 구형에서부터 와이어 모양까지 다양한 자가조립 몰폴로지로 제어할 수 있다. 즉, 고분자의 양이나 용매, TiO_2 전구체, 산을 통하여 몰폴로지를 조절할 수 있다. 실리콘 웨이퍼에 코팅한 샘플을 주사전자현미경 (SEM) 이나 투과전자현미경 (TEM) 을 이용해 삼차원 이미지로 얻을 수 있었고, TiO_2 결정은 고해상도 TEM 을 이용하여 확인하였다. 자가 조립 혼성 물질의 다양한 몰폴로지는 태양전지 응용을 위해 테스트한 결과, 1 sun, 1.5 AM 조건에서 10 nm 이하의 활성층 두께에서도 디바이스는 0.15 % 효율을 보였다. One-pot 방법에서 전구체를 바꾸어가며 개선한 결과 태양전지 효율은 더 증가하였다. 폴리에틸렌글라이콜로 개질시킨 titanate 를 기능적인 블록 공중합체 PEO-b-PTPA 와 함께 전구체로 이용하여 자가조립 네트워크 몰폴로지를 얻은 후, 태양전지특성 측정을 하였다. 태양전지 성능에서 일반적으로 중요하다고 보는 연결된 네트워크의 형성이 혼성물질의 몰폴로지 디자인에 따라 다르다는 것을 발견하였다. 활성층의 두께를 증가 시키더라도 연결된 네트워크는 여전히 존재한다는 것을 전도성 주사 힘 현미경이용하여 알아내었다. 특별한 기능기로 처리한 타이타늄 전구체를 이용하여 제작한 혼성 벌크 헤테로 정션 태양전지로 1 sun, 1.5 AM 조건에서 최고 0.4 % 효율을 얻을 수 있었다.

CONTENT

ABREVIATION

AAO	Anodized Aluminum Oxide
AM	Air mass
ATO	Anodized Titanium Oxide
CMC	Critical micelle concentration
CMT	Critical Micelle Temparture
CV	Cyclovoltammetry
DMF	N, N-Dimethylformamide
dp	Dispersity
DSSC	Dye sensitized solar cell
EGMT	Ethyleneglycole modified titanate
EISA	evaporation-induced self-assembly
EL	electroluminescence
FF	Filling Factor
FTO	Fluorine doped tin oxide
GISAXS	Grazing incidence small angle x-ray reflectivity
HOMO	Highest Ocupied Molecular Orbital
HRTEM	High Resolution Transmission Electron Microscopy
Isc	Short Current
ITO	Indium doped tin oxide
LC	Liquid crystalline
LCD	Liquid crystal display
LED	Light emitting diode
LUMO	Lowest Unocupied Molecular Orbital
M	molar
MDDOPP	poly(2-methoxy-5-dodecyloxy-*p*-phenylenevinylene)
Mn	Number Average Molecular Weight
N	Degree of polymerization
η	Power conversion Efficiency
$N\chi$	Degree of segrgation
OLED	Organic light emitting diode
OOPPV	poly(2,5-dioctyloxy-*p*-phenylenevinylene)
OPV	Organic photovoltaic
P2VP	Poly(2-vinylpyridine)
P3HT	Poly(3-hexylthiophene)
PANI-PSA	Poly(aniline) -phenolsulfonate
PCBM	[6,6]-phenyl-C_{61}-butyric acid methyl ester
PEDOT	poly(3,4-ethylenedioxythiophene)
PEDOT:PSS	Poly (3, 4-ethylenedioxythiophene):poly (styrene sulfonate)
PEO	Poly(ethylenoxide)
PEP	Poly(ethylene-propylene)
PFPE	perfluoropolyether
PFS	Poly(4-fluorostyrene)
PI	Poly(isoprene)
PLA	poly(D,L-lactide)
PMMA	Poly(methylmethycrylate)

PP	Poly(propylene)
PPV	Poly(phenylenevinylene)
PS	Poly(styrene)
PV	Photovoltaic
PVA	Poly(vinylalcohole)
PVDF	Polyvinylidene fluoride
PVP	Poly(vinyl pyrolidone)
RAFT	Reversible Addition Fragmentation Chain Transfer Polymerisation
RT	Room temperature
SEM	Scanning electron microscope
T	Temperature
TEM	Transmission Electron Microscopy
TEOS	Tetraethylorthosilicate
TFA	Trifluoroacetic acid
THF	tetrahydrofurane
THF	Tetrahydrofurane
TTiP	Titanium tetra isopropoxide
UV	Ultra violet
Voc	Open Circuit Voltage
XRD	X-ray diffraction
XRD	X-Ray Diffraction
XRD	X-Ray diffraction
Φ	composition
χ	Segment-segment interaction parameter

1 MOTIVATION

The energy demand of our constantly growing world population is increasing. At the same time we are running short of fossil fuel that is fare the basis of our energy supply. Furthermore the CO_2 emission involved in burning fossil fuels and wood in the actual dimensions is nowadays known to be environmentally critical and therefore needs to be reduced. Nuclear power and renewable energy resources are effective alternatives. While nuclear power comprises several safety risks renewable energies are safe and can be tapped from available resources like tides and ocean currents, geothermal energy, wind power and solar energy. Among these solar energy is most viable to solve our increasing energy demand.[1] While classical solar cells like single-crystal and polycrystalline silicon photovoltaics (PV) are currently dominating the market due to their high power conversion efficiency, they are manufactured at high cost.[2] Therefore much research has been done to look for alternative organic and hybrid materials that can replace silicon. Organic and hybrid solar cells offer certain advantages over classical solar cells[3]:

- potential to be flexible and semitransparent
- to be manufactured in a continuous printing process
- to coat large areas
- to be easily integrated in different devices
- manufactured at significant low cost compared to classical devices

Besides, there are still many combinations of different materials that can be investigated for PV application. With a power conversion efficiency of over 10 % the Dye Sensitized Solar Cell (DSSC) has the highest efficiency among the organic/hybrid solar cells which is very close to commercial silicon devices. DSSCs prepared with a liquid electrolyte are so called “Grätzel-Cells. For easy and low cost manufacturing the liquid electrolyte in these “Grätzel-Cells” has to be replaced by a hole conducting polymer or a low molecular weight organic material leading to solid state dye sensitized or bulk heterojunction hybrid solar cells. Although highest efficiencies are so far found for hybrid solar cell blends of CdSe and CdTe[4] in combination with poly-thiophenes, in this work TiO_2 phases in combination with P3HT (poly-hexylthiophene) or PTPA (poly-triphenylamine) are investigated. Depending on the kind of hole conductor efficiencies of up to 4 % can be obtained with the TiO_2/spiro-MeOTAD material nowadays[5] and because of environmental impact and low cost TiO_2 seems to be more applicable.

In this work several hybrid nano structured materials for promising solar cell application were introduced based on a semiconducting metal oxide and a hole conducting organic species. An approach was designed that allows easy processing and leads to reproducible nano structured hybrid morphologies under ambient condition. Therefore the synthesis of a functional block copolymer as a templating agent was demonstrated. Using the self-assembling nature of a block copolymer, an orthogonal functionality was incorporated into the hybrid system that resulted in materials that are directly usable for device fabrication. Furthermore systematic investigations have been done on hybrid solar cells to study external and experimental influences on the device performances.

2 INTRODUCTION

In this PhD thesis new and simple approaches for the preparation of hybrid solar cells are introduced and investigated. A one-pot synthesis based on a sol-gel approach that form self assembled morphologies as well as a simple blend structure undergoing self-assembly is designed. Self-assembled systems and templating methods are introduced in the following chapters (2.3 and 2.4). Selected morphologies with orthogonal functionalities are tested in solar cell application. Therefore an introduction to certain morphologies which are favoured and the kind of requirements which are needed for hybrid solar cells are discussed in chapters 2.2 and 2.1, including a small overview about organic solar cells in general.

2.1 ORGANIC PHOTOVOLTAICS

2.1.1 CONCEPT OF ORGANIC AND HYBRID PHOTOVOLTAIC

Applying a semiconducting organic material as active material in a solar cell device to harvest light and convert it into electrical energy, leads to organic photovoltaics. The difference between organic and inorganic photovoltaics is mainly based on the difference in charge carrier generation during illumination. In a conventional device the charge carriers are generated in bulk as a hole and electron and are not bound to each other. Because of the electric field given by the p-n-junction hole and electron separately move towards their electrodes. In contrary the charge carriers in organic semiconductors are bound hole-electron pairs, so called excitons. The exciton only dissociates at the interface of the donor and acceptor material, but the electric field in the organic device is much smaller compared to inorganic ones and therefore the exciton diffusion length is of about 10 to 20 nm.[6]

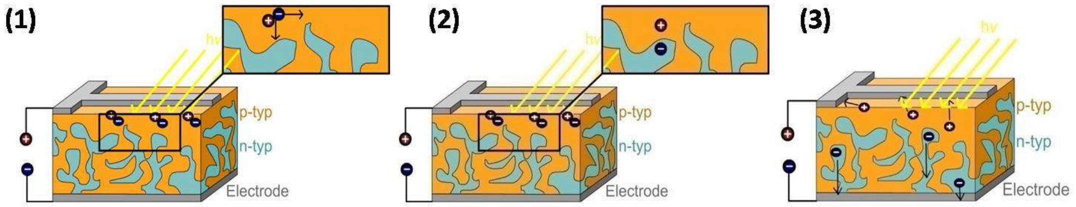

Figure 1: Schematic concept of the photocurrent generation in organic solar cells. (1) Creation of the exciton upon light irradioation and travelling of the hole electron pair towards the heterojunction interface. (2) Charge separation of the exciton at the semiconductor interface. (3) Transport of the holes and electrons towards the electrodes.

Because of the importance of the morphology of organic heterojunction, the surface should be maximised for an efficient charge separation. Moreover a network system is required to obtain percolating structures for the charges to travel towards the electrodes. Further on the structure of the heterojunction should phase separate in the nanometer regime as the diffusion length of the exciton is limited.

At least the following steps limit the overall power conversion efficiencies [7]:

- Photon absorption and exciton creation (Figure 1, (1))
- Exciton diffusion to donor/acceptor interface (Figure 1, (1))
- Exciton split at donor/acceptor interface (Figure 1, (2))
- Carrier diffusion to respective electrodes (Figure 1, (3))
- Carrier collection by the electrodes

The operation of solar cells can be described with energy band diagrams. While in inorganic devices a valence and a conducting band display the energy levels where the photoconversion takes place, in organic devices these energy levels are represented by the HOMO and LUMO of the active material. In case of a hybrid solar cell, the acceptor material is a semiconducting metaloxide and offers its conducting band for electron diffusion. The material with the lower ionization potential is the donor while the material with the larger electron affinity is the acceptor.

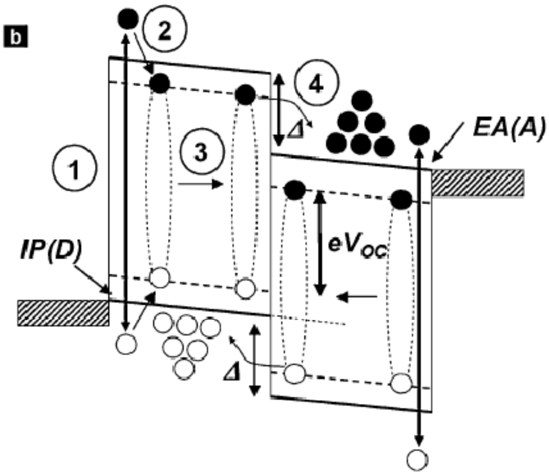

Figure 2: Energy level diagram of an organic heterojunction upon illumination. IP (D) denotes the ionization potential of the HOMO of the donor material while EA (A) denotes the electron affinity of the LUMO of the acceptor material.[8]

In Figure 2 a mechanism of a simple donor/acceptor heterojunction is shown. The exciton creation upon light absorption takes place in the donor material (1) followed by the formation of an exciton (2). The exciton diffuses through the film (3) and dissociates at the interface of the donor and acceptor (4) driven by the energy level offset of these materials that draws the hole and the electron towards the respective electrodes. In Figure 3 the mechanism is shown for a dye sensitized hybrid solar cell. If the donor material consisting of a hole conducting polymer does not absorb enough energy in the visible light, a dye can be added to increase the absorption. After absorption of a photon by the sensitizer dye, an electron is transferred to the LUMO of the acceptor material or the conducting band of the semiconducting inorganic phase (Figure 3, 1). The donor material thereupon provides electrons for the dye (Figure 3, 2) and holes in the organic donor material are transferred towards the electrode via a hopping mechanism. Interfacial recombination processes act as loss mechanism in competition with the hole transport mechanism by direct combination with either the dye or the hole conductor (Figure 3, 3 and 4).[9] *Zhu* et al. proposed two possible mechanisms for dye sensitized solid state hybrid solar cells: the former described dye-regenerating mechanism and in case of using a hole conductor like P3HT that absorbs the sun light, a mechanism where the dye could act as an electron mediator or funnel.[10] They suggested both mechanisms to be possible depending on the relative HOMO and LUMO energy levels between the dye and the hole conductor.

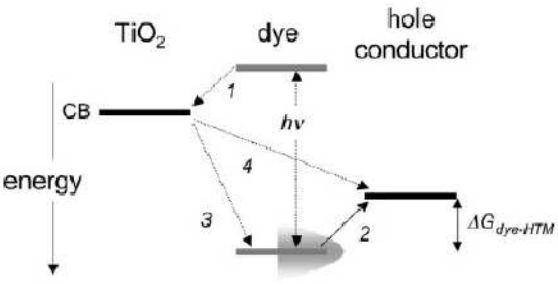

Figure 3: Charge transfer process occuring at the dye sensitized hybrid solar cell.[9]

It is important for the dye that the energy band fits exactly between the energy level of the acceptor and donor.

2.1.2 *EFFICIENCY*

To compare photovoltaic devices with each other and to identify their efficiency the power conversion efficiency η_{eff} is calculated as follows:

$$\eta_{eff} = \frac{V_{oc}*I_{sc}*FF}{I_{light}} \qquad \text{Eqn.1}$$

V_{OC} is the open circuit Voltage (measured in V), I_{SC} is the short circuit current density (measured in A/m^2), FF is the fill factor and I_{light} is the intensity of the light that is used during the measurement (Figure 4). V_{OC} is the maximum possible voltage that can be obtained across the cell when no current is flowing. It displays the difference between the work function of the electrodes. At open circuit all photoinjected electrons recombine.[11] When the electrodes are short-circuited, I_{SC} is the maximum current obtained. I_{SC} depends on the light intensity that shines through the device.

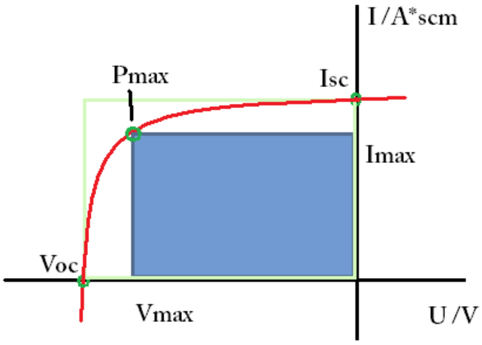

Figure 4: Sketch of an I-V curve at light illumination with the distinct areas and points that are important for the efficiency measurement.

The fill factor FF is the ratio of the maximum power output (P_{max}) and the theoretical power output. FF is defined as:

$$FF = \frac{I_{max} * V_{max}}{V_{OC} * I_{SC}} \qquad \text{Eqn. 2}$$

P_{max} is the point on the I-V curve where the maximum power is produced. This point is given by the product of I_{max} and V_{max} creating the maximum area under the curve (blue square in Figure 4). The theoretical maximum power is given by the product of V_{OC} and I_{SC} (light, green square in Figure 4). A small FF can occur when charge accumulates between the active layer and the electrode.[12] Further on the FF is influenced by the device thickness and the illumination intensity. Thicker layers of the organic materials show higher resistivity.[13] With an increase of illumination the amount of charge carriers is lifted due to higher absorption but at the same time this enables a higher charge recombination rate.

2.1.3 TYPES OF ORGANIC PHOTOVOLTAICS

Up to now there exists a huge variety in organic solar cell design (Figure 5). On the one hand there are pure organic solar cells. The polymer-polymer solar cells consisting of a all polymer components and bulk heterojunction solar cells consisting of hole conducting polymers and fullerenes. On the other hand there are hybrid solar cells, consisting of either a liquid electrolyte, small organic hole conducting molecules like pentacene or polymers like P3HT in combination with an inorganic semiconductor. One is speaking of DSSC, if the inorganic part is sensitized with a dye.

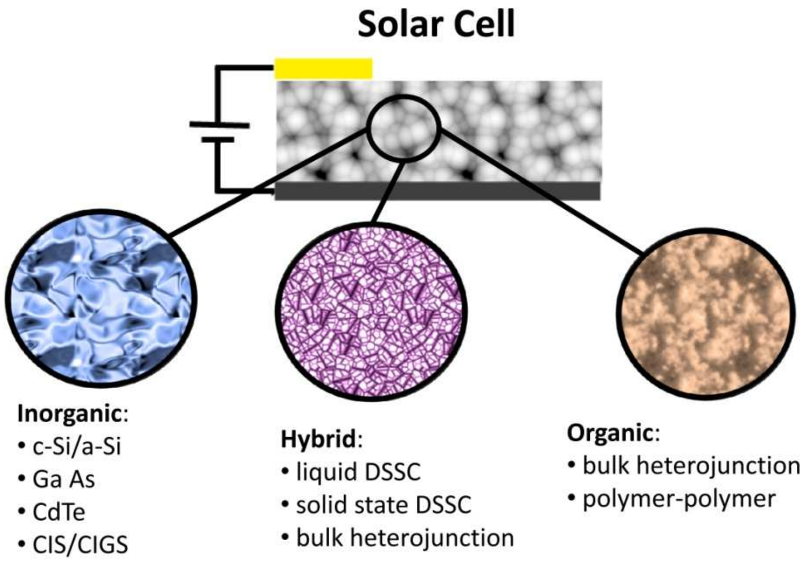

Figure 5: Examples of different types of photovoltaics.

2.1.3.1 All-Organic Solar Cells

In polymer solar cells, both the hole and the electron conducting material is composed of a polymeric structure. Nanoscale morphologies can either be created by a block copolymer or a blend of the active material. *Lindner* et al. used a block copolymer bearing a donor and an acceptor part showing the morphology with a cross-sectional cut in a TEM picture.[14] They could obtain a power conversion efficiency of 0.07 %. Using a blend morphology instead of a block copolymer *McNeill* et al. achieved with P3HT as acceptor and poly((9,9-dioctylfluorene)-2,7-diyl-alt-[4,7-bis(3-hexylthien-5-yl)-2,1,3-benzothiadiazole]-2′,2″-diyl) F8TBT as donor material a power conversion efficiency of 1.8 %.[15] With different polymeric materials similar efficiencies have been reported.[16, 17] *Kitzke* et al. showed a new method of gaining nanoscale donor-acceptor polymer blends by using miniemulsion processing.[18] Blending of individual donor-acceptor particles was compared with donor-acceptor janus particles already containing both functionalities.

Probably the most popular blended organic solar cells are the fullerene-polymer devices. With reproducible 4 to 6 % they are reaching the highest efficiencies among the solid state organic solar cells.[19-21] The two components have to phase segregate on suitable length scales to form desired percolating networks of donor and acceptor material with a minimal external influence. These self-assembled, nanometer sized morphologies can be controlled by varying solvent, concentration, blend ratio, processing parameters etc.[22, 23] So far the blending seems to be more successful than the block copolymer approach. Well ordered honeycomb structures were obtained from a block copolymer of an acceptor block and a fullerene containing donor block.[24] But until now they do not seem to find an application in efficient devices.

2.1.3.2 Hybrid Solar Cells

2.1.3.2.1 Liquid Electrolyte Dye Sensitized Solar Cells

In polymer solar cell devices the electron accepting material is still a limiting factor with respect to its insufficient conductivity and fullerene-polymer cells are an expensive alternative. Therefore, the use of inorganic metal oxides, such as TiO_2 and ZnO as electron conducting part is not only favoured because of its low cost and availability, but also because of its processability and morphologic variety in combination with polymeric materials. Photoconversion in a DSSC is based on the injection of an electron from the photoexcited state of a light absorbing material into the conduction band of a nanocrystalline semiconducting metal oxide.[25] For an efficient absorption of the solar spectrum numerous dyes have been synthesized and tested in organic solar cells. The most successful DSSCs so far are the "Grätzel-cells" showing the highest power conversion efficiency up to 11 %.[26] In such "Grätzel-cells", I^-/I^{3-} dissolved in acetonitrile is commonly used as electrolyte. Typically the iodine electrolyte penetrates into a porous TiO_2 phase, previously soaked with a dye solution. To absorb as much light as possible a matching dye is as important as a high TiO_2 surface area, because the dye will be adsorbed at the interface. In search for crystalline TiO_2 percolating networks, many research groups propose to use copolymer templates to assist structure formation. Efficiencies between 9 and 10 % are reached with self-assembled crystalline TiO2 particles by either using surfactant-directed[27] or a block copolymer-directed mesoporous structures.[28] *Snaith* et al. used a gyroid phase formed by a block copolymer to build a replica of TiO_2 for DSSCs.[29] However, the charge transport was found to be faster in 1D wire structures than in 3D gyroid arrays, even though the overall power conversion efficiency reached about 3 % for the gyroid structure.[30] Highly porous titania films with different pore sizes by altering the ratio of the block length of the polymer and the polymer-precursor were produced. Pore sizes of 30 nm were found to be most efficient. There will be no further discussion about the liquid DSSCs in further detail, because the focus in this work lays on the solid state bulk heterojunction solar cells.

2.1.3.2.2 Hybrid Bulk Heterojunction and Solid State Dye Sensitized Solar Cells

The previously discussed Grätzel-cells are reaching the highest efficiencies in organic solar cells so far, but they also bring along some disadvantages. The corrosive liquid electrolyte for example still is a challenge for the device engineering concerning leak-proofness. Promising replacements for the liquid electrolytes are the various p-type semiconducting polymers, based e.g. on triaryls, pyrrols, anilines and thiophenes. This gives rise to the development of flexible and printable devices. Table 1 summarizes recent research on solid state hybrid and DSSCs based on TiO_2. Depending on the kind of hole conductor efficiencies, up to 4 % can nowadays be obtained with the 2,2′7,7′-tetrakis-(*N,N*-di-*p*-methoxyphenyl-amine)-9,9′-spirobifluorene (spiro-MeOTAD) material. But also the dye used makes a difference in the overall efficiency as well as the layer thicknesses, the measurement e.g. measuring at 1 sun, the device preparation conditions like annealing, barrier layer and protecting layers usage, etc). These efficiency dependencies complicate the comparison of the devices of different groups.

hole conducting material	TiO_2 structure	Efficiency / % (illumination)	Literature
TPD-MEH-M3EH-PPV	Porous network	0.58 (100 mW/cm^2)	2005[31]
MEH-PPV	Nanorods	0.39 (100 mW/cm^2)	2006[32]
MEH-PPV	Network	0.7 (100 mW/cm^2)	2006[33]
P3OT	nanocrystal layer	0.16 (80 mW/cm^2)	2002[34]
P3HT	Porous network	1.5 (33 mW/cm^2)	2003[35]
P3HT	Particles	0.42 (100 mW/cm^2)	2004[36]
P3HT	Nanorods	0.51 (100 mW/cm^2)	2008[37]
P3HT	ZnO-TiO_2 nanorods	0.29 (100 mW/cm^2)	2007[38]
Spiro-OMeTAD	Porous network	4.1 (100 mW/cm^2)	2005[5]
Spiro-MEOTAD	Gyroid	1.7 (100 mW/cm^2)	2008[29]
Spiro-OMeTAD	Porous network	1.5 (100 mW/cm^2)	2009[39]

Table 1: Recently published results of solid state bulk heterojunction hybrid solar cells. Compared are different hole conducting materials and various TiO_2 structures.

Hybrid materials can be easily obtained in various morphologies by using sol-gel processing. Using a sol-gel mixture to create hybrid systems has certain advantages. The desired morphological features in hybrid materials can be deliberately adjusted not just by the variation of the block length of the copolymer, but also by the variation of the concentration of the sol-gel mixture.[23] To gain a deeper insight in the relationship of structure and concentration of the components the mapping of a ternary phase diagrams is helpful. Another benefit of this procedure is the generality of these phase diagrams for different hybrid systems. For DSSCs a defined structure of crystalline TiO_2 plays an important role. As seen in Table 1 the TiO_2 morphology ranges from defined gyroid networks to random spherical porous clusters. These structures are commonly self-assembled organic and inorganic materials that are made from blends or templates. In blended systems the formation of an interconnected pathway in a self-assembled fashion by the incorporation of particles or rods is desired. The advantage of this approach results from the possibility of a separate optimization of the particles or rods and the additional polymer. This for examples enables previously calcination of the inorganic part at high temperatures to become crystalline. Furthermore, the organic part can be tuned to improve the miscibility of the organic and inorganic part in a blend[40] or to selectively dissolve the inorganic part in a certain phase. As inorganic part not only TiO_2 can be used as donor material in hybrid solar cells. *Huynh* et al. obtained power conversion efficiencies of about 1.7 %, by blending previously prepared CdSe nanorods with P3HT.[41] ZnO can be used as donor material by blending particles with acceptor materials.[42] Examples of recently published results are shown in Table 2.

Acceptor	Donor	Efficiency / %	Literature
P3HT	CdSe rods	1.7 (100 mW/cm^2)	2002[41]
P3OT	CdTe rods	1.1 (100 mW/cm^2)	2005[4]
MDMO-PPV	ZnO particles	1.6 (75 mW/cm^2)	2004[42]
PPV	CdSe rods	2.8 (90 mW/cm^2)	2005[43]
P3HT	ZnO rods	0.2 (100 mW/cm^2)	2006[44]
P3HT	ZnO nanoparticles	0.9 (75 mW/cm^2)	2006[45]

Table 2: Comparison of different donor materials of devices made of hybrid blends, were the donor part is previously prepared.

Compared to blended systems, the structures obtained via block copolymer templates are very defined and controlled. This can be achieved by using low molecular weight surfactants or amphipilic block copolymers. Depending on the concentration of the amphiphile and the time of gelation, when the solidification in the sol-gel mixture occurs, it can be distinguished between surfactant templating, evaporation-induced self- assembly and sol-gel templating.[46] Many sol-gel polymer mixtures contain a sacrificial polymer that is just used for templating and burned off after processing. The benefit of this method is that common block copolymers, such as PEO-*b*-PS can be used; they are easily accessible, well-known and commercially available in various block length ratios. *Oey* et al. used a PEO-*b*-PS polymer to obtain porous TiO_2 films, which were prepared by a casting method. After calcinations the backfilling with a hole conducting polymer poly(2-methoxy-5-(2'-ethyl-hexyloxy)-*b*-phenylene vinylene (MEH-PPV) leads to power conversion of 0.7 %.[33] *Crossland* et al. showed the gyroid structure to be prepared via this method.[29] Depending on the kind of dye, they obtained solar cells from a TiO_2–spiro-MeOTAD hybrid material, exhibiting power conversion efficiencies between 0.7 and 1.7 %. *Snaith* et al. used PI-*b*-PEO copolymers as structure directing agents in a sol-gel based synthesis.[39] Using the same templating polymer, *Nedelcu* et al. achieved TiO_2 networks with controlled pore size and film thickness.[39] After backfilling the pores which remained after calcination with a hole conducting material Spiro-OMeTAD, they obtained power conversion efficiencies up to 1.5 %, depending on the thickness and porosity of the active layer.

The post synthetic strategy, where the templating amphiphile does not carry functionality, causes difficulties concerning the stabilization of the calcined film and gain a proper refilling density. In an one-pot strategy these challenges can be avoided. Furthermore the extra steps such calcining the templating, sacrificial polymer and refilling the remaining skeleton with a desired hole conducting material can be circumvented. Thus a one-pot synthesis is a faster way of producing functional hybrid materials. *Wang* et al. showed the preparation of a hybrid solar cell by using a ZnO precursor and PVP-PVA as template. The resulting hybrid composite consisted of a conjugated polymer and ZnO crystals and showed an efficiency of about 0.03%.[47]

2.2 SELF ASSEMBLED SYSTEMS IN PHOTOVOLTAICS

Self-assembled systems have found their way into all fields of organic photovoltaics, be it hybrid-, polymer-polymer-, fullerene-polymer- or dye-sensitized solar cell devices. Their structures are based on organic, inorganic or hybrid materials. One can roughly distinguish between blend structures and block copolymer structures. In a blend system the phase separating components form non-covalently bound morphologies while in copolymer structures the amphiphilic polymers themselves phase separate. All these systems can be used in bulk heterojunction solar cells (BHJ), where donor and acceptor materials are blended together to form a heterojunction.[48] In any case a self-assembled active layer is formed where creation, separation and diffusion of the exciton, a hole/electron pair, takes place. Therefore, this layer is a crucial part of the solar cell. To design an efficient photovoltaic device, the heterojunction morphology as well as its optoelectronic properties are essential for a successful result. First of all the material has to be able to absorb the light and create an excited state that leads to an exciton. When the exciton is created it has to diffuse towards the interface of the electron and the hole transporting material. Since the diffusion length of excitons in polymeric materials typically ranges from 10 to 20 nm, the structure of the active material has to display a nanostructure in these dimensions. This results in a very high surface area that is beneficial for an efficient charge separation. At the same time the nanostructure has to have a percolation way for the photogenerated charges to pass towards the electrodes. Therefore certain structures like pillars and networks have been proposed to be most favourable. With lithography or diverse templating systems[46] these kinds of nanostructures can be obtained. Here it will be concentrated on a comparison of active materials that are organized via a self-assembled process. In hybrid systems amphiphilic polymers can be used to act as a surfactant, template or functional template to structure direct the active material. In special cases an organic and inorganic part can form covalently bond self-assembled structures.[49] It is known that block copolymers can form various morphologies from spheres in a matrix to pillars, layers and network structures via self-assembly under appropriate conditions. Changing the molecular weight fraction, block ratio[50] and amphiphilicity, these morphologies can be controlled in the nano- and micrometer regime. Pillars, layers and networks perfectly fulfil the requirement for the creation of a percolated system (Figure 6, top). Network structures for example appear in complicated bicontinuous cubic phases, such as gyroids. In blended systems distinct micro- or nanostructured materials can be formed too. Linked particles or rods phase separate via self-assembly to form network structures (Figure 6, bottom).

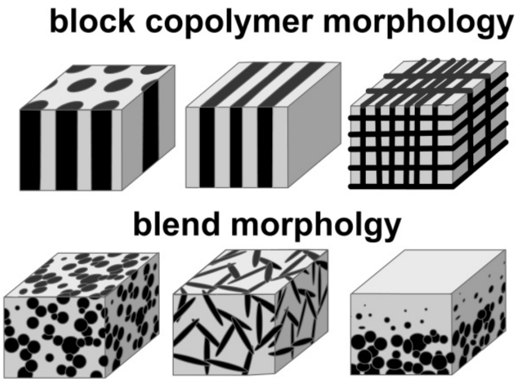

Figure 6: From left to right, pillar, layer and network morphologies of block copolymers at the top and blended morphologies of spheres, rods and gradient systems on the bottom.

Copolymer systems are found in all-polymer solar cells where block copolymers consisting of a donor and an acceptor material function as the active material. Non-functional block copolymers can be used as templating material for inorganic and organic networks by selectively disposing parts of the polymer or the whole polymeric structure. This method is implemented in hybrid or dye sensitized solar cells. Self-assembled morphologies made of blended systems lead to fullerene-polymer or hybrid solar cells.

2.3 SELF-ASSEMBLED SYSTEMS

Self-assembly is an appropriate way to organize matter on the nanometer scale over large areas. Very general the self-assembly process starts at the transition from a dispersed state to condensed state, whether the system is made of molecular species, polymers or microscopic objects.[51] In the following chapters polymeric or surfactant assisted self-assembled systems leading towards organized matter will be introduced.

2.3.1 PHASE DIAGRAMS OF BLOCK COPOLYMERS - BULK

The mixing of two polymers can be expressed with the Flory-Huggins Interaction. The phase behaviour of this blend is described by Flory-Huggins segment-segment interaction parameter (χ), the degree of polymerization (N) and the composition (ϕ). These parameters are found in the Flory-Huggins formulation for the Gibbs free energy of mixing of polymer blends:

$$\Delta G_{mix} = RT\tilde{n}_c\left(\frac{\phi_A}{N_A}ln\phi_A + \frac{\phi_B}{N_B}ln\phi_B + \chi\phi_A\phi_B\right) \qquad \text{Eqn. 3}$$

In this equation the influence of enthalpic and entropic factors on the phase state is expressed. In the case of diblock copolymers the combination of monomer A and B determines the energy of mixing that can be approximated by χ. The product Nχ, determining the degree of segregation, gives evidence, if the system is dominated by entropic or enthalpic contributions resulting in ordered or disordered structures.[52] The Interaction energies ε_{AA}, ε_{BB} and ε_{AB} between the segments of monomer units A-A, B-B or A and B are described with χ_{AB} as follows:

$$\chi_{AB} = \frac{1}{k_B * T}\left(\varepsilon_{AB} - \frac{1}{2}(\varepsilon_{AA} + \varepsilon_{BB})\right) \qquad \text{Eqn. 4}$$

Higher ε_{AB} than ε_{AA} and ε_{BB} interactions bring a positive value for χ causing an increased energy of the complete system. A negative value of χ indicates that there is a favorable interaction between segment A and B. Consequently the overall system energy is lowered by an A-B contact compared to the sum of A-A and A-B contacts.

Block copolymer directed structures are accessible in various formations and functionalities. Amphiphilic block copolymer systems tend to microphase separate to form distinct nanostructures because of the different chemical and physical properties of the blocks (Figure 7). Depending on the volume fraction of the blocks ordered structures as cubic packed spheres, hexagonal cylinders, gyroid or lamellar structures are obtainable. Besides these architectural factors of the polymer phase separation, also external parameters like temperature, solvent annealing, shear field, electric and magnetic fields are playing a role.[53]

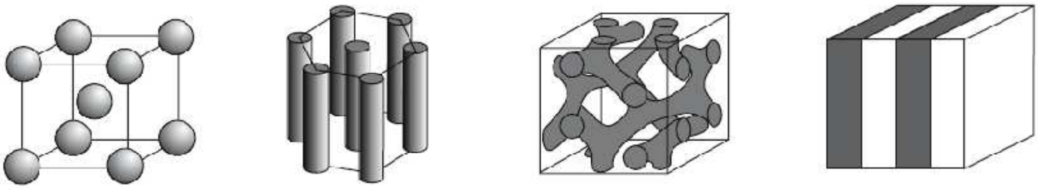

Figure 7: Morphologies of diblock copolymers. Cubic packed spheres, hexagonal packed cylinders, double gyroid and lamellar. Inverse phases are not shown.[54]

2.3.2 *PHASE TRANSITION OF SURFACTANT SYSTEMS - EMULSION*

Amphiphilic polymers or surfactants form diverse aggregates in water-oil mixtures driven by the hydrophobic attractions and the hydrophilic ionic and steric repulsions of the molecules. The packing of the amphiphiles depends on the volume fraction of the hydrophobic and hydrophilic part. The geometry is further influenced by experimental conditions like temperature, pH, solvent etc. In water-oil mixtures micellar systems are formed, which strongly depend on surfactant concentration that has to be above the critical micelle concentration (CMC). Depending on the composition of surfactant, oil and water, the system changes between spherical and rod-like micelles, hexagonal, cubic and lamellar phases. Mapping a ternary phase diagram is helpful to indicate certain morphologies in dependency on the concentrations of the oil, water and surfactant phases (Figure 8).

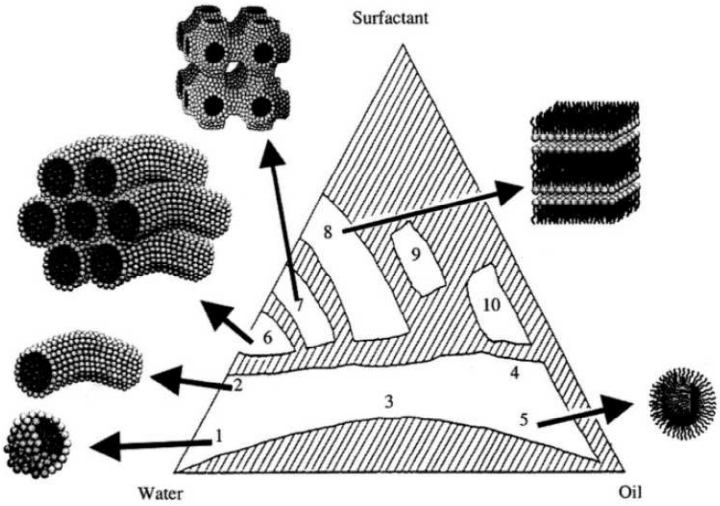

Figure 8: Schematic diagram of a surfactant-water-oil system. 1. Spherical micelles. 2. Rod-like micelles. 3. Irregular bicontinuous phase. 4. Reverse cylindrical micelles. 5. Reverse micelles. 6. Hexagonal phase. 7. Cubic phase. 8. Lamellar phase. 9. Reverse cubic phase. 10. Reverse hexagonal phase.[51]

Not only low-molecular weight (low-M_n) surfactants can be used in micellar systems but also block copolymer macrosurfactants. Common polymeric surfactants are e.g. poly(ethylene oxide) – poly(propylene oxide) (PEO-PPO) and poly(ethylene oxide) – poyl(butylenes oxide) (PEO-PBO), commercially available as Pluronics. They represent a bridge between classical low-M_n and non-ionic surfactants.[55] Like low-M_n surfactants the block copolymer macrosurfactants create micelles in selective solvents for one block at a certain temperature (CMT) and concentration (CMC). The critical concentrations for low-M_n surfactants are higher than those for macrosurfactants.[56] Depending on the block length and environment, the micellar structure can range from star like micelles (small core and big corona) to crew-cut micelles (larger core and stretched coronal chains). PEO blocks containing amphiphilic polymers are commonly known for diverse morphologies in organic solvent/water mixtures.

In the presented work amphiphilic block copolymers made of PEO and poly(triphenylamine) (PTPA) blocks are prepared and investigated. For the PEO block the CMT is of special interest because dehydration of the PEO block takes place at elevated temperature.[56] While the PTPA block of the PEO-*b*-PTPA block copolymer is hole conducting the PEO block is coordinating to the metal oxide. The amphiphilic nature of the block copolymer stems from the solubility of PEO block in water, while the PTPA block is insoluble. This block copolymer is used in a micellar system not only for plain solvent/polymer mixtures, but also applied for sol-gel systems to template hybrid materials via self-assembly.

2.4 TEMPLATED HYBRID MATERIALS VIA SELF-ASSEMBLY

To obtain nanostructured hybrid materials, different approaches that make use of self-assembly processes of amphiphilic molecules or amphiphilic block copolymers in distinct environments, have been invented. In a self-assembly process a template for an inorganic phase is formed, which is introduced either as a molecular precursor or added as pre-formed nanoparticles. Depending on the templating strategy, the amphiphilic molecule or amphiphilic block copolymer is either penetrated by the inorganic phase during synthesis or backfilled with inorganic material after template formation. By using polymers as surfactants, an inorganic phase can be shaped in the ten-nanometer-regime during a sol-gel synthesis. Thus, the size of the templated metal oxide structures can be rationally controlled by the molecular weight of the templating amphiphile on a size scale, which is appropiate for photovoltaic applications. For electronic devices like integrated circuits, a common but expensive route of lithographic techniques exists. These are top down routes like nanomolding [57], nanoimpriting [58] and relief grating [59]. While the precision of lithographic approaches is very high, it is still difficult and costly to cover large surface areas with nanostructured materials by lithographic technique. Bottom up approaches using self-assembly, however would enable to coat large surface areas with active materials which are structured in the nanometer range. Therefore copolymers are used as amphiphiles to structure directly as micellar systems (2.3.2) or as bulk materials (2.3.1) in phase separated morphologies (Figure 9).

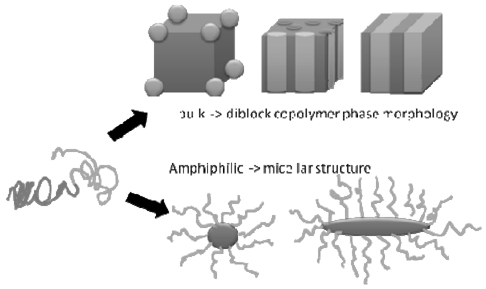

Figure 9: Block copolymer self assembled structures as micellar systems and bulk morphologies (adapted from literature[60]).

This means in combination with an inorganic phase one can distinguish between micellar sol-gel and bulk templating techniques. *Soler-Illia* et al. used commercially available Pluronics (PEO-*b*-PPO) to template meso-structured metal oxide based hybrid networks. [61] Depending on the amount of water they proposed different mechanisms of the hybrid structures formation (Figure 10). With a high amount of water a micellar structure is preferred and small inorganic clusters arrange around these micelles. While in systems with low amount of water the inorganic phase has to arrange itself in the domains of the favoured part of the block copolymer domains.

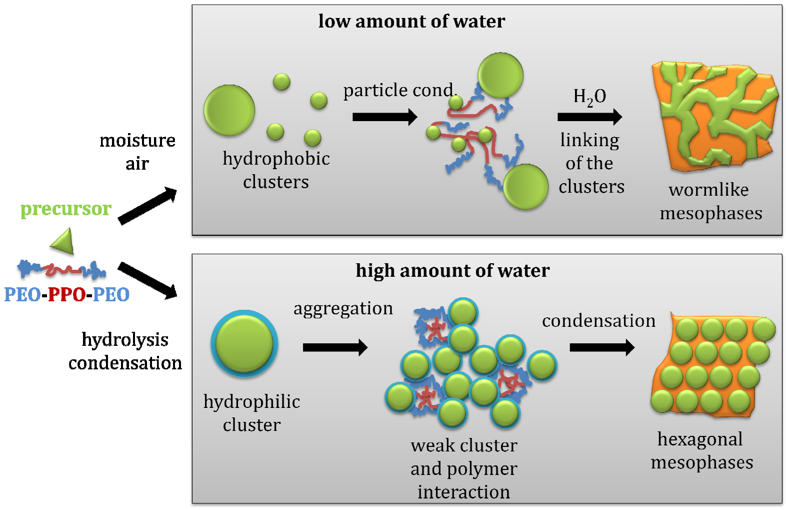

Figure 10: Formation of hybrid mesophases with different content of water in the system (adapted from literature[61])

2.4.1 SOL GEL TEMPLATING SYSTEMS

Low molecular weight surfactants as well as amphiphilic block copolymers can show lyotropic phase behaviours leading to even more diverse morphologies.[62, 63] In addition, polymers can be used to solubilise inorganic materials in organic solutions, if the inorganic material is either coordinated to one part of the amphiphile via specific chemical bonds or if the inorganic material is synthesized from an aqueous sol-gel solution. The precise control of the lyotropic phase separation is not only a solubilisation process of the inorganic phase, but also a direct templating step. Depending on the concentration of the amphiphile and the time when the sol-gel reaction mixture solidifies, one can distinguish between different synthetic approaches. (i) Surfactant templating: Just the right amount of surfactant and inorganic precursor are used to prevent aggregation, flocculation and Ostwald ripening (2.4.1.1). (ii) Evaporation-induced self- assembly templating: Successive concentration of a sol-gel solution by evaporation to yield in a hybrid material that is determined by the liquid crystal phase of the templating amphiphile (2.4.1.2). (iii) Sol-gel templating in a template consisting of a polymer matrix with marginal residual solvent, where the inorganic phase is completely surrounded by the stabilizing and structure directing high molecular weight organic matrix (2.4.1.3). In this case the structure of the resulting hybrid material can be directly controlled by variation of the molecular weight and composition of the amphiphilic template.

2.4.1.1 Growth stabilization by low molecular weight amphiphiles

For the use of catalysts, sieves and membranes for sensors a range of accessible pore sizes and compositions are needed. Supramolecular templates for metal oxides could be achieved by the use of short-chain amphiphiles. The inorganic frameworks can be composed of silicate, silica, main-group and transition-metal oxides, sulphides and phosphates.[64] In 1992 *Beck* et al. published a method to obtain mesoporous solids from the calcinations of aluminosilicate gels in the presence of surfactants.[65]

To obtain well-defined nano particles, which are not agglomerating, the synthesis in small reactors of self-organized systems has been conducted. These small reactors can either be micelles or droplets in micro- or miniemlusions. Polymers or surfactants stabilize the large surfaces of the resulting e.g. metalparticles. Further, these small reactors can arrange in a lattice structure leading to well-ordered hybrid materials with defined morphologies.[62] But not just a controlled organization of the particles is favoured, also the size itself to influence the properties of the metal or metal compounds. For the preparation of quantum dots to be used for application in LEDs, diverse core-shell quantum dots (e.g. CdSe/ZnS) are fabricated with the aid of surfactants that control the particle size and also stabilise their surface[66, 67].

Artemyev et al. demonstrated the electroluminescence (EL) of densely packed CdS quantumdots which where stabilized by surfactants to reduce the size of the nanocrystals to about 2 nm in diameter.[68] They pointed out that not only the size and properties of the nanocrystals, but also the stabilizing component influences the nature of the EL. *Yang* et al.[69] described an approach in which a functional templating agent was applied in the synthesis of their silica-chromophoric nanocomposites. A chromophoric amphiphile, which acted as photoactive as well as structure directing material, was used in combination with a sol-gel technique to co-assemble a nanocomposite film that showed enhanced emission. This co-assembly introduces another structural level. In this sense amphiphiles are not only useful in the shape definition of the primary structural units, but may also be used in order to structure these particles on a higher hierarchical level. This ability for structure generation will be addressed in greater detail in the following sections.

2.4.1.2 Evaporation-Induced Self-Assembly

Sol-gels which follow the evaporation-induced self-assembly are made of a hydro-alcoholic inorganic precursor and an amphiphile at low concentrations, typically below the critical micelle concentration (CMC). Reaction of the sol-gel precursor takes place in free solution and results in small particles which are then concentrated via spin coating, dip coating, ink-jet printing or aerosol deposition to form a uniform hybrid gel film, which is patterned due to the self-assembly of the amphiphiles once their concentration exceeds the CMC.[70] Starting from very dilute solutions, the resulting mesophases are mainly depending on the surfactant/inorganic precursor ratio, the nature of precursor and the humidity during the evaporation process.[70]

Surfactant-templated inorganic materials by evaporation induced self-assembly (EISA) using low molecular weight amphiphiles are also known to form mesostructured hybrid materials. Since evaporation only changes the concentration, the freshly formed micelles may have sufficient time to order into highly correlated mesophases. Since ordering during drying is a slow process, EISA is most often used in connection with dip-coating as a sample preparation process. The self-assembly process is driven by evaporation during film preparation and while the formation of a meniscus acts as an ordering interface, the change of surfactant concentration during evaporation may also change the lyotropic phase. Therefore, both variables, amphiphile concentration and evaporation rate, play an important role and determine the orientation of the mesostructure.[71] If no ordering meniscus is present, as in the case of solvent evaporation from a bulk solution, lyotropic phases are formed and as a result, the formation of nanoscale hybrids, which have been templated by low molecular weight surfactants, is driven by an interplay between the liquid crystal templating mechanism and the cooperative self-assembly mechanism.[72] This can be seen as an extension to the EISA process, where the highly correlated mesostructures are already formed in solution and not during the preparation of the active material.

2.4.1.3 Lyotropic templating of electroactive functional materials

The creation of the morphology is a self assembly process in lyotropic solution and as such can be controlled during the preparation procedure. Inside the aggregates the metal oxide is formed by hydrolysis followed by a condensation. Structure and morphology of the resulting network depend on the type of sol-gel precursor, the temperature, the amount and concentration of acid, the solvent, and the alkoxide. Acidic condition enhances the speed of hydrolysis which should be finished before condensation takes place.[73] Most experiments addressing the lyotropic templating of sol-gel mixtures have investigated the formation of mesoporous silica. The hydrolization behaviour of molecular precursors, such as tetraethyl orthosilicate, is easily controlled, which is crucial for a successful templating.[61] Nevertheless, it is possible to reduce the hydrolysis speed via appropriate e.g. titania precursors under acidic conditions.[74-79] Different morphologies can be created by controlling the chemical parameters, like concentration of precursor, acid and surfactant to determine the formation of the hydrolysed and condensed inorganic network. After sample preparation a temperature step is typically applied in order to remove the surrounding organic matrix and to transfer the initially amorphous titania into a crystalline modification. This temperature treatment commonly deteriorates the structural order. Thus, if only a removal of the organic matrix is intended, UV treatment of the hybrid material results in highly ordered structures without deterioration.[77] For hexagonally packed titania films *McGehee* et al. demonstrated that it is possible and beneficial to incorporate thin templated titania layers into a working solar cell device.[75, 80] A porous TiO_2 film with pore diameters of about 10 nm and a filling of P3HT a pore power conversion efficiency of 1.5 % could be reached.[75]

In a lyotropic approach the structure directing block copolymer can be directly mixed with a metal precursor to obtain hierarchically structured materials.[77, 78] The advantage of using a block copolymer template lies in the precise positioning of the inorganic part within the polymer matrix and the control of the overall structure due to the design of the respective block copolymer itself.[81] *Huo* et al. published a detailed discussion about the formation of hydrophobic-hydrophilic interacting hybrid composites. They described the formation of silicate phases that are stabilized by the electrostatic interactions between the soluble inorganic specie and the templating molecules (model shown in Figure 11).[64] Templating molecules react with inorganic species to form cooperative nucleation sites resulting in the formation of liquid crystals by precipitation into organized arrays. In the end, condensation of the inorganic phase occurs while the templating/surfactant phase reorganises to reduce interface charge densities.

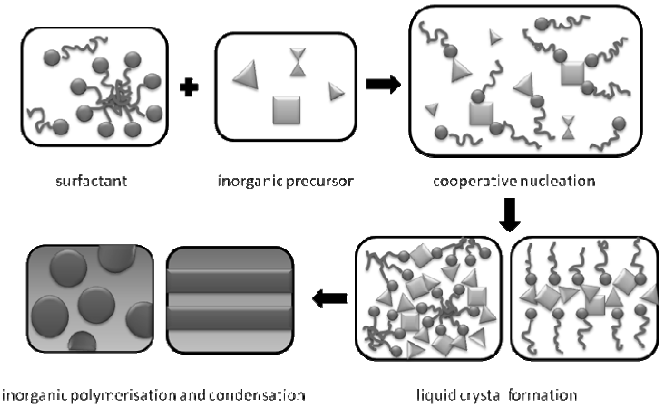

Figure 11: Cooperative templating model for biphase materials (adapted from literature[64])

Changing the amphiphilic nature of the copolymer by changing the block length ratio will lead to different predesigned morphologies. In this way *Cheng* and *Gutmann* could show a variety of structures that allow for the synthesis of inorganic materials by a sol-gel process within a lyotropic template. Upon variation of the amount of precursor, solvent and acid, the formation of diverse crystalline TiO_2 structures ranging from spheres to wires and hollow nano doughnuts could be rationalised by a comprehensive phase diagram.[82] They were able to prepare active hybrid materials with identical morphologies, but different characteristic sizes. This was achieved by using two amphiphilic block copolymers of different molecular weight, but comparable composition and identical inorganic precursors and preparation protocols.

2.4.2 *INTEGRATED FUNCTIONAL TEMPLATES*

Hybrid nanostructured systems can be reached by one-pot-synthesis (chapter 2.4.2.1) or post-synthetic strategies (chapter 2.4.2.2) (Figure 12). The post-synthetic strategy is a common lyotropic approach, where the templating amphiphile does not carry an electronic functionality. Thus, it is sacrificial and has to be removed before the templated functional material is used. This inherently adds extra processing steps in the manufacturing of optoelectronic materials and consequently, the use of a block copolymer that already incorporates the desired electronic functionality would be advantageous. The disadvantages in the post-synthetic strategy are the problems which can be caused by removing of the templates, what results in a film deformation due to heating process. Another disadvantage is the extra step of refilling with the problem of the proper filling density. In the one-pot-synthesis the surfactant or template has not to be removed, it is either not perturbing or brings a functionality with itself.

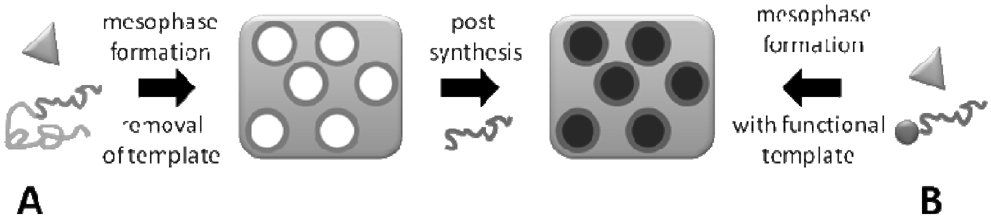

Figure 12: Common templating technique with post synthetic strategy to add the functionality (route A) and an integrated functional template – a one-pot-synthesis (route B).

2.4.2.1 One-Pot-Synthetic Strategy

The integrated use of templating amphiphiles with electronic functionality is challenging, since it requires very specific preparation conditions, but has meanwhile been investigated by several groups. *Wang* et al. showed the preparation of a hybrid solar cell consisting of ZnO and poly(vinyl pyrolidone)/poly(vinyl acetate) (PVP/PVA).[47] The Zn precursor was added to a solution of a polymer mixture leading to a hybrid composite of a conjugated polymer and ZnO crystals. Besides active layer materials, *Memesa* et al. investigated the use of integrated functional templates in materials for barrier layers. They were able to show that it is possible to integrate isolating domains in between conducting titania pathways into defect free films.[83] These non-optimised hybrid films were able to support charge densities comparable to charge carrier densities in conventional blocking layers.

In this work a new block copolymer is introduced with an approach that is able to cover exactly the need of functional hybrid templating systems for optoelectronic application.

2.4.2.2 Post Synthetic Strategy

2.4.2.2.1 Templating from Structured Bulk Phases of Block Copolymers

If the templating amphiphilic block copolymer is sufficiently mobile at room temperature, i.e. the glass transition temperature of all blocks is well below room temperature, templating does not need to rely on the formation of lyotropic phases. *Wiesner* et al.[84] demonstrated a technique to obtain crystalline metal oxide-carbon composites by mixing poly(isoprene)-b-poly(ethylene oxide)

(PI-*b*-PEO) with metal oxide precursors. As a result they obtained hexagonally structured hybrid films and metal-oxide-carbon composites after heating the film under argon. Further heating in air revealed pure, crystalline metal oxides. For solid-state-dye sensitised solar cells a defined structure of crystalline TiO_2 plays an important role. *Snaith* et al. also used PI-*b*-PEO copolymers as structure directing agent in a sol-gel based synthesis.[85] They used a gyroid phase formed by a block copolymer to build an electrochemical replica of TiO_2 for DSSCs.[86, 87] The charge transport was found to be faster in 1D wire structures than in 3D gyroid arrays, even though the overall power conversion efficiency reached about 3 % for the gyroid structure.[87] Highly porous titania films were produced with different pore sizes by altering the ratio of the block length of the polymer and the polymer-precursor. Pore sizes of 30 nm were found to be most efficient.

The templating via bulk block copolymer phases is, however, not limited to amphiphilic templating of alcoholic sol-gel solutions. If one of the blocks specifically binds to a molecular precursor, it is possible to use the block-copolymer microphase separation to selectively confine the reactants of a chemical reaction into a well-defined spatial region. Using noble metal precursors and ionic interactions, *Fahmi* et al. demonstrated the preparation of 1D metal nanostructures.[88-90] Sphere, rod- and ring-like structures of metal loaded copolymer micelles could be fabricated with controlled size and distribution of the metal particles in the films.

2.4.2.2.2 Inverse Opals

The use of monodisperse latex particles, which are ordered into closely packed arrays, opens a way to several highly macroporous materials being either hybrid or inorganic materials. Inverse opals can be obtained by several filling techniques of the colloidal crystal, like sol-gel chemistry, polymerization, salt deposition, chemical vapour deposition, spraying techniques, electrodeposition and more.[91] By coating latex particles with alkoxide precursors of different metals like Ti, Zr, Al, Fe etc., highly ordered composite structures have been be obtained.[92] Via this method *Jones* et al. prepared a copper phthalocyanine (CuPc) interconnected porous film and infiltrated it with [6,6]-phenyl-C_{61}-butyric acid methyl ester (PCBM).[93] With regard to solar cell application, it is however more common to use inverse opals as photonic crystals to increase the photocurrent of a solar cell. A photonic crystal that has been attached onto a conventional photoelectrode can act as a dielectric mirror and as a medium for enhancing light absorption.[94]

2.4.2.2.3 Anodic Titanium Oxide (ATO templates)

In contrast to the template-based approaches, where the template is used as an sacrificial mold and is removed after the patterning process, anodic titanium oxide (ATO) templates offer the possibility to build up nanostructured inorganic-organic hybrid systems, which can be used directly in hybrid solar cells. Titanium oxide templates serve as an electron conducting material and by coating the walls of the pores first with a light-absorbing dye and then infilling the template of the nanoporous structure with a hole-conducting organic or polymeric material, a large donor/acceptor interface can be generated, which is one of the requirements for high efficient photovoltaic devices. Highly ordered titania nanotube arrays with a length of 360 nm and pore diameters of about 50 nm are made by anodization of titanium films that had been sputtered on fluorine-doped tin oxide (FTO) substrates, followed by an annealing step of the TiO_2 to obtain an enhanced transparency of the ATO template. These ATO templates could then successfully be integrated into a dye-sensitized structure using a commercially available ruthenium-based dye and a photocurrent efficiency of 2.9 % under air mass (AM) 1.5 illumination was measured.[95] The overall efficiency could be further increased to 6.1 % by using antenna dye-sensitized arrays of ~15 µm long titania nanotubes.[96] *Zhu* et al. compared dye-sensitized solar cells, which were based on anodized titania nanotubes, with devices based on nanoparticle films of the same thickness. Intensity modulated photocurrent and photovoltage measurements showed that the charge-collection efficiency for the nanotube-based system is 25 % larger compared to the efficiency for nanoparticle-based cells.[97] Besides hetero-junction solar cells that utilize a liquid electrolyte, also solid state titania nanotube-based solar cells were fabricated using a carboxylated polythiophene derivative with power conversion efficiencies of 2.1 % under AM 1.5 sun.[98] *Zhang* et al. could grow P3HT onto the surface of TiO_2 nanotubes grown in anodic aluminium oxide (AAO) membranes (Figure 13).[99] With this method they could achieve a higher filling density than with usual infiltration methods.

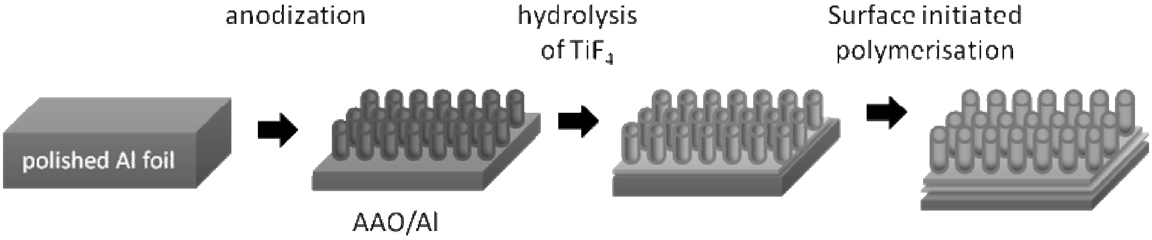

Figure 13: Schematic presentation to form P3HT-titania hybrid nanotube arrays (adapted from literature[99])

Kang et al. used porous alumina templates for growing CdS nanorods through AAO membranes on Ti substrates.[100] But their overall power conversion efficiency just reached 0.6 %. An alternative to the common AAO templates was shown by *Law* et al., who used directly grown ZnO nanowires for solar cell applications.[101] They grew ZnO nanotubes directly on FTO, while *Unalan* et al. grew them from single walled carbon nanotubes resulting in combination with P3HT in plastic solar cells with a power conversion efficiency of 0.6%.[102] However, ZnO nanotubes were not only used for solar cell application but also for templates. *Rattanavoravipa* et al. coated ZnO wires with TiO_2 to test them in a P3HT/Fullerene device resulting in a power conversion efficiency of 0.7 %.[103]

In literature, most synthetic strategies to crystallize TiO_2 are however based on high temperature or corrosive chemicals and thus damage or destroy the templating polymer. One way to avoid high temperatures is the use of ultrasound to get crystalline TiO_2 out of $TiCl_4$[104]. Gopal et al.[73] obtained a crystalline phase out of $Ti(O^iPr)_4$ even at room temperature. Depending on the heating rate the precursor becomes anastas or rutile.

2.4.2.2.4 *Templating of Pre-Fabricated Functional Particles*

So far, the amphiphilic templating relied on the structuring of a reactive system, which is transformed into a structured functional material afterwards. It is, however, also possible to prepare nanoparticles first and then align the nanoparticles in an ordered arrangement using a template. This constitutes a bottom-up approach to structure already existing nanoparticles. In this bottom-up fashion, monodisperse quantum dots like CdS and CdSe are accessible which are used in LED and solar cell application. [105, 106] Therefore the exact size control is of great importance for tuning the optoelectronic properties. Such pre-formed semiconductor particles have proven to be efficient in the preparation of hybrid solar cells.[41, 74, 105]

Self-assembled nanostructures of organic materials can be used to structure directly inorganic materials, thereby introducing magnetic, electronic or optoelectronic functions. A variety of nanostructured morphologies can be obtained by using block copolymer thin films.[60] The nanodomains can be tuned by different means, such as changing the molecular composition, the thin film parameter or by applying an external field. The selective decoration of the polymer structure with inorganic particles has been described in literature.[107] Figure 14 shows a schematic diagram of the process of decorating a nanostructured self-assembled block copolymer thin film with inorganic particles. Exposure of PS-*b*-PEO structures to water resulted in a selective swelling of the PEO. The swollen PEO domains functioned as a reaction vessel for the hydrolysis of a silicon oxide precursor yielding patterned SiO_2 nanoparticles on the top surface of the block copolymer film.

Figure 14: Using PEO-*b*-PS scaffolds to grow silicon oxide particles from the swollen PEO domain (adapted from literature[108])

Lopes et al. published a method to align metals on a spin-coated thin film of a PS-*b*-PMMA block copolymer, whose lamellar domains were oriented perpendicular to the surface.[109] The metal arranged selectively along one of the block copolymer domains resulting in a self- assembled nanopatternd array. Other groups tried to load block copolymer structures with metal or metal oxide particles by filling metal salts into a porous polymer scaffold, which was obtained by selective reduction of one block.[110-112] A similar approach addresses the addition of already prepared metal nanocrystals to a block copolymer solution. *Thomas* et al. could show that different nanoparticles (Au and SiO_2) organize size selective in block copolymer domains of PS-*b*-PEP.[113] Similar work has been presented by *Russell* et al., who were loading PS-*b*-P2VP with CdSe particles.[114] Ochsmann et al.[115] were able to obtain a monolayer of CdS nanostructures on top of a PS-*b*-PEO film. AFM and GISAXS revealed spherical nanostructures (d = 15 nm) corresponding to the dimensions given by the block copolymer film.

3 EXPERIMENTALS

3.1 CHEMICALS - MATERIALS

Titaniumtetraisopropoxide (TTIP, 99.999%), DMF (HPLC grade), CH_2Cl_2 (HPLC grade), MeOH (99.8 %) THF (anhydrous 99.9 %), hexane (95 %) and $Zn(OAc)_2$ (98 %) were purchased from Sigma Aldrich. HNO_3 was purchased from Riedel-de-Haen (65 %), Isopropanol was purchased from Fluka. HCl was purchased from Riedel-de-Haen (37 %). Clavios P (poly(3,4-ethylenedioxythiophene) poly(styrenesulfonate), PEDOT:PSS) was obtained from Starck and used as obtained without filtration.

FTO glasses were obtained from AGC Fabritech in Japan (24 mm×24 mm; < 12 Ω sheet resistance; > 80 % effective transmittance; 10-20 % haze).

3.2 SYNTHESIS

Cis-Ru(SCN)₂(4,4´-dicarboxylic acid-2,2´-bipyridine)(4,4´-dinonyl-2,2´-bipyridine) (Z907) was synthesized according to literature[116].

Poly(ethylene)oxide **2** (PEO) was anionicly synthesized by using potassium isopropylate. The active chain end was quenched with dry and oxygen free methanol. The precipitate was dried in vacuum.

Triphenylamine **4** (TPA) was synthesized according to literature[117].

3-Benzyl-sulfanylthiocarbonylsulfanylproionicacidchloride ***1*** (BSPAC) the RAFT agent was synthesized according to literature.[118],[119]

MacroRAFTagent **3** (PEO-RAFT)
8.12 g (5800 g/mol, 0.0014 mol) PEO was solved in 80 mL CH_2Cl_2 and after adding 0.6 mL Pyridine it was flushed with argon for 30 min. The solution was given on to the RAFT-acidchloride and stirred for 24 h at room temperature. The solution was extracted three times with 50 mL of water and the combined water phases washed with CH_2Cl_2. The combined organic phases were dried with $MgSO_4$ and after concentration in vacuum precipitated in hexane.
^{1}H NMR ($CDCl_3$) δ (ppm): 7.31 (m, 5H, Phenyl); 4.60 (s, 2H, Ph-CH_2-S); 4.28 (t, J = 4.7 Hz, 2H, CH_2-COO); 3.64 (m, 576H, PEO); 2.80 (t, J = 6.8 Hz, 2H, S-CH_2-C)
GPC (DMF, PEO standard): M_n = 8700 g/mol, M_w = 9900 g/mol, dp = 1.14

Poly(ethyleneoxide)-b-poly(triphenylamine) **5** (PEO-*b*-PTPA)
0.48 g PEO-RAFT, 3.2 mg AIBN, 1.7 g TPA and 6 mL of DMF were put into a schlenk flask under argon and after three pump and freeze cycles, the mixture was stirred for 3 days at 60 °C. After evaporation of DMF, the solid was solved in a small amount of THF and precipitated in hexane (2 times).
^{1}H NMR ($CDCl_3$) δ (ppm): 6.98-6.45 (m, 512H, PTPA); 3.65 (s, 428H, PEO)
GPC (DMF, PEO Standard): Mn = 9800 g/mol, Mw = 17900 g/mol, dp = 1.8
P1: 6 000 – 10 000 g/mol; P2: 5 000 – 5 00 g/mol
More details found in Results and Discussion chapter 4.1.

Ethylene glycol-modified titanate (EGMT)
Was prepared according to literature.[120]

Synthesis of crystalline TiO_2 rods
0,55 ml of $TiCl_4$ (stored under argon) were taken out in an argon counter stream and then dissolved in 100 mL of ethanol. Within 15 minutes 40 mL of a 1 M NaOH solution were added under stirring. Stirring was continued for another 30 min. The suspension was filtered and the precipitate was washed with water until no chloride ions were found in the filtrate anymore, which was tested by addition of a 0.1 M AgNO3 solution to the filtrate. A white precipitate was obtained. 50 mL of 10 M NaOH solution and the precipitate were mixed and stirred for 30 min. 25 mL of the suspension were transferred into a 50 mL Teflon vessel. Afterwards the sealed autoclave was treated in a preheated furnace at 200°C for 24 h. The Sample was naturally cooled down to room temperature. The residual NaOH-solution was removed by centrifugation, followed by washing with 0.1 M HNO_3 until acidic reaction. The sample was subsequently washed with 0.1 M HCl once and with water until neutral reaction of the supernatant solution was reached. In the end the TiO_2 rods were dried over night in a desiccator over silica gel and in vacuum.
Poly-(triphenylamine) (PTPA) and *Poly-(3-hexyl-thiophene)* P3HT were synthesized according to literature.[117, 121]

3.3 SAMPLE AND DEVICE PREPARATION

3.3.1 MORPHOLOGY PREPARATION

3.3.1.1 Hybrid Materials from TTiP Precursor

For titanium *tetra*-isopropoxide (TTiP) TiO_2 precursor systems samples were prepared according to the following procedure: 0.01 g of diblock copolymer PEO-*b*-PTPA (P1) and 0.005 g ruthenium dye (Z907) was solved in 1 g DMF/isopropanol (8.4:1). Afterwards a variable amount of HNO_3 (10 M) was added, followed by the precursor (TTiP) (Table 3). The emulsion was put into an ultrasonic bath for

20 min. Then the mixture was stirred while heating to 90 °C (5°/min) and after reaching this temperature for further 15 min. The weight fractions of the HNO_3 solution and of the organic solvent DMF/isopropanol varied from 0 % to 10 %.

Sample	DMF / wt%	HNO3 / wt%	TTiP / wt%	shape
[M77]	0.36	0.63	0.01	**foam**
[M81]	0.98	0.01	0.01	**wire/sphere**
[M82]	0.96	0.02	0.02	**wire/sphere**
[M83]	0.91	0.01	0.08	**foam**
[M84]	0.91	0.08	0.01	**spheres**
[M88]	0.90	0.08	0.02	**agg. spheres**
[M89]	0.50	0.30	0.20	**foam**
[M90]	0.79	0.20	0.01	**agg. spheres**
[M91]	0.87	0.08	0.05	**scales**
[M92]	0.90	0.05	0.05	**scales**
[M97]	0.97	0.01	0.02	**wire/sphere**
[M98]	0.95	0.04	0.01	**wire**
[M99]	0.99	0.005	0.005	**flakes**
[M100]	0.94	0.04	0.02	**wire**
[M101]	0.92	0.04	0.04	**foam**
[M102]	0.94	0.02	0.04	**wire**
[M103]	0.88	0.08	0.04	**scales**
[M104]	0.94	0.01	0.05	**wire**
[M105]	0.93	0.06	0.01	**wire/sphere**
[M111]	0.94	0.03	0.03	**wire**
[M114]	0.92	0.06	0.02	**sphere**
[M117]	0.97	0.02	0.01	**wire**
[M118]	0.93	0.06	0.01	**foam/sphere**
[M120]	**0.90**	**0.02**	**0.08**	**foam**

Table 3: Composition of TTiP mixtures.

3.3.1.2 Hybrid Marterials from EGMT Precursor

For ethylene glycol modified titanate (EGMT) TiO_2 precursor systems samples were prepared according to the following procedure: 0.01 g block copolymer PEO-PTPA (P2) and a standard ruthenium dye (Z907) (0.005 g) was dissolved in DMF (1 g). After addition of a variable amount of HCl (0.1 mM) and EGMT (Table 4) the mixture was heated to 90 °C for 15 min.

Sample	DMF / g	HCl / g	EGMTA / g	shape
[M137]	1	0.25	0.01	**foam**
[M138]	1	0.50	0.01	**sphere**
[M155]	1	0.40	0.02	**sphere/worms**
[M156]	1	0.10	0.01	**sphere**
[M157]	1	0.05	0.01	**platelets**
[M158]	1	0.05	0.02	**sphere**
[M159]	1	0.05	0.05	**sphere/worms**
[M171]	1	0.10	0.10	**cluster**
[M172]	1	0.30	0.02	**sphere**
[M175]	1	0.40	0.01	**foam**
[M190]	**1**	**0.10**	**0.005**	**foam**

Table 4: Composition of EGMT mixtures.

3.3.1.3 Hybrid Materials from $Zn(OAc)_2$ Precursor

For $Zn(OAc)_2$ precursor systems samples were prepared according to the following procedure: In a PEO-*b*-PTPA (P2, 0.01 g), ruthenium dye (Z907, 0.005 g) solution, dissolved in DMF (1 g), a variable amount of KOH (0.03 M in MeOH) was added drop wise, then a variable amount of $Zn(OAc)_2{*}2H_2O$ (98 %) was added and stirred for 2 h at 60 °C (Table 5).

Sample	DMF / wt%	MeOH/KOH / wt%	$Zn(OAc)_2{*}2H_2O$ / wt%
[M131]	0.920	0.050	**0.03**
[M132]	0.935	0.050	**0.015**
[M133]	0.962	0.008 + 0.02 MeOH	**0.010**
[M134]	0.940	0.050	**0.010**
[M135]	0.943	0.042	**0.015**
[M136]	**0.945**	**0.050**	**0.005**

Table 5: Composition of $Zn(OAc)_2$ Mixtures.

3.3.1.4 Film Preparation

Hybrid films for morphology investigation were prepared on Si(100) substrates by drop coating or spin coating (1000 rpm, 120 s) using a Süss Micro Tec Delta 80 spin coater under ambient conditions (temperature 21 °C; relative humidity 30-40 %; rotation speed of 2000 rpm; acceleration speed of 2000 rpm/s; open cover). The film thicknesses used in solar cells were measured by X-Ray reflectivity profiles or SEM.

3.3.2 SOLAR CELL DEVICE FABRICATION

3.3.2.1 One-Pot Systems

TiO_2 barrier layer were prepared according to literature (for TTIP and $Zn(OAc)_2$ systems[122], for EGMT systems[123]) and spin coated (1000 rpm, 60 s) on commercially available FTO glasses. Coated glasses were put into an oven at 450 °C for 2 h. Active layers were prepared as described in chapter 3.3.1.1, 3.3.1.2 and 3.3.1.3 and spin coated or drop coated on the according barrier layer. On top of the active layer in some cases a PEDOT:PSS (poly(3,4-ethylenedioxythiophene) poly(styrenesulfonate)) layer was spin coated (2000 rpm, 60 s) and finally gold electrodes with 100 nm thickness were evaporated. Preparation and measurements were held under ambient condition.

3.3.2.2 Blend Systems

The whole Preparation was held under ambient condition. The TiO_2 barrier layer was prepared according to literature[123] and spin coated (1000 rpm, 60 s) on commercially available FTO glasses. The coated glass were put into an oven at 450 °C for 2 h. Blend materials were prepared by mixing TiO_2 rods (0.01 g) with P3HT (0.01 g) or Ru-dye Z907 (0.005 g) and PTPA (0.01 g) dissolved in THF or chlorobenzene (1 mL) upon 5 min of ultrasound irradiation. Films were drop casted on the barrier layer and dried over night under ambient condition. On top of the active material in some cases a PEDOT:PSS layer was spin coated (2000 rpm, 60 s). Finally gold electrodes with 100 nm thickness were evaporated. Measurements were taken under ambient condition as well as in protecting atmosphere (after storage of the devices in a glove box for least 12 h).

3.4 MEASUREMENTS

3.4.1 CYCLOVOLTAMETRY - CV

All cyclovoltametry (CV) data were obtained using a three electrode cell in an electrolyte of 0.1 M tetrabutylammonium tetrafluoroborate in acetonitril, using ferrocene as the internal standard and Ag/Ag^+ as reference electrode. The CV scans were performed anodically, proceeding from 0 V to 2.0 V (10 mV/s). The reversible oxidation of the triphenylamine moiety occurred at 1.2 V (E_{ox}). As the potential gets reversed from 2.0 V to 0 V the corresponding reversible reduction occurred at 0.6 V.

3.4.2 SCANNING ELECTRON MICROSCOPY - SEM

In a scanning electron microscope (SEM) an electron beam is used to image a pattern or object by scanning the surface. The electron beam interacts with the surface and shows information about the topography but can also give a contrast between different materials. Scanning electron microscope images were obtained on a field emission SEM (LEO 1530 "Gemini") and FEI Nova 600 Nanolab Focused Ion Beam. The acceleration voltage was 1 - 2 kV.

3.4.3 TRANSMISSION ELECTRON MICROSCOPY - TEM

The transmission electron microscope (TEM) works similar to a usual light microscope however instead of light an electron beam is used to shine through the sample. A resolution smaller than 1 nm is obtained by this method. It is possible to resolve lattice specimen of a crystal with high resolution TEM (HRTEM). TEM measurements in the work presented were done with a Hitachi Model H-7600 and HRTEM with a FEI Tecnai F20.

3.4.4 *FOCUSED ION BEAM – FIB*

A focused ion beam (FIB) is used primarily to cut or polish surfaces and to apply materials like wolfram, platinum or silicon dioxide, but also to image a surface topography. A FEI Nova 600 Nanolab Focused Ion Beam was used to polish cross sections of solar cells and to cut through ZnO/polymer film with a gallium ion beam.

3.4.5 *SCANNING FORCE MICROSCOPY – SFM*

Scanning force microscopy (SFM) is used to image surfaces in a very high resolution by scanning topography with a very small tip in contact or tapping mode. Images can be analyzed for surface roughness, height profiles and phase contrast. PEO-*b*-PTPA films were recorded in tapping mode at room temperature (RT) at Veeco MultiMode Scanning Probe Microscopy with an OMCLAC 240 TS (RF 70 kHz) and OMCLAC 160 TS-W2 tip. The offset and tilt background of all images were removed by processing all images with a first order flattening procedure with the Nanoscope V5.31r1 Software. The offset and tilt background of all images were removed by processing them with a first order flattening procedure.

It is possible to gain information of the sample conductivity with conductive scanning force microscopy (C-SFM) while recording the surface topography. The measurement is accomplished in contact mode while the current induced between the metal coated scanning tip and a conductive sample is monitored with constant bias. Cross sections of solar cell devices were accomplished by MFP3D with ORCA current amplifier, Asylum Research.

3.4.6 *SPECTROSCOPIC MESUREMENTS - UV-VIS*

UV-VIS measurements where conducted on a PERKIN ELMAR Lambda 900 UV/VIS/NIR Spectrometer.

3.4.7 *X-RAY DIFFRACTION – XRD*

Θ-Θ measurements were conducted on Siemens D500 diffractometer equipped with a Cu anode generated at a current of 30 mA and a voltage of 30 kV. Scans were taken in a 2θ range from 10° to 40° or 80° with a step size of 0.05° or 0.1° and integration time of 30.0s.

3.4.8 *GISAXS*

Grazing Incidence Small Angle X-Ray Scattering (GISAXS) measurements were conducted in Hamburg at DESY at the beamline BW4. Si-wafers were mounted in a sample-detector distance of about 2.0 m. Measurements were conducted with a beam wavelength of $\lambda = 0.138$ nm and a beam size of 0.017 mm.

3.4.9 *X-RAY REFLECTIVITY*

With x-ray reflectivity film thicknesses can be obtained by the study of the electron density gradient perpendicular to the film interface. The principle of x-ray reflectivity is based on the interaction between x-ray and matters on the surface and inside the film while x-ray penetrates the film. X-ray reflectivity experiment was conducted using a surface XRD-TT3003 diffractometer equipped with Göbel mirror and a Cu-anode. The modelling of the experimental profiles was conducted using the Parratt 32 software, version 1.5, provided by the Berlin Neutron Scattering Centre at the Hahn-Meitner-Institute.

3.4.10 SOLAR CELL DEVICE MEASUREMENT SETUP

All solar cell devices were measured in the set up seen in Figure 15, left. A 1.5 AM filter was put in the optical path of the solar simulator (Figure 15, left 1). 1.5 AM filter simulates the air mass of the solar irradiance with the sun 45° above the horizon that represents the absorption loss of the solar spectrum in northern Europe, resulting in about 100 mW/cm^2 of light energy.[124] The intensity of the solar simulator was calibrated to 1 sun (100mW/cm^2) with a standard Si-cell (ISE Freiburg) and was changed by the aperture of the light source and the distance between device and light source. The sample holder allowed measurements under ambient and protecting air conditions due to the vacuum chamber (Figure 15, left, 2). With the I-V supply unit voltages from -1.5 to 0.3 V were impressed on the device in the dark and under illumination and the according amperage was measured. This was done for each pixel 1 to 6 seen in Figure 15, right. For better contact, silver paste was applied on the gold pixels as well as on the FTO electrode. The active area of each pixel was measured with an optical microscope. The active area is limited by the etched FTO part and the gold pixel itself (Figure 15 – red box). Interpretation of the obtained I-V data were accomplished with a python program (see appendix, “solarfrickler”).

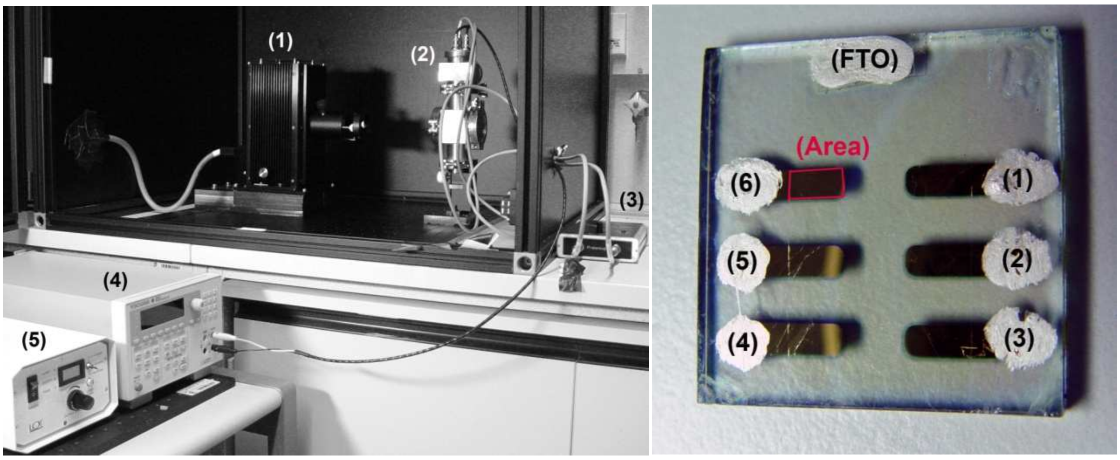

Figure 15: Solar cell device measurement setup. (1) Solar simulator with 1.5 AM filter, (2) device holder in vacuum chamber, (3) switchbox for pixel choice, (4) I-V supply unit, (5) solar simulator transformer (left). Pixel to be measured (1-6), FTO electrode and area used in calculation (red square) (right).

4 RESULTS AND DISCUSSION

Hybrid materials for optoelectronic application were nanostructured via a new functional block copolymer PEO-*b*-PTPA introduced in chapter 4.1. The hybrid material was obtained in a one-pot synthesis combining sol-gel chemistry and block copolymer templating (chapter 4.2.1). It could be shown that PEO-*b*-PTPA forms various morphologies in combination with different TiO_2 (chapters 4.2.2 and 4.2.3) and ZnO precursors (chapter 4.2.4).

The introduced hybrid materials were tested in solar cell application (chapter 4.3). In the first section (4.3.1) a convenient blend approach is used, comparing the hole conducting polymers PTPA and P3HT to find the advantages and disadvantages of using PTPA and P3HT in hybrid solar cells. But also to investigate the influence of device preparation as well as measurement conditions on the device performance for different hybrid blends. Further on an improvement of the solar cell efficiency was obtained by the development of a functional template system introduced in chapter 4.3.2. Different metal oxide/PEO-*b*-PTPA systems are presented.

4.1 SYNTHESIS AND CHARACTERIZATION OF PEO-*B*-PTPA

The novel amphiphilic block copolymer poly(ethyleneoxide)-*b*-poly(triphenylamine) (PEO-PTPA) was synthesized via the following procedure: PEO **2** with one hydroxyl endgroup was obtained via anionic polymerization and the PTPA block by radical polymerization. The acidchloride of the RAFT-starter 3-benzyl-sulfanylthiocarbonylsufanylpropionicacidchloride (BSPAC) **1** [125] as well as the triphenylamine monomer[117] was synthesiszed according to literature.

In a first step an acidchloride of the RAFT starter was added to dry poly(ethyleneoxide) (PEO) to form a macroinitiator **3** (Scheme 1).

In a second step triphenylamine (TPA) was polymerized using the RAFT technique and the functionalized PEO as the chain transfer agent (Scheme 2).

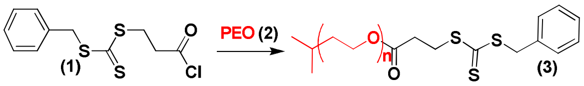

Scheme 1: Synthesis of Macro-RAFT-agent.

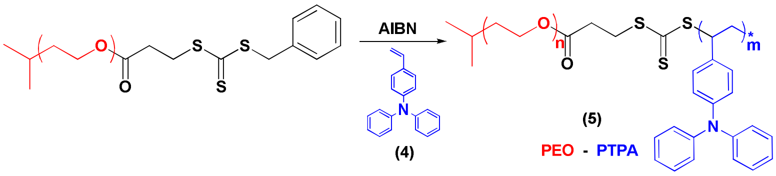

Scheme 2: RAFT polymerisation of PTPA with Macro-RAFT-agent.

Upon termination a block copolymer of PEO-b- PTPA **5** was obtained. Results are shown in Table 6. TGA measurements for P1 resulted in a decomposition temperature of about 400 °C. Therefore the block copolymer is definitely stable around 200 °C and annealing or gentle heating procedures should not be a problem.

Sample	M_n PEO* / g/mol	M_n PTPA** / g/mol	T_g*** / °C	Dispersity*
P1	6 000	10 000	52	1.8
P2	5 000	5 000	56	1.9

Table 6: Characterization of PEO-*b*-PTPA. *measured by GPC, ** measured by NMR, ***measured by DSC

PEO-*b*-PTPA **5** was investigated by SEM, TEM and CV. The block copolymer (P1) was dissolved in THF to drop coat a film and put on a carbon coated TEM grid. The polymer showed phase separation of the blocks (Figure 16). The electron density of the three phenyl rings in the PTPA block is high enough to give a good contrast in electron transmission (dark regions) compared to PEO (light regions). The size of the domains of about 100 nm is common for the phase separated morphologies of block copolymers[126]. Results could be confirmed with AFM data (Figure 17). A very rough film is formed when spin coated from a THF solution seen in the height image (Figure 17, left), but the phase image clearly shows a phase contrast between the blocks (Figure 17, right). While in a DMF/HNO_3/isopropanol mixture a micellar structure was obtained showing the successful synthesis of an amphiphilic block copolymer (Figure 16, right picture).

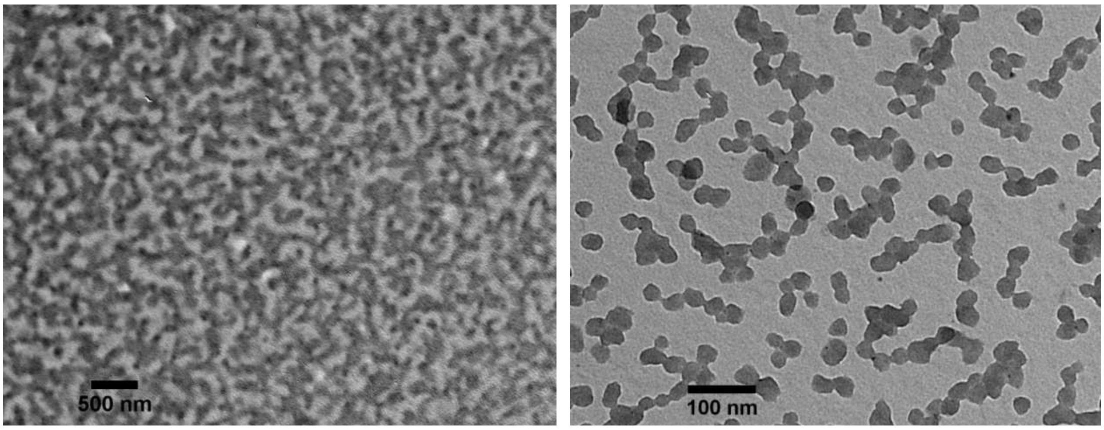

Figure 16: TEM pictures of block copolymer (P1) film dip coated from THF (left) and dip coated from HNO_3/DMF/isopropanol (right).

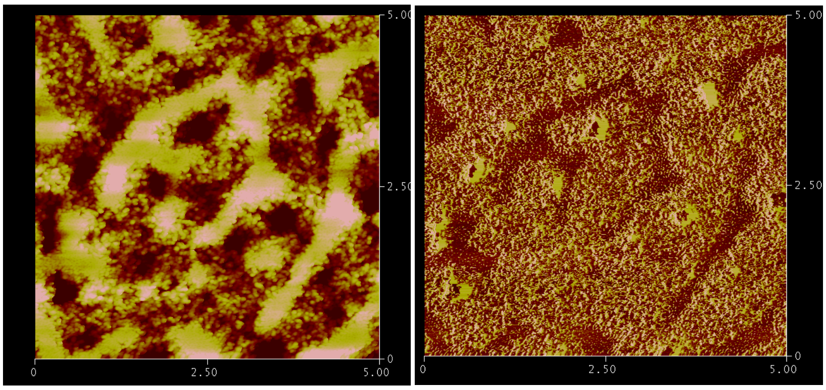

Figure 17: AFM picture taken of a spin coated polymer (P1) sample from THF. Image sizes are 5 X 5 μm^2; height image contrast from 0 – 300 nm with a scan rate of 0.7 Hz (left); phase image with a phase contrast from 0 – 100° (right).

Varying the water amount in a PEO-*b*-PTPA/DMF mixture changed the micellar structure (Figure 18). At low water concentration small micelles were formed. Increasing the amount of water the micelles increased in size from 40 nm (1 wt % of water, Figure 18 (a)) to about 200 nm (30 wt % of water, Figure 18 (e)). With 50 wt % of water the spheres collapsed to form wormlike micelles (Figure 18 (f)). For a random copolymer DNQMA-HMEA (2-diazo-1,2-naphtoquninone – hydroxyl ethyl metacrylate) in water/DMF *Tian* et. al.[127] found similar morphological transitions from spherical micelles (<20 wt% water), through wormlike micelles (60 wt% water) to large vesicles (100 wt% water).

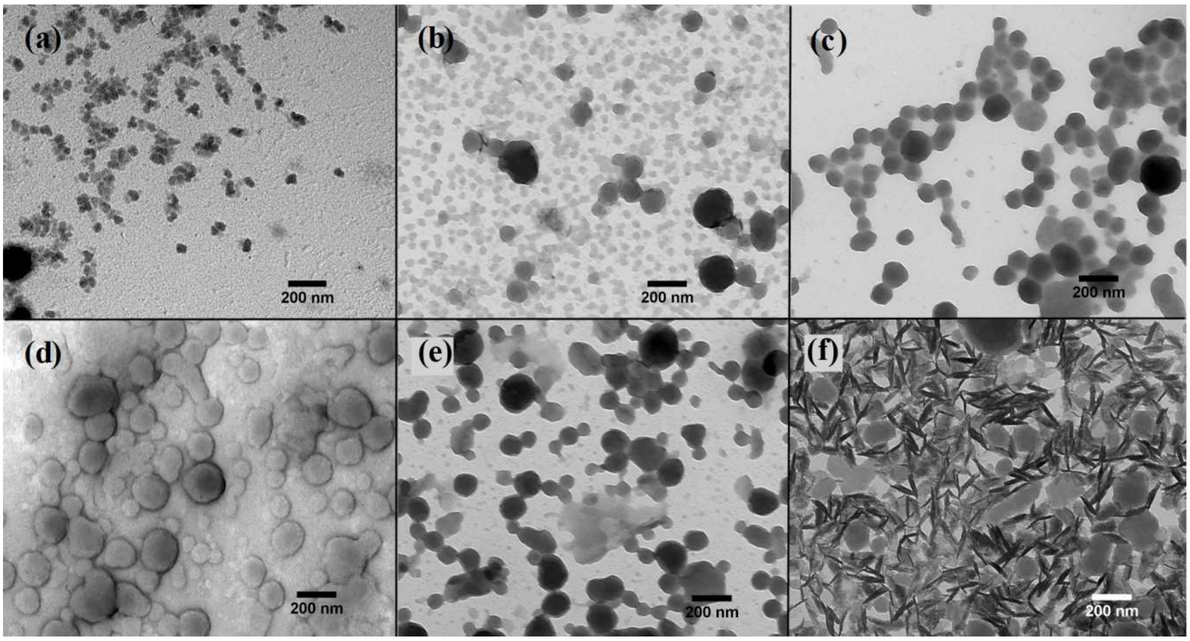

Figure 18: TEM pictures of PEO-*b*-PTPA (P1) in DMF with different amounts of water. 1 wt % (a) 2 wt % (b) 4 wt % (c) 10 wt % (d) 30 wt % (e) 50 wt % (f).

PTPA is a conjugated p-type polymer, which shows high hole-transport mobility.[128] CV measurements show that the prepared PEO-*b*-PTPA has a similar redox behaviour (Figure 19).

The HOMO level was calculated using the empirical formula $E_{HOMO} = -e(E_{ox} + 4.4)$ eV to be -5.6 eV[129, 130], which is in agreement with characteristic values of polymeric triphenylamine moieties.[131] Thus the block copolymer can be used as an amphiphilic hole conducting material.

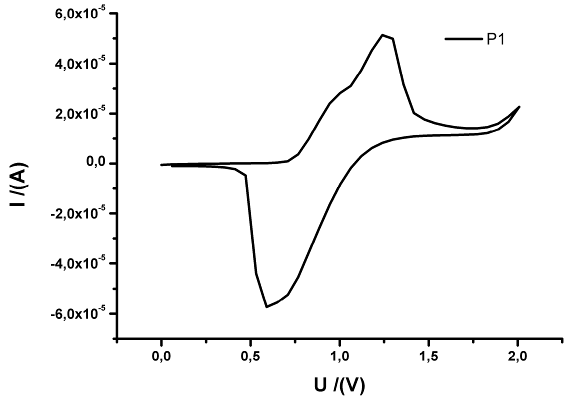

Figure 19: CV measurement of PEO-*b*-PTPA.

4.2 MORPHOLOGY CREATION OF HYBRID SYSTEMS

The hybrid material described in the following consists of the previously introduced hole conducting block copolymer and an electron conducting nanostructured metaloxide. The metaloxide phase is incorporated into the block copolymer PEO-*b*-PTPA due to the preference of the sol-gel precursor to coordinate onto the PEO-block. The tendency of PEO to penetrate into the metal oxide phase was investigated previously by Cheng et al. with a PEO-*b*-PS block copolymer acting as a template agent for TiO_2.[132] PEO-*b*-PTPA in combination with TTiP (4.2.2) and EGMT (4.2.3) as TiO_2 precursors and $Zn(OAc)_2$ (4.2.4) as ZnO precursor are forming a variety of solid bulk morphologies that were investigated in a convenient one pot synthesis (Scheme 3).

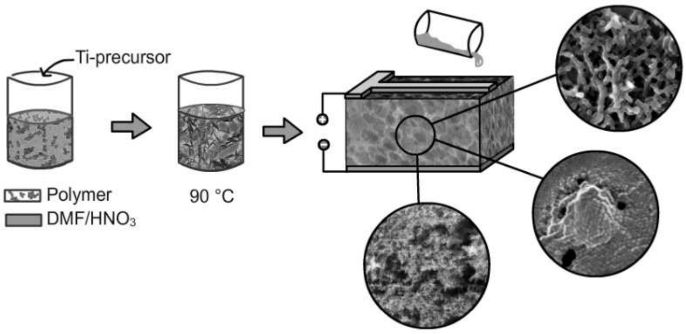

Scheme 3: One-pot synthesis of solid state DSSCs.

Upon the amphiphilicity of PEO-*b*-PTPA in the discussed DMF/acid mixture, a micellar system is formed since the acid phase is a poor solvent for the PTPA block but a good solvent for the PEO block. In combination with a TiO_2 precursor a sol-gel is formed that follows the nanostructure of the block copolymer because of the preferred migration of the Ti phase into the PEO phase. With the intent to crystallize the metal oxide phase without destroying the polymer the mixture was heated to 90 °C. To prove the amount of crystallinity in the hybrid films turned out to be difficult. More investigations had therefore been done using a dummy polymer PEO-*b*-PS, following the same one-pot approach in combination with EGMT and TTiP (following chapter).

4.2.1 THERMAL CRYSTALLIZATION OF TIO_2 FROM SOL-GEL SYSTEMS

Titanium dioxide is known to be applicable in hybrid solar cells, especially successful shown in DSSCs. While TiO_2 appears naturally in three different crystal structures, namely brookite, rutile and anatase, the latter is proposed to be most beneficial for solar cell application. The difference in photovoltaic performance was found in slower electron transport in the rutile phase as well as in the distinction to absorb the dye, owing to a smaller surface area per unit volume of rutile in comparison towards anatase.[133]

Anatase, rutile and brookite consist of $[TiO_6]^{2-}$ octahedra, where titanium is surrounded by 6 oktahedral oxygens. In case of anatase the octahedra are face shared while in rutile they are edge shared as seen in Figure 20. Shared edges and even more shared faces reduce the stability of the ionic crystal. -In face shared octahedra the center cations are closer to each other and therefore anatase is less stable than rutile, due to repulsive forces.[134]

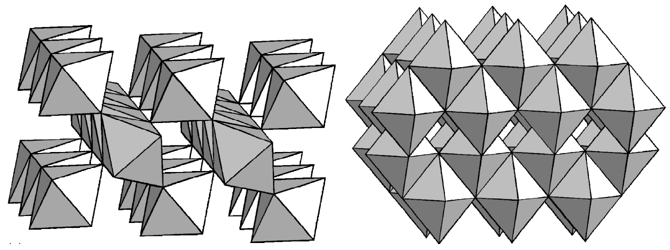

Figure 20: Arrangement of octahedra in rutile (left) and anatase (right).[73]

Most methods which are published to obtain rutile or anatase crystal structures out of diverse precursor systems mostly include corrosive chemicals and/or high temperatures. In this work a method had to be found to obtain anatase TiO_2 nanostructures without destroying the functional organic template. There had been recently publications on hydrothermal,[135, 136] sol-gel[73] and/or sonochemical[104, 137] processing avoiding the sintering step. The formation of either rutile or anatase and the shape of these crystals can be controlled by e.g. temperature (rutile at $T < 60$ °C and anatase at $T > 70$ °C),[138] anions (e.g. NO_3^-, Cl^-, OH^-, SO_4^-),[139] pH[140] and surfactants.[141]

Yin et al.[135] described the formation of single TiO_6 octahedra upon acid influence on the hydrated, condensed octahedral eliminating water molecules as seen in Figure 21. Therefore the nucleation of anatase is enhanced by chloride ions, but on the same hand the crystallization process is slowed down by repulsion of the charged octahedra. Further they described a preparation to obtain a broader size distribution of the crystallite in the presence of amorphous TiO_2 while using nitric acid. They proposed that the nictric acid is able to slow down the nucleation process due to the poorer nucleophilicity of the nitrate anion towards the titanium compared to chloride anion.

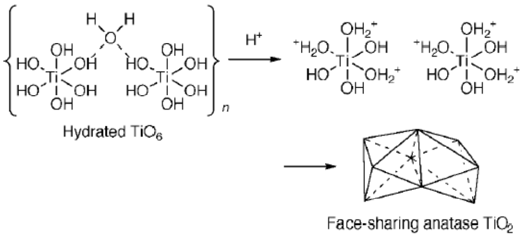

Figure 21: Nucleation process of anatase TiO_2.[135]

Cozzoli et al. discribed a modified sol-gel method to slow down the hydrolysis rate of TTiP in water by using a surfactant.[141] They also claimed the influence of the surfactant on the shape of the resulting crystalline particles.

Therefore PEO-*b*-PS (6 000 - 19 000 g/mol) is used as a kind of surfactant and template in Ti-precursor sol-gel systems. The PEO part might be able to exchange most of the –OR groups from the TTiP or EGMT precursor to form a chelated Ti-O-Ti network surrounded by polymer. In the prepared acid/DMF mixtures the amphiphilic block copolymer induces a micellar system. For small amounts of precursor and acid most likely an amorphous Ti-O-Ti core consisting of TiO_6 oktahedra and a polymer shell is formed. For higher amount of precursor and acid the core consists of polymer micelles that are decorated with a Ti–O-Ti network of TiO_6 oktahedra. In Figure 22 (a) a SEM picture of TiO_2/PEO-*b*-PS film prepared from TTiP/HNO_3/DMF mixtures is shown. A sphere like morphology [M179] is created whereby polymeric spheres are decorated by a TiO_2 phase. The calcined sample Figure 22 (b) shows a porous TiO_2 network that remained after removal of the spherical polymer micelles. A similar morphology [M180] was found for the TiO_2/PEO-*b*-PS film prepared from EGMT/HCl/DMF mixture as seen in Figure 22 (c). But the calcined sample (Figure 22, (d)) of this morphology [M180] does not reveal a TiO_2 structure as porous as that of the TTiP precursor morphology [M179].

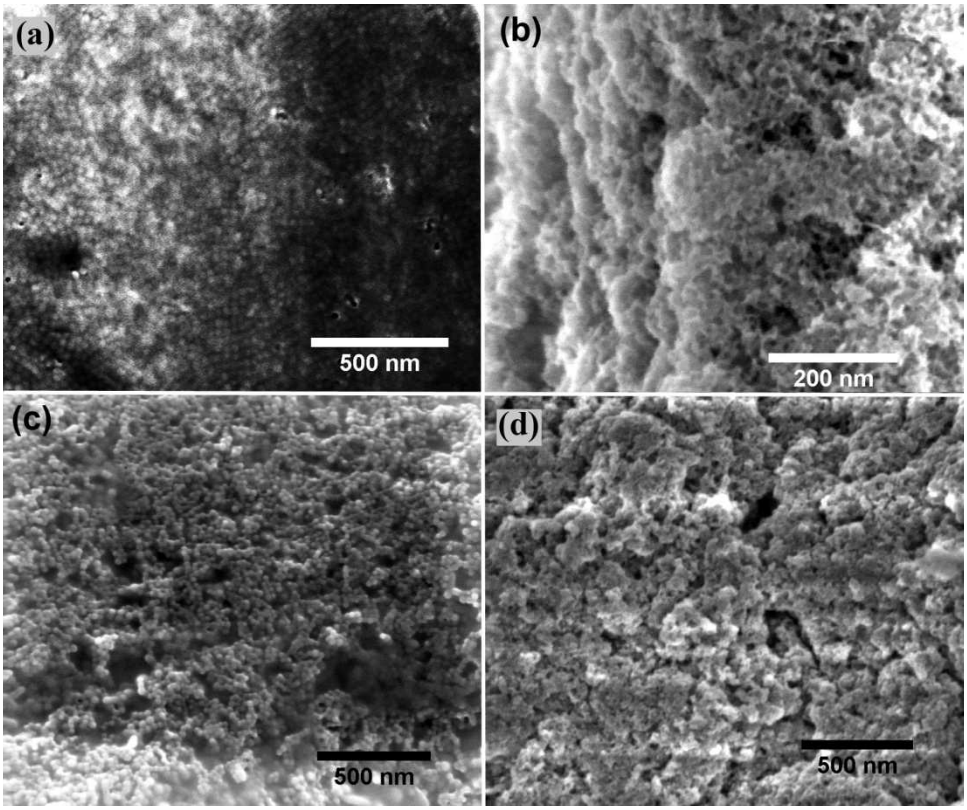

Figure 22: SEM picture of PS-*b*-PEO morphologies prepared of 0.01 g PS-*b*-PEO, 1 g DMF, 0.078 g HNO_3, 0.0125 g TTiP [M179] (a, b); 0.01 g PS-*b*-PEO, 1 g DMF, 0.4 g HCl, 0.02 g EGMT [M180] (c, d). Drop coated films on Si-wafer (a, c) after calcination, 450 °C for 2 h (b, d).

To obtain the nanostructured morphologies [M179] and [M180] the precursor, acid and block copolymer, dissolved in DMF was mixed together and heated to 90 °C.

In Figure 23 XRD patterns of PS-*b*-PEO films prepared from different emulsions and sol-gel systems firstly indicate that the block copolymer itself shows a crystal structure when processed from DMF/acid mixtures (black curves). The XRD pattern of the hybrid film prepared from EGMT/HCl/DMF/PS-*b*-PEO mixtures leading to the sphere like morphology [M180] (Figure 23, left, red curve) corresponds with the first two peaks of the XRD pattern from the pure polymer (HCl/DMF/PS-*b*-PEO) mixture (Figure 23, left, black curve). But the higher order deflections of the polymer pattern are vanished for the hybrid film. The same is found for the TTiP/HNO_3/DMF/PS-*b*-PEO mixture (Figure 23, right, red curve) compared to the pure polymer film (HNO_3/DMF/PS-*b*-PEO) (Figure 23, right, black curve).

Secondly an influence of the processing on the crystal structure of PS-*b*-PEO films is visible. PS-*b*-PEO seems to crystallize in different modifications when processed from different acids.

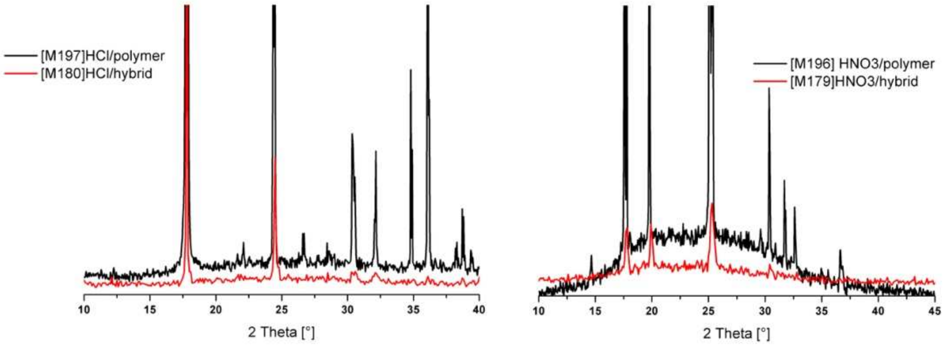

Figure 23: XRD pattern of polymer and hybrid films drop casted after heating to 90 °C for 15 min. Prepared from HCl/DMF/polymer and HCl/EGMT/DMF/polymer mixtures (left) as well as from HNO_3/DMF/polymer and HNO_3/TTiP/DMF/polymer mixtures (right).

Nevertheless no diffraction pattern corresponding to an anatase or rutile phase of TiO_2 could be observed. The peaks only correspond to the crystal structure of the block copolymer. In Figure 24 hybrid films of EGMT and TTiP systems processed from PEO-*b*-PTPA/acid mixtures are compared after different heating processes. It is shown that a longer heating process does not improve/influence the crystallinity of the hybrid films.

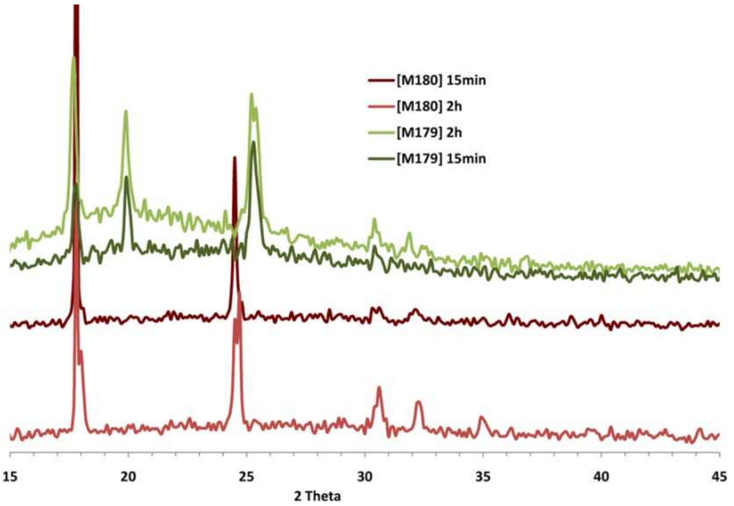

Figure 24: XRD patterns of films drop coated from EGMT/HCl/DMF/PS-*b*-PEO mixtures [M180] and TTiP HNO_3/DMF/PS-*b*-PEO mixtures [M179] after heating to 90 °C for 15 and 120 min.

For samples prepared from TTiP/polymer/HNO_3 mixtures HR-TEM crystals of about 3 nm were found (chapter 4.2.2). The peak broadening (Δ2Θ) at full width half maximum of the diffraction pattern can be correlated with the size of the crystals by the Scherrer equation:

$$\frac{K*\lambda}{B*\cos\theta} = \Delta 2\theta \qquad \text{Eqn. 5}$$

With the particle size (B), the shape factor K (with the typical value of 0.9), the x-ray wavelength λ (0.154 nm) and the Bragg angle Θ. For an average particles size of about 3 nm a peak broadening of 2.7 ° was calculated. Consequently the peaks should be resolved well. However, in the HR-TEM picture (Figure 26) few, spherical crystals are seen that indicate a deformation of the crystal lattice in the shell region of the particles. Since there are no pattern found that corresponds to an anatase lattice, the amount of crystallinity might be too low to be detected by the x-ray diffraction.

4.2.2 HYBRID MORPHOLOGIES BASED ON TI-ORTHO-ISO-PROPOXIDE

To obtain crystalline TiO_2 nanoparticles in a polymer matrix a synthetic route had to be established in order to crystallize the titanium dioxide at moderate conditions in order to prevent the polymer from damage. According to *Gopal* et al.[73] TTiP crystallizes if put into HNO_3/isopropanol/H_2O and heated to 90 °C (5 °C/min). In this work a modified procedure was designed by adding a templating polymer. The block copolymer P1 (PEO-*b*-PTPA) was dissolved in DMF/isopropanol before adding HNO_3 and the precursor TTiP (Scheme 4). The resulting mixture was put into an ultrasonic bath for 10 min until a homogenous gel was produced. Upon heating to 90 °C the resulting TiO_2 phase in the polymer matrix became crystalline. After heating the mixture, films were drop casted. Upon solvent evaporation the morphology of the TiO_2 phase in the dry film is determined by the lyotropic phase of the block copolymer.

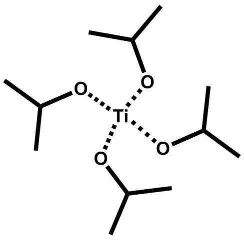

Scheme 4: Ti-ortho-iso-propoxide (TTiP)

Before adding the precursor the block copolymer is forming micelles in a DMF/isopropanol/HNO_3 mixture about 30 nm in diameter (Figure 16 (right)). After the precursor addition the TTiP precursor diffuses into the hydrophilic PEO domain of the micelles. Since the titania precursor binds selectively through hydrogen bonding to the PEO block[142] a spatial localization of Ti-O-Ti condensation takes place. For appropriate amounts of precursor, a TiO_2 wire morphology is created at 90 °C. The diameter of the wires doubled compared to the diameter of the micelle formed by the pure copolymer, indicating swelling of the micelles by the TTiP precursor (Figure 25).

In Figure 25 TEM images of the wires before and after staining with RuO_4 is shown. RuO_4 is commonly used for labelling the phenyl rings in block copolymers at a nanometer scale[143]. Before staining only the metal oxide phase is visible due to its high electron density. After staining with RuO_4 a PTPA polymer shell around all rods can be seen with good contrast. This is a direct prove that the PTPA block creates a shell surrounding the TiO_2/PEO core.

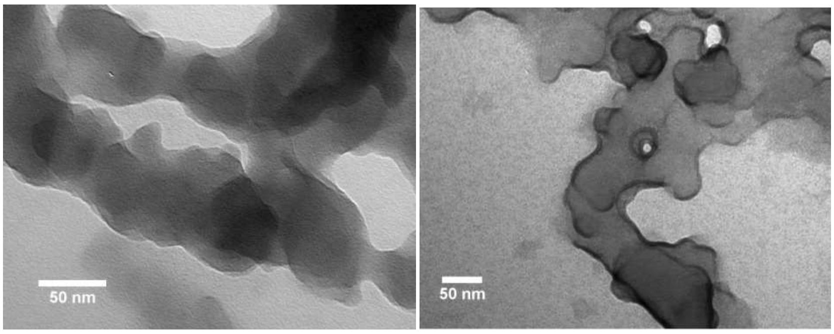

Figure 25: TEM picture of block copolymer with TiO_2 in wire domains [M102]. Without staining (left), with RuO_4 staining (right).

With HR-TEM measurements the lattice structure of the TiO_2 can be observed (Figure 26). Since the examined film was dip coated from the pure suspension the particle concentration was very high and a multilayer film was created. Therefore only crystalline particles are visible but no clear morphology of particle aggregates is observed. While the observed wire like morphology is interesting for further application, due to the presence of a clear charge percolation pathway, it is not the only morphology obtained.

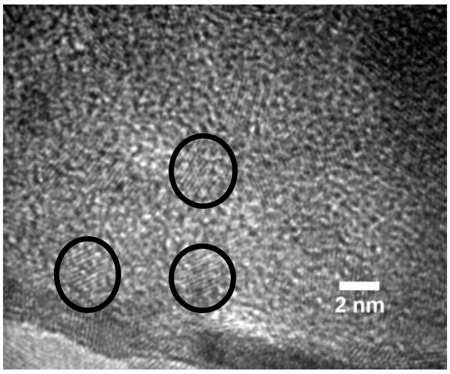

Figure 26: HR-TEM picture of the wire-morphology. Some crystalline domains are highlighted.

Further morphologies created by block copolymer P1 and TiO_2 were investigated by SEM and TEM. In Figure 27 the resulting mapped phase diagram is indicating the presence of a total of 5 phases with different morphologies. These morphologies are analogue to the structures found within the PS-*b*-PEO/TiO_2 system that were investigated previously by *Cheng* et al..[144]

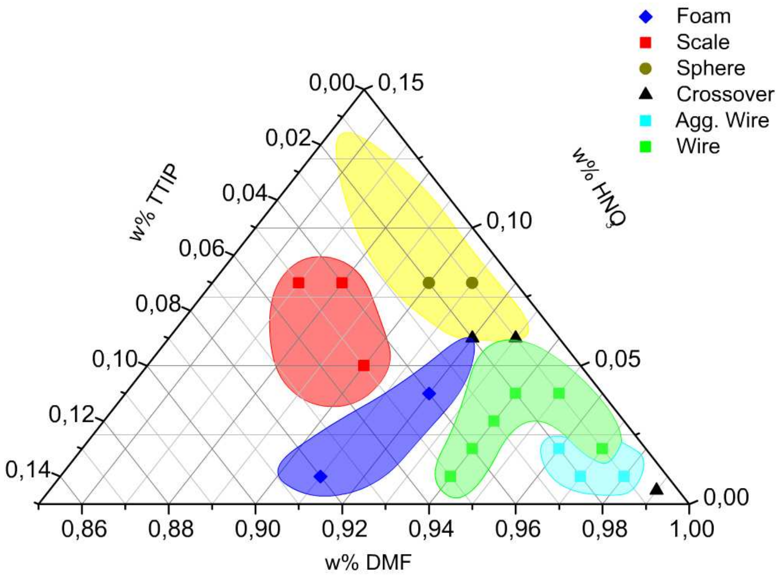

Figure 27: Phase diagram of the different morphologies created by different weight ratios of precursor, solvent and acid.

Images of the different morphologies are shown in Figure 28. Increasing the amount of TTiP the micelles seem to collapse, spheres flattened and scales were formed (Figure 28 (b)). Raising the amount of the precursor TTiP to about 0.08 wt% the micelles were completely destroyed and a large scale pore network of titanium oxide was obtained which resembled a foam (Figure 28 (a)). A further decrease of the acid concentration and increase of solvent amount revealed the previously shown wire like morphology (Figure 28 (c)). With lower amounts of acid, but high amounts of solvent the wires seem to aggregate into spheres (Figure 28 (d)).

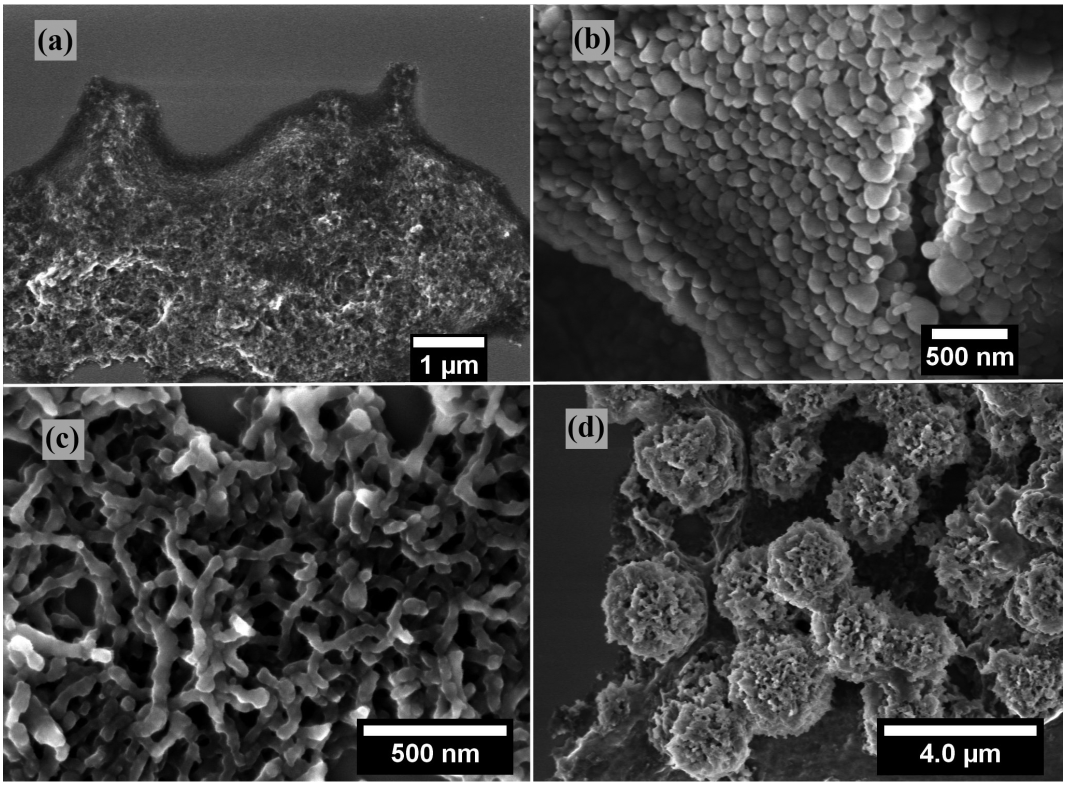

Figure 28: Picture of different morphologies: foam [M83] (a), scales [M91] (b), wires [M102] (c), aggregated wires [M97] (d).

The SEM pictures (Figure 29) of the calcined samples selectively show the structure of the embedded titanium dioxide skeleton. Depending on the overal morphology titania frameworks with a varying degree of porosity were found. With a high amount of metal oxide a very porous network of fine TiO_2 needles is found resulting in a foam like structure (Figure 29 left). The original morphology before calcination corresponded to a foam like structure similar to that in Figure 28 (a). In contrast to the foam like structure a very densely packed TiO_2 skeleton is found (Figure 29 right) for the initial scale like structure (Figure 28 (b)).

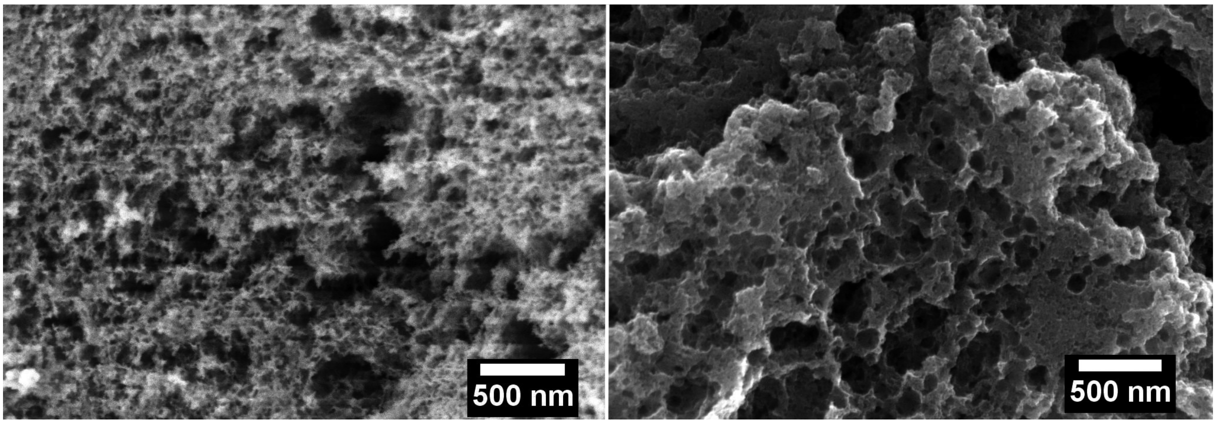

Figure 29: Calcined at 450 °C for 4h. Foam like structure [M83] (left) and scale like structure [M91] (right).

With a high concentration of acid (0.08 wt %) and a low concentration of the titanium precursor (0.01 wt %) monodisperse spheres around 50 nm diameter were created (Figure 30 left). To investigate the pure TiO_2 morphology the templating block copolymer was removed by calcinating the film (Figure 30 right). Calcination proved that the sphere like morphology consists of PTPA spheres surrounded by a TiO_2 skeleton. Investigating a fracture surface of the film, it is easily seen that the PTPA spheres are homogeneously distributed through the whole film. On the surface of the spheres the TiO_2 forms a sponge like network enabling charge percolation. Furthermore it can be seen in higher resolution SEM images (Figure 31) that the TiO_2 phase consists of small grains that form the porous skeleton. Closer inspection of the titania network (Figure 31) shows that the polymer spheres also interconnect, what creates a second percolating network.

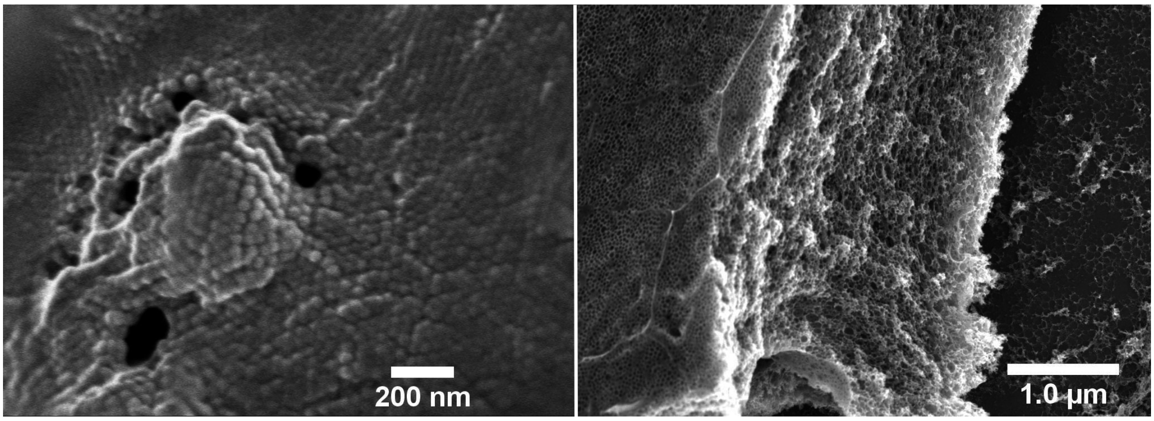

Figure 30: SEM pictures of a film creating a sphere like morphology [M84]. Before calcinations (left) and after calcination (right).

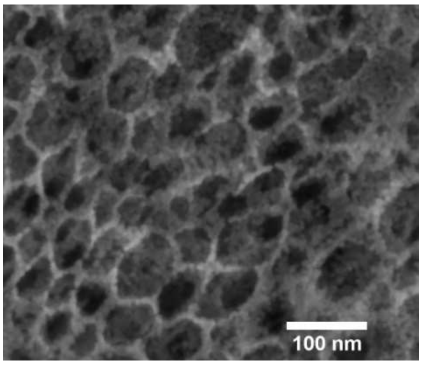

Figure 31: SEM picture of a closer view of morphology [M84] after removing the polymer by calcination.

For a small amount of TTiP and HNO_3 a wire morphology could be observed and smaller weight percentages than 0.05 of HNO_3 lead to aggregated wire structures. With a large amount of water the micelles were swelling in an uncontrolled way and diameters of several hundred nanometers were found (Figure 32 (a)). At a lower amount of about 0.08 wt % acid the micelles became monodisperse with an average size of 50 nm (Figure 32 (b)). With a further decrease of the water content, the micelles stick together, to form wormlike micelles (Figure 32 (c)) indicating a crossover that finally leads to the wire structure (Figure 32 (d)).

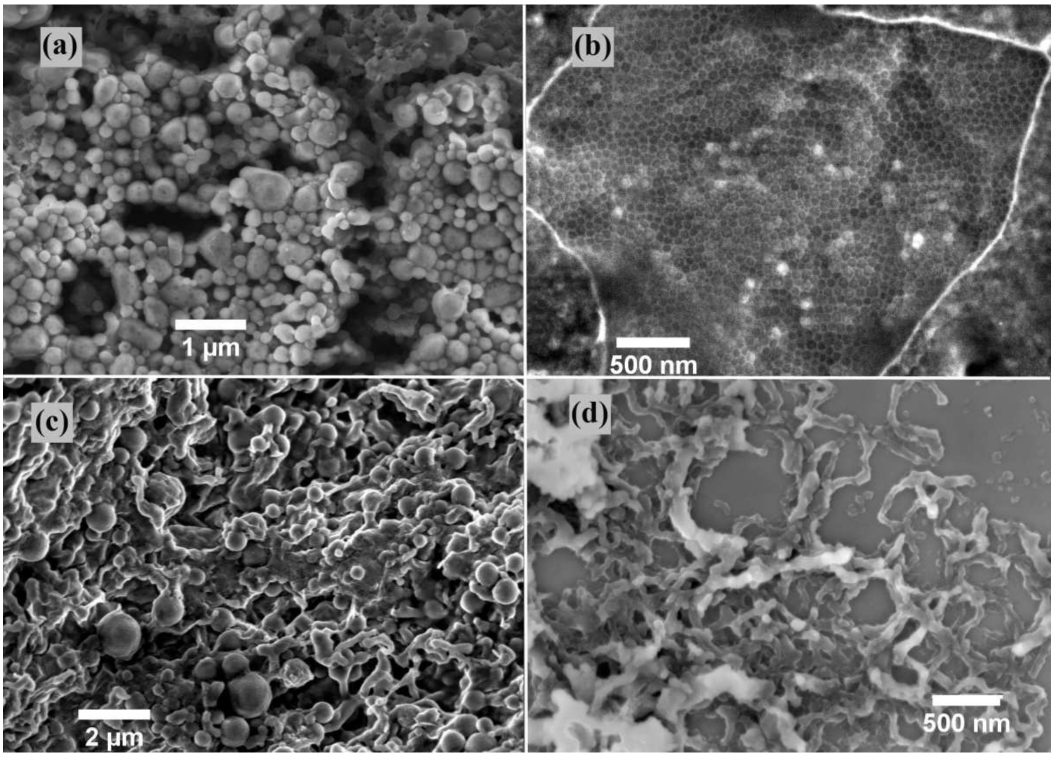

Figure 32: SEM pictures showing morphologies due to a decreasing amount of HNO_3, TTiP is fixed to 0.01 wt %. (a) 0.2 wt % HNO_3 [M90], (b) 0.08 wt % HNO_3 [M84], (c) 0.06 wt % HNO_3 [M105], (d) 0.04 wt % HNO_3 [M102].

4.2.3 *MORPHOLOGY CREATION BASED ON ETHYLENEGLYCOLE MODIFIED TITANATE*

To overcome the problem of TiO_2 to become crystalline without destroying the functional templating block copolymer, the method described previously was used (4.2.2) to obtain hybrid nano structures in combination with an alternative precursor EGMT (Scheme 5) that is already crystalline and has been processed in combination with amphiphiles.[120] PEO-*b*-PTPA is an amphiphile that structure directs the hybrid material in a sol-gel process and functions as a hole conductor in the solar cell device later on.

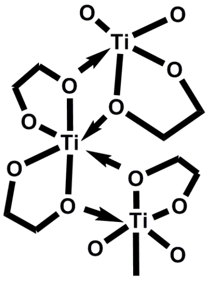

Scheme 5: Ethylene glycol-modified titanate (EGMT).

As described for the TTiP precursor in the previous chapter different morphologies can be obtained in a controlled fashion, by varying PEO-*b*-PTPA (5 000 – 5 000 g/mol, pd = 1.9, P2) , EGMT, DMF and HCl in an one-pot synthesis and heating it to 90 °C for 15 min. With a 1:1 ratio of precursor and polymer a platelet structure [M156] was obtained (Figure 33, c, d). The formation of platelet structures is not uncommon for PEO block copolymers in organic solvents. *Lin* et al. characterized these morphologies obtained from PEO-*b*-PS polymers with X-Ray techniques.[145] They found the PEO block to crystallize in the middle of the plates with hairy PS rods surrounding the outside. Structures left over after removal of the polymer in the investigated sample (Figure 33 (d)), show clotted TiO_2 platelets. The fact that still layered structures are found in the calcined sample leads to the assumption that the TiO_2 precursor is located in between the polymer lamellae. With a smaller amount of HCl (Figure 33 (a), (b)) the PEO/titanate phase is less swollen and the platelet structure is reduced to a flake like structure [M157], seen in the calcined sample (Figure 33, (b)).

With the variation of the precursor, solvent and acid concentration a transition towards spherical micellar systems are obtained heading towards foamy sol-gel hybrid nanostructures of TiO_2 and polymer.

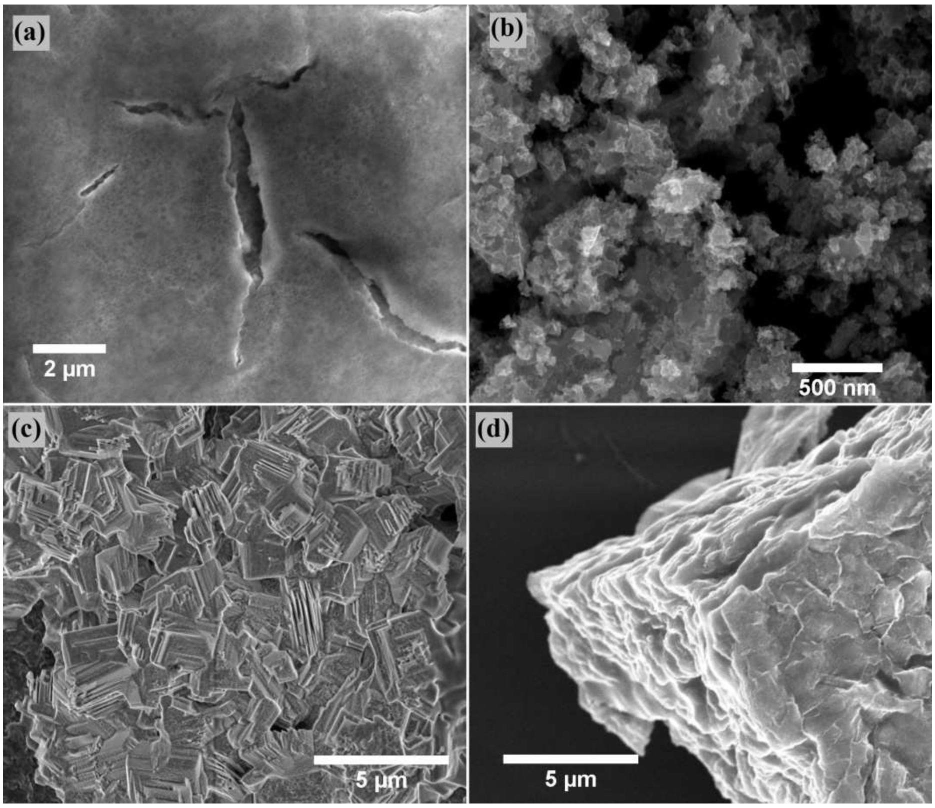

Figure 33: SEM picture of (a) flake like morphology [M157] and (b) after calcination; (c) platelet morphology [M156] and (d) after calcination.

In the solar cell devices reported in this work, foam and sphere like morphologies (Figure 34) were used with a Ruthenium-dye as absorbing material. Since sphere and foam like structures are able to form percolated systems. With small amounts of precursor and acid a very fine TiO_2 foam like structure is formed with densely packed particles of about 10 to 20 nm that are surrounded by a polymeric film [M190] (Figure 34 (a), (b)). With an increasing amount of acid the EGMT-precursor phase can swell more and finally gets less dense and becomes foamier [M175] (Figure 34 (e), (f)). But with an increase of titanate, polymer spheres are created that are decorated by an TiO_2 phase [M172] (Figure 34 (c), (d)).

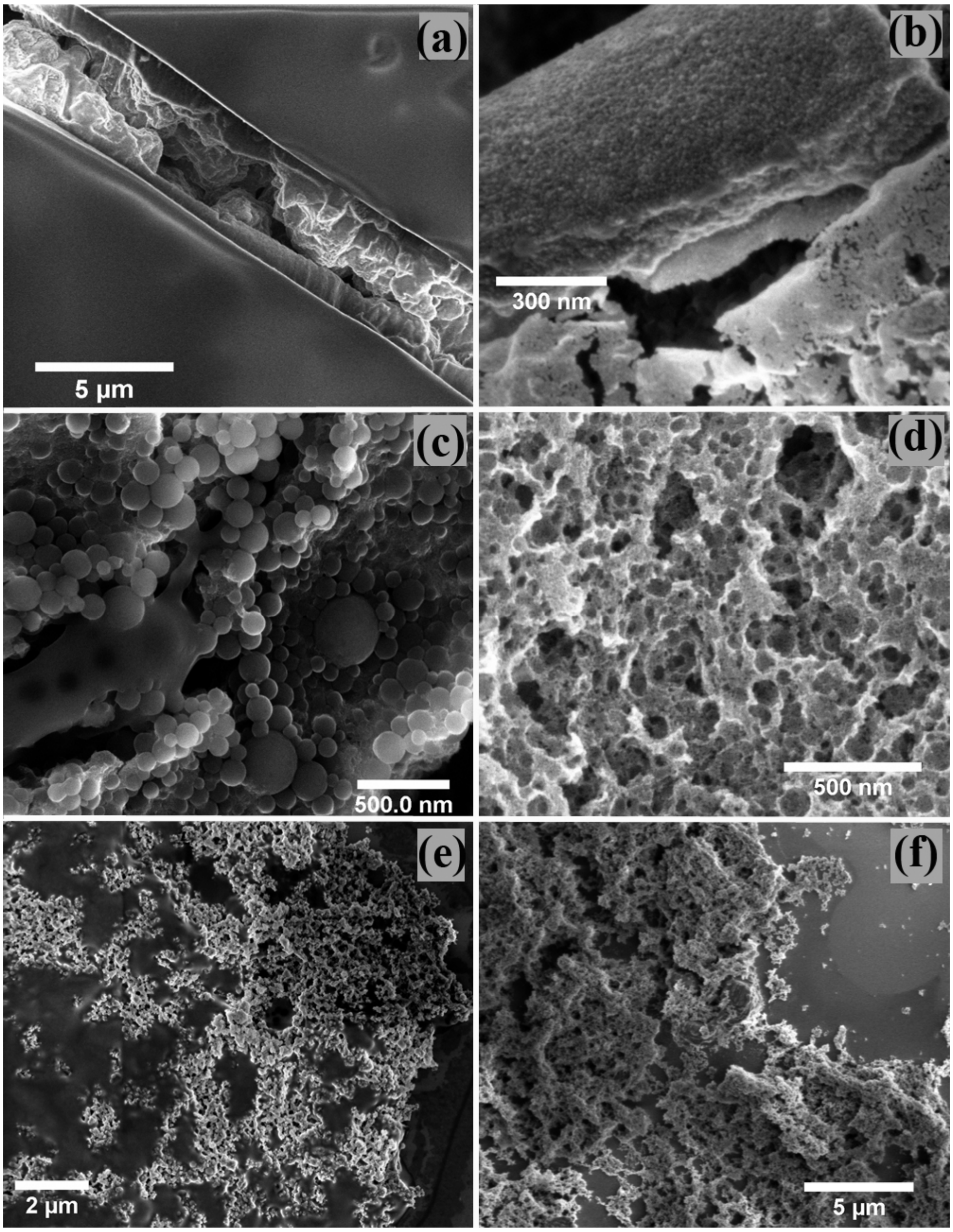

Figure 34: SEM pictures of different morphologies. The active material as prepared (left side (a), (c), (e)) and the remaining TiO_2 structures after burning away the polymer (right side (b), (d), (f)). (a) [M190] before (b) and after calcination; (c) before [M172] (d) and after calcination; (e) before [M175] (f) after calcination.

To show that the structures are extended over the whole sample GISAXS measurements were done on films of sphere [M155] and platelet [M157] morphologies. Information about the lateral structure of the hybrid material was taken from an out-of-plane (OOP) scan along the q_{II} plane at the Yoneda peak's maximum as seen in the graphs (Figure 35). The unified fit model (dashed curves) was calculated by a method published previously by *Lenz* et al.[146]

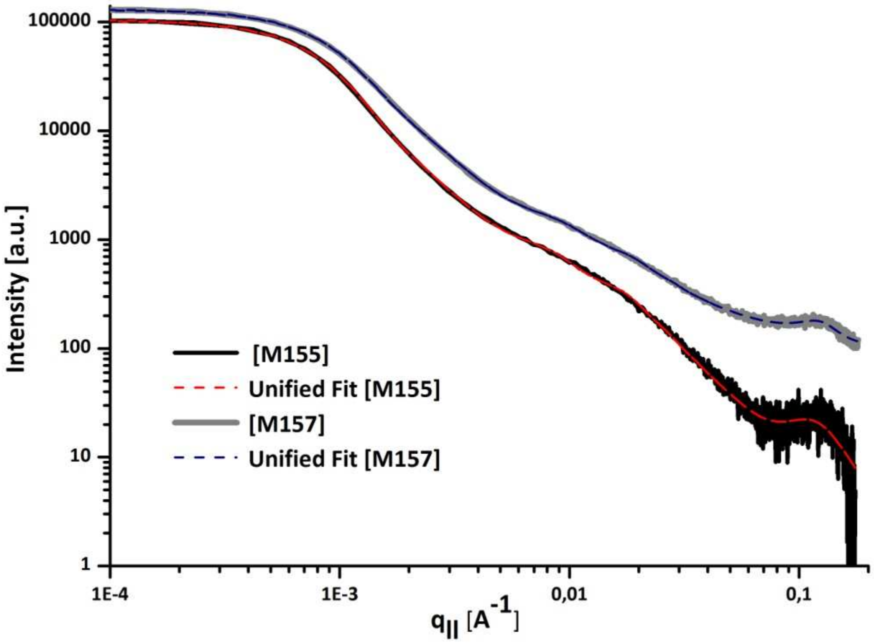

Figure 35: OOP cut along q_{II}on GISAXS data taken from a hybrid film assembling in a sphere like morphology [M155] and a platelet morphology [M157].

The Porod regime ($q_{II} > 0.02$ Å^{-1}) of both samples show that the titanium dioxide phase is composed of small particles (R_g = 2.8 nm (M155) and R_g = 2.4 nm (M157)) that are densely packed. They arrange in clusters of similar size (R_g = 23 nm (M155) and R_g = 29 nm (M157)) and correlation distance of about 70 nm for both morphologies taken from the second level unified fit model ($q_{II} > 0.005$ Å^{-1}). But the fractal dimension shows low correlated 3 D arrangement for (M155) (P = 2.1) indicating the sphere like structure that is formed in larger scale (Figure 36 (right)). The fractal dimension for (M157) indicates a 2 D packing (P = 1.5) that fits well to the lamellar structures which are formed and displayed in Figure 36 (left).

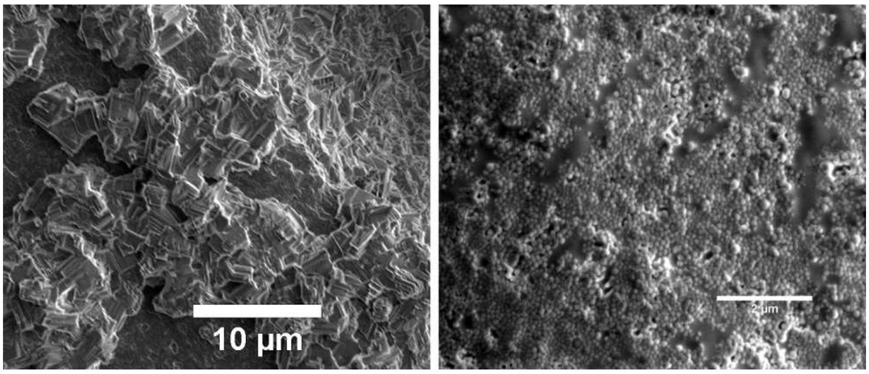

Figure 36: SEM pictures of the platelet [M157] (left) and the sphere [M155] (right) like structures.

It was shown that TiO_2 phase embedded in a polymer matrix for both morphologies is made of small particles which are clusterd and either arranged in a lamellar or sphere like structure template by the block copolymer. The GISAXS data further indicate uniformity of the structure through the film (3.3 × 0.017 mm^2 given by the beam spot at a sample tilt of 0.55°). This proves that the structures are not just found on selected areas of the samples chosen for SEM measurements.

With a polymer to TiO_2 ratio of 1:2 in 0.4 g acid and 1 g of DMF a porous structure was found as seen in (Figure 37 (a), (b)). It can be interpreted as a crossover between the sphere like and wire like structure similar to the crossover morphologies found in the phase diagram of the TTiP precursor (Figure 32 (c)). Interestingly by burning away the polymer and calcination of the TiO_2 phase in some cases brick like crystals are obtained as seen in Figure 37 (d). This entails the influence of calcination on the morphology. Furthermore severe shrinkage of the films are monitored often accompanied by cracks or agglomeration.

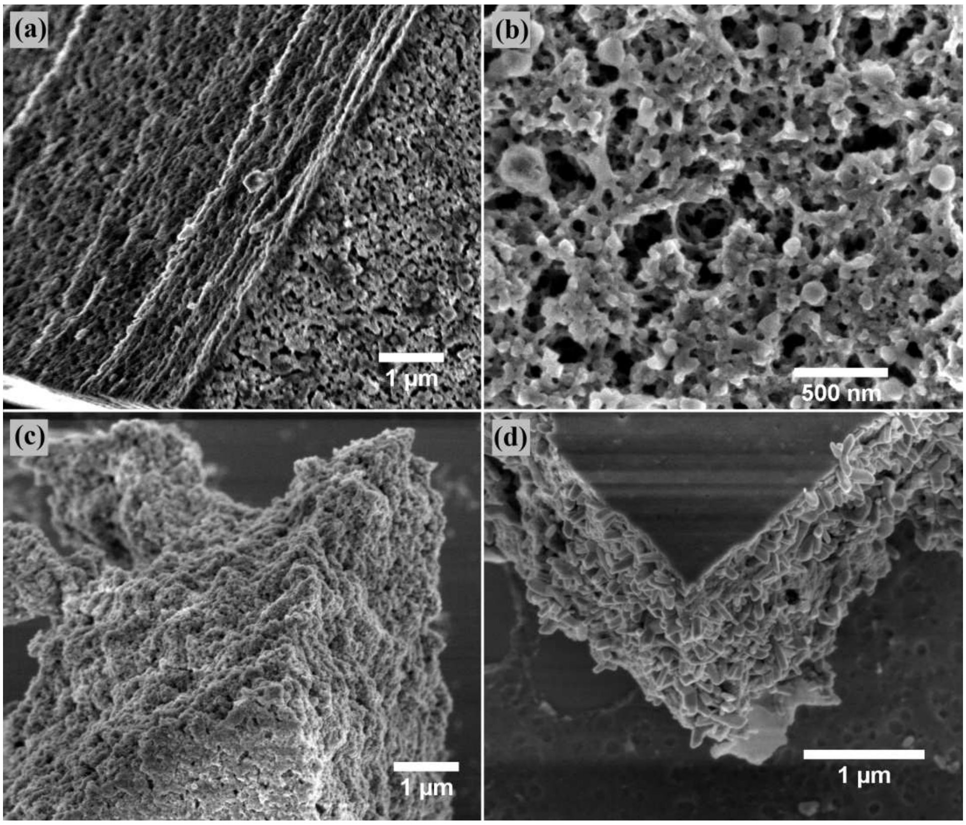

Figure 37: SEM pictures of morphology [M155] (a,b) as prepared and (c,d) after calcination.

But this is not the only external influence that could be observed on morphologies. Humidity has a great impact on the film formation and nanostructure. Morphologies shown previously are prepared in humidity from 30 to 40 %. In summertime when the humidity in the lab reached about 70 % a liquid film was seen on the surface of the samples probably because of the hygroscopic nature of the PEO block. It was found that upon exposure of the films to high humidity a strange behaviour as seen in Figure 38 could be investigated. It seems that the TiO_2 phase either pushes the polymer out of the film by a post crystallization process or the polymer is undergoing a moisture expansion out of the TiO_2 skeleton. For that reason no films were prepared for solar cell application when the laboratory humidity exceeded 40 %.

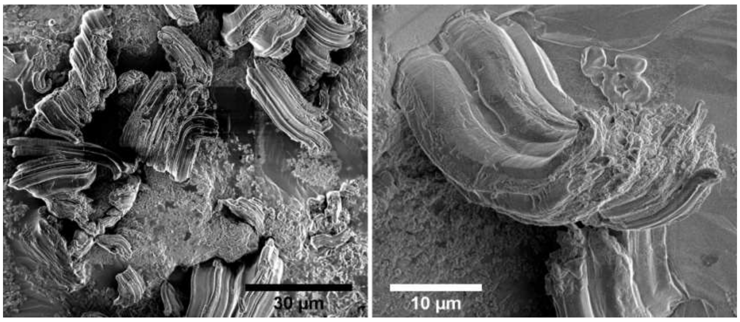

Figure 38: SEM pictures of EGMT morphologies [M175] prepared at high humidity.

4.2.4 *HYBRID MORPHOLOGY CREATION BASED ON ZINC ACETATE*

It could be shown that the principle of templating a hybrid structure with the aid of PEO-*b*-PTPA is not limited to TiO_2 systems. Using zinc acetate ($Zn(OAc)_2$) as precursor hybrid ZnO globular structures in the µm regime could be prepared (Figure 39, a). Again in a one pot approach all components were mixed in certain ratios and heated to about 60 °C. At first a fixed amount of polymer (P2) was dissolved in 1 g of DMF, upon a variable addition of 0.03 M KOH in MeOH the mixture became turbid indicating the formation of aggregates. But after a variable addition of $Zn(OAc)_2 {*} 2H_2O$ and heating to 60 °C the solution cleared. Samples were prepared by spin coating on Si-wafer and dip coating for TEM-grids (dilute solution) respectively.

In Figure 39, c the sample is shown after burning away the polymer (450 °C, 2 h) leaving behind the ZnO skeleton. It is clearly seen, that the micelles are made of a polymer core surrounded by a ZnO shell nicely seen in the cross section done by focused ion beam (FIB, Figure 39, b). In the TEM picture (Figure 39, d) of the hybrid film it is further seen that the ZnO phase is made of distinct nanoparticles of about 5 to 10 nm.

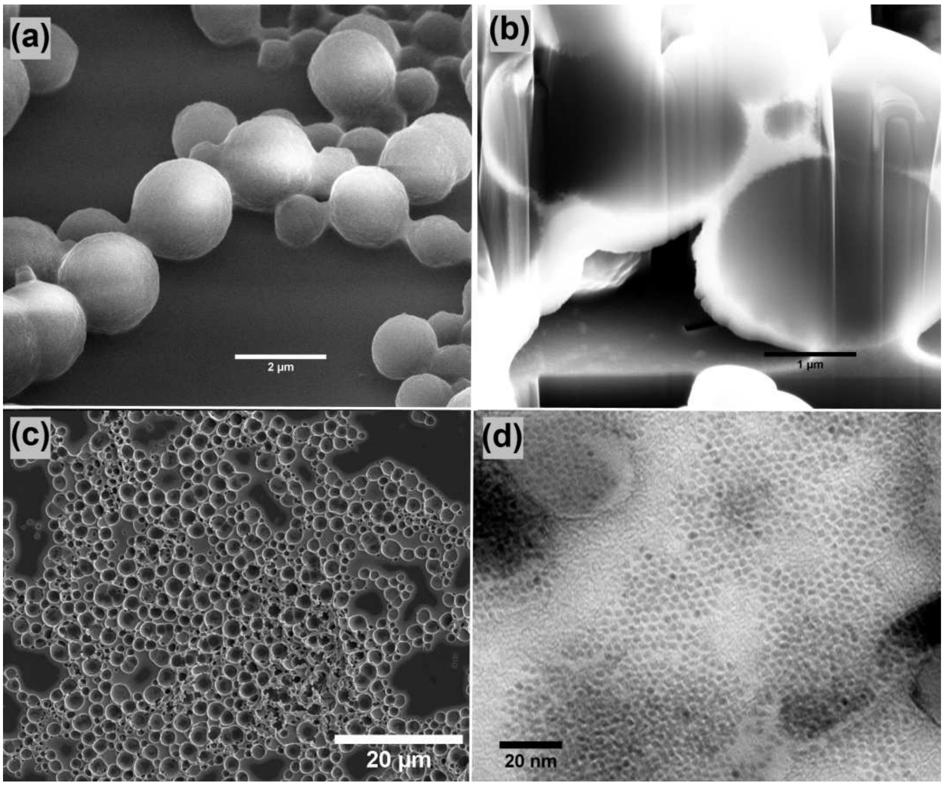

Figure 39: ZnO morphologies prepared of mixtures made of 0.01 g polymer (P2), 1 g DMF, 0.01 wt% of $Zn(OAc)_2$ and 0.05 wt% of KOH/MeOH [M134]. SEM pictures of a film drop cast on Si-wafer (a); a cross-section of spheres cut by a FIB (b); a calcined sample (c). TEM picture of a film dried on carbon coated copper TEM-grid (d).

With an increase of ZnO precursor the micelles tend to stick together seen in Figure 40 (a), (b), (c) going into direction of wormlike structures as indicated by the TEM picture (Figure 40, c). By decreasing the amount of methanol (Figure 40 (d), (e), (f)) a ZnO matrix is formed embedding polymer micelles. The ZnO matrix is found to be very porous as seen in the higher magnification of the calcined sample (Figure 40 (e)).

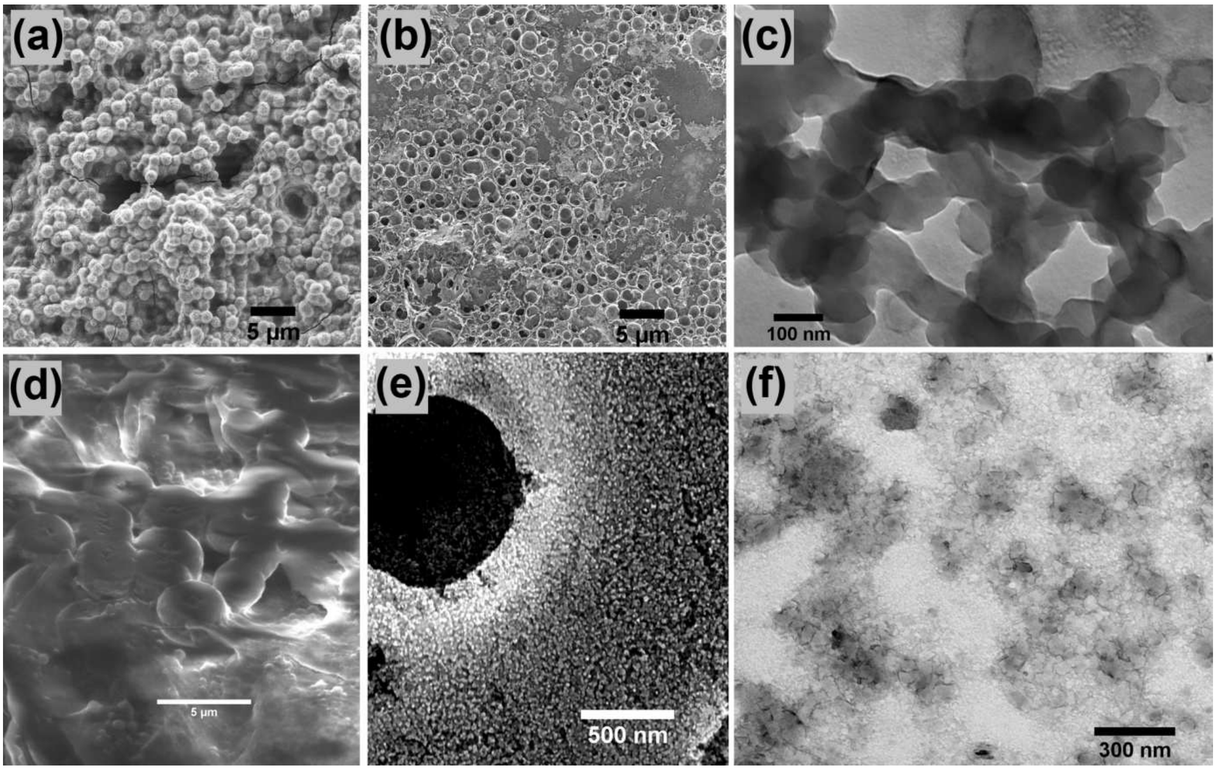

Figure 40: ZnO morphologies of 0.02 wt % $Zn(OAc)_2$, 0.05 wt % KOH/MeOH [M132] (a, b, c) and 0.02 wt % $Zn(OAc)_2$, 0.04 wt % MeOH/KOH [M135] (d, e, f). SEM pictures of films as prepared (a, d); SEM pictures of films after calcination (b, e); TEM pictures hybrid mixtures (c, f).

4.3 SOLAR CELL DEVICES

The active layer of a hybrid solar cell device consists of a mixture of a material that is able to absorb the solar light and materials which function as a hole and an electron transporter. The photoactive material can either be the polymeric/organic part itself or an additional dye. The electron transporting material is carried out by a semiconducting metal oxide like TiO_2 or ZnO. In combination with the polymeric hole conducting material a hybrid system is formed. The structure created by the hole and the electron transporting material providing a percolated network can either be templated by a functional or non functional block copolymer. It also can be obtained by the phase separation of the hybrid blend. In this work the functional (4.3.2) morphologies as well as the blend systems (4.3.1) are tested in solar cell devices.

The hole and electron conducting materials and the dye are required to display special properties in solar cell devices. The material need to face the following aspects of a device performance: (1) On the anode side, in case of an inverse set up, the electrode and electron transporting material have to be transparent to the visible spectrum to enable the absorption of light by the dye or hole transporting material. (2) A method has to be found to assemble a heterojunction that offers a high surface and at the same time a good percolating network. (3) The energy levels of the hole and electron transporting materials and the dye have to fit in a way that charge can be transferred between HOMOs and valence bands and LUMOs and conducting bands. As seen in Figure 41 the energy levels of the materials discussed in the following chapters confirm the requirements.

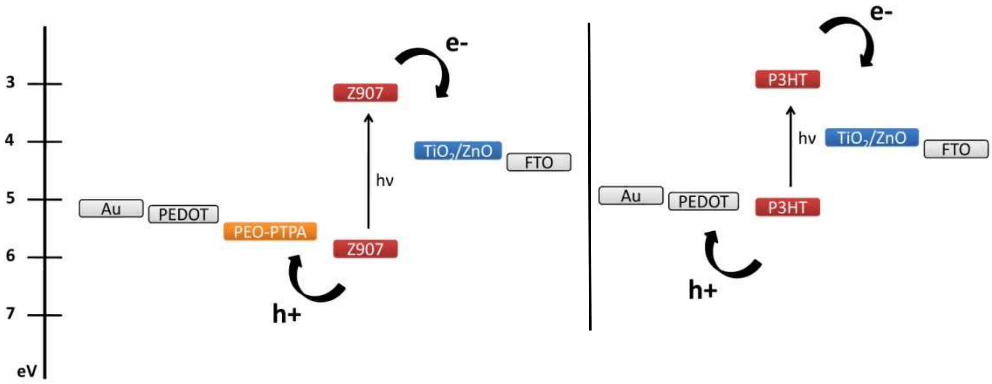

Figure 41: Energy levels for a hybrid solid state DSSC; Au (5.2 eV) and FTO (4.4 eV) as electrodes[147], PEDOT (5.2 eV)[148], PEO-PTPA (5.6 eV)[149] and P3HT (3.5/5.2 eV)[150] as hole transporting material, a sensitizing dye Z907 (3.8/5.8 eV)[151] and TiO_2 (4.2 eV)[21] or ZnO (4.2 eV)[152] as electron transporting material.

All devices were prepared with a transparent, crystalline TiO_2 barrier layer in between the active material and the FTO electrode. The importance of a barrier layer is shown in Figure 42. A simple device with and without a barrier layer between the electrode and an active layer resembled from a simple blend (TiO_2/PTPA/Ru-dye) is prepared and measured in the dark. Without a barrier layer the devices exhibit a short circuit resulting in a linear I-V relationship (grey squares). These cells showed no power conversion efficiency at all. With a crystalline TiO_2 layer spin coated from a sol-gel the typical diode behaviour is found (black rectangles). This gives the proof to the blocking ability of the used barrier layer. If the barrier layer exceeds a certain thickness (about 150 nm) a negative effect can be observed.[153] Therefore the barrier layer prepared in this work was kept at 100 nm.

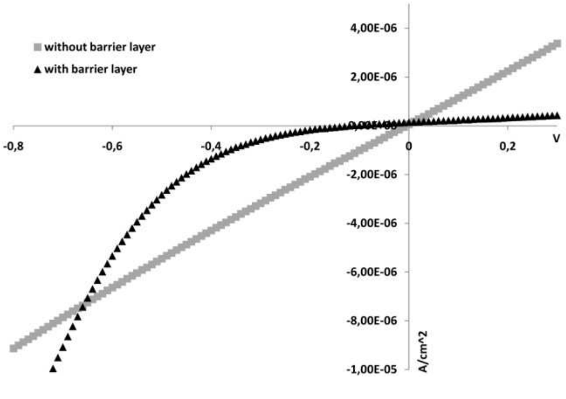

Figure 42: Dark current measurements of solar cell devices with and without a barrier layer.

4.3.1 *Self-Assembled Blend Morphology Hybrid Solar Cells*

The DSSC in form of the “Grätzel-cell” shows the highest power conversion efficiency in the area of hybrid and organic solar cells. In most Grätzel-cells a liquid, volatile and corrosive electrolyte is used, commonly I^-/I^{3-} dissolved in acetonitrile. Sealing of cells based on this electrolyte is rather difficult, which is a major drawback in terms of long term stability. In search of alternatives to the liquid electrolyte in DSSCs various solid state and dye sensitized solid state hybrid solar cells have been investigated throughout the last years. A variety of inorganic/organic combinations have been found to be suitable as functional hybrid materials for solar cells. Semiconducting metalchalcogenides and oxides like CdSe, CdTe, PbS, PbSe, ZnO, TiO_2 and hole conducting organic materials like MEH-PPV (poly(2-methoxy-5,(2-ethyl)hexoxy-phenylenevinylene)), P3HT, Spiro-OMeTAD (2,20,7,70-tetrakis-(N,N-di-4-methoxyphenylamino)-9,90-spiro-bifluorene), PTPA were found to be promising for photovoltaic application.[154] In the following it will be focused on blended systems of organic and inorganic materials to form interconnected pathways in a self-assembled fashion by the incorporation of particles or rods in a polymer matrix. Blending the components desired for an active layer in solar cells offers certain advantages. The components can be optimized separately and this, for example, enables previous calcination/annealing steps of the incorporated inorganic semiconductor at high temperatures. Not only this leads to well crystallized particles, but also enables to use particles of a desired crystallographic phase. Furthermore, the organic materials can be tuned to improve the miscibility of the organic and inorganic phase in a blend[40] or to selectively dissolve the inorganic part in one phase.

Although highest efficiencies are so far found for hybrid solar cell blends of CdSe and CdTe[4] in combination with poly(thiophenes), in this work TiO_2 phases in combination with P3HT or PTPA are investigated. Since of mild environmental impact and its low cost TiO_2 seems to be more promising component than Cd-based blends. Additionally, TiO_2/spiro-MeOTAD cells show up to 4% efficiency, depending on the kind of hole conductor.[5]

Depending on the combination of hole and electron conductor and on the additional dye in case of DSSCs the overall power conversion efficiency is strongly influenced. Also device properties like e.g. layer thickness, measurement techniques (e.g. measuring at 1 sun) and device preparation conditions (annealing, use of barrier and protecting layers, etc.) have an impact on the solar cell efficiency. These facts render a comparison of the devices assembled by different research-groups difficult.

In this study two different hole conducting polymers are used in combination with TiO_2. In order to allow a direct comparison of these materials the device preparation and measurement were conducted under equal conditions. While experimental conditions, such as the choice of solvent and photovoltaic characterization conducted in inert atmosphere is of importance for blends prepared from P3HT/TiO_2, PTPA/TiO_2 blends show weaker power conversion efficiencies but enhanced air and long-term stability as well as less sensitivity in terms of experimental conditions during preparation. The influences of the device preparation as well as measurement conditions on the device performance for different hybrid blends were investigated.

4.3.1.1 Comparing TiO_2/P3HT and TiO_2/PTPA Blend Systems in Hybrid Solar Cells

Hybrid solar cells were prepared from blend systems using crystalline TiO_2 nanorods with either one of the hole conducting polymers P3HT or PTPA. The TiO_2 rods were prepared from a $TiCl_4$ precursor leading to a crystalline product with distinct diameter but polydisperse rod length, ranging from about 1 to 10 µm (Figure 43). The reason for the rod formation is the presence of residual chloride ions that could not completely be removed by the washing procedure (chapter 3.2). Chloride ions are believed to be a structure directing agent to favour growth of short rods over long wires.[155]

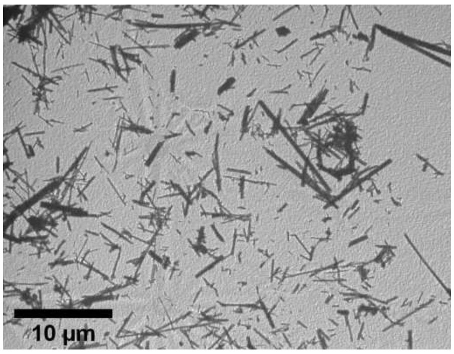

Figure 43: TEM picture of TiO_2 rods.

Alivisatos et al. showed the advantages of using rods instead of particles in a blend to create an interpenetrated network system that simplifies electron conduction through the active material. In small particle networks charges have to overcome more grain boundaries than in networks formed by rods.[41]

The hole conducting part of the hybrid blends are P3HT (with a M_n of about 4000 g/mol) and PTPA (with a M_n of about 26 000 g/mol and a pd of 1.3) polymers. The blends were prepared by mixing the TiO_2 rods with the polymer phase in either THF or chlorobenzene. The weight ratio of polymer and TiO_2 used was chosen to be 1:1, since this ratio had been reported by *Yu* et al. to be most efficient in P3HT:TiO_2 blends compared to several other ratios.[156]

SEM picture of drop casted films show that the TiO_2 rods are nicely distributed throughout the films, for P3HT blends (Figure 44, a) as well as for PTPA blends (Figure 44, b). By burning away the polymer matrix (P3HT and PTPA) the TiO_2 network is revealed showing that the rods are touching each other to create a percolating network (Figure 44, c, d).

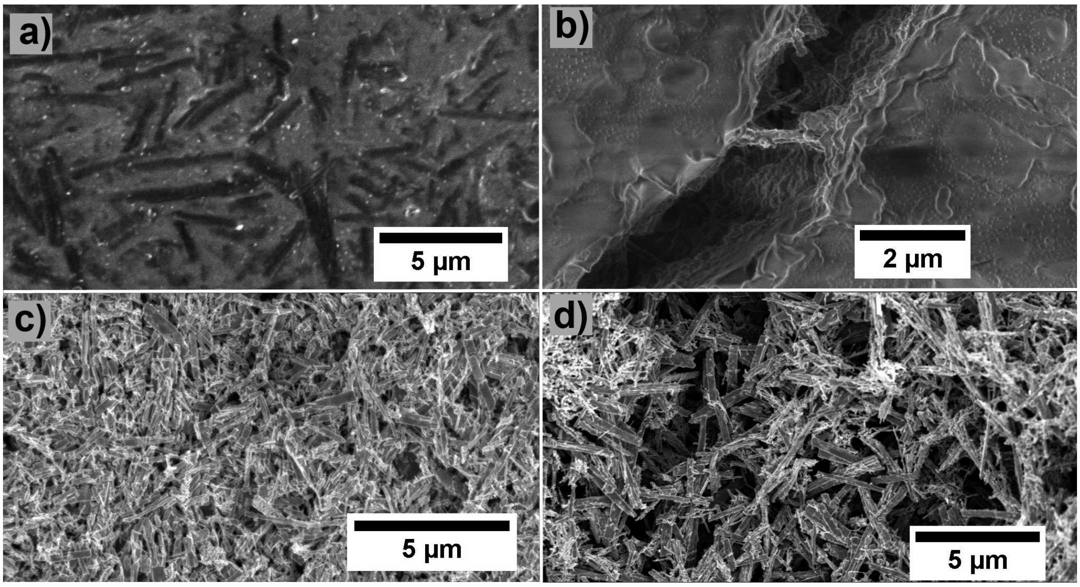

Figure 44: SEM picture of polymer-TiO_2 blends. TiO_2 rods in a P3HT matrix (a); TiO_2 rods in a PTPA matrix (b); Calcined sample of TiO_2-rods from P3HT matrix (c); Calcined sample of TiO_2 from PTPA matrix (d).

The polymer/TiO_2 blends were prepared under ambient condition and tested in solar cell devices as follows. An inverse assembly was used with FTO coated glass as transparent electrode and gold as counter electrode. The active TiO_2-polymer layer was embedded in a TiO_2 barrier layer on top of the FTO and a PEDOT:PSS protecting layer underneath the gold electrode (FTO/ncTiO_2/blend/PEDOT:PSS/Au). The active layer thickness of the drop coated blend mixtures were around 2 µm as seen in Figure 45.

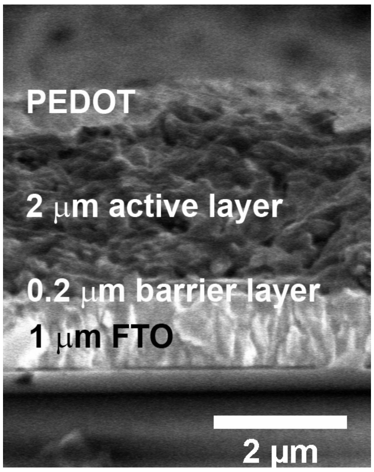

Figure 45: SEM picture of a cross section of a P3HT/TiO_2 hybrid solar cell.

Results of blends drop coated from THF solution and measured at 1 sun (100 mW/cm^2) with 1.5 AM filter are shown in Table 7.

Device assembly*	FF /%	Voc /V	Isc/ A/cm^2	Eff /%
PTPA	29	-0.16	$0.7*10^{-4}$	0.002
PTPA/PA	28	-0.11	$0.6*10^{-4}$	0.001
PTPA/PEDOT	30	-0.23	$1.0*10^{-4}$	0.007
PTPA/PEDOT/PA	30	-0.19	$1.2*10^{-4}$	0.006
P3HT	36	-0.75	$1.5*10^{-4}$	0.03
P3HT/PA	41	-0.77	$2.0*10^{-4}$	0.11
P3HT/PEDOT	28	-0.37	$2.5*10^{-4}$	0.03
P3HT/PEDOT/PA	37	-0.48	$6.3*10^{-4}$	0.11

Table 7: Measurements of solar cell devices under 1 sun and 1.5 AM. (FF: fill factor, V_{OC}: open circuit voltage, I_{SC}: short circuit current, Eff: power conversion efficiency). The blend materials were drop casted from THF solution. (PA): Measured in protecting atmosphere. * All results are averages over 8 cells containing 6 pixel each (active area about 0.07 cm^2).

4.3.1.2 Comparison of PTPA and P3HT

Comparing the results found in Table 7 P3HT is performing much better in solar cell devices than PTPA using identical TiO_2 nano-rods. The reason for this is mainly due to the difference in optical properties of the films. For an efficient exciton creation, light has to be absorbed by the polymer or an additional dye. In the case of P3HT the absorption matches the suns spectrum (Figure 46), whereas PTPA does not absorb light in the visible range. Therefore a Ru-Dye (Cis-Ru$(SCN)_2$(4,4´-dicarboxylic acid-2,2´-bipyridine)(4,4´-dinonyl-2,2´-bipyridine), Z907) is additionally introduced into the PTPA- TiO_2-blend. However the standard Ru-dye does not absorb as much sunlight as the P3HT, as seen in the corresponding UV-VIS spectra. That might be one of the reasons why the PTPA-Ru-dye system works less efficient in a solar cell. Another reason might be the undefined localization of the dye molecules in the blend. As discussed in literature[9] the absorbing species should be adsorbed at the surface of the semiconducting metal oxide to inject electrons efficiently. To recover the dye the polymer phase has to transfer electrons towards it and therefore it is most convenient to sandwich the dye in between the hole and electron conducting part, i.e. the polymer and TiO_2 phase respectively. In the discussed blend of TiO_2, Ru-dye and PTPA the dye is distributed throughout the hole active material and therefore opens ways of recombination and loss mechanisms. The importance of the interface modification is already reported in literature. *Goh* et al. studied the positive influences of the interface modification of hybrid TiO_2/P3HT devices with interfacial dipoles and additional Ru-dyes adsorbed at the interface between TiO_2 and P3HT.[157] They improved the power conversion efficiency from 0.35 to 0.6 % with additional Ru-dye adsorbed at the TiO_2 interface measured at 1.5 AM but without reported illumination intensity. *Lin* et al. reported the suppression of recombination at P3HT/TiO_2 nanorod interfaces by the attachment of Cu and Ru dye species and an additional capping of the rods with anthracene-carboxylic-acid.[158] They even reached promising efficiencies of up to 2.2 % at 1.5 AM and 100 mW/cm^2 illumination.

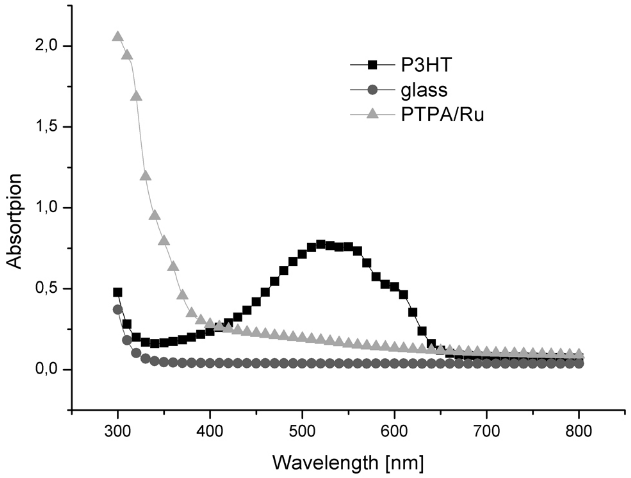

Figure 46: UV-VIS diagram of blend films spin coated on glass slides.

Comparing the charge carrier mobility of PTPA (about $1*10^{-6}$ $cm^2/(V*s)$) and P3HT (about $4*10^{-5}$ $cm^2/(V*s)$ for $M_n \approx 6\,000$ g/mol) reported in literature[159, 160] it is obvious why they perform differently when introduced in solar cell devices. The short circuit current (I_{SC}) of P3HT blends is higher than for PTPA blends. An even bigger difference is found for the open circuit voltage (V_{OC}) that is much higher for P3HT blends.

However the additional PEDOT layer seems to be sufficient for PTPA blends but not for devices prepared of P3HT blends. This is remarkable because as it is seen in the SEM image in Figure 44 a, the TiO_2 rods are clearly visible at the surface of the P3HT/TiO_2 blend film. Therefore a short circuit caused by a contact of the rods and the gold electrodes should be prevented by the PEDOT:PSS layer. An explanation might be a mismatch of the energy levels between the P3HT and PEDOT:PSS. In literature the donor material P3HT as well as PEDOT:PSS are cited with an HOMO of 5.2 eV[148, 149].

Solar cell measurement in air of P3HT and PTPA leads to divergent effects concerning the efficiency as seen in Table 7. Therefore the influence of oxygen seems not to be attributed to the semiconducting metal oxide as it is reported in literature[161] but rather to the different hole conducting polymer. In the introduced systems P3HT blends show much better performance in inert atmosphere as it is also known for fullerene/P3HT blends. P3HT is well known for the decrease in charge carrier mobility when measured [162] and prepared under ambient condition[163]. Although all devices were built under ambient conditions, the ones measured under protective atmosphere were stored under argon for at least 12 h prior to measurement. Since this treatment was found to be beneficial towards an increase in power conversion efficiency, this could be an indication for reversible oxygen doping of the P3HT/TiO_2 matrix. However, in order to recover their initial photovoltaic performance Wang et al. found oxygen to be indispensable for P3HT/TiO_2 hybrid solar cells during long-term measurements.[164] Since P3HT/TiO_2 blends reported in this work are much more efficient when measured under inert gas it was not possible to take advantage of this effect. In Figure 47 the I-V-curves of devices measured at constant illumination (1 sun and 1.5 AM) are shown for the P3HT (a) and PTPA (b) blends. For both blends a decrease in I_{SC} and V_{OC} can be detected. For the P3HT blend the curve changed dramatically upon illumination (Figure 47, a) while measured in inert atmosphere. The same dramatic decrease in efficiency was found for long-term measurements done in air. Lira-Cantu et al. proposed the influence of the UV light to be the reason for the unsatisfying long-term stability.[161] That does not seem to be a suitable explanation here; since light has to pass through FTO coated glass and thus only little UV light should reach the active layer. Since P3HT blends show a decay of efficiency by an order of magnitude (Table 8), although measured in inert atmosphere, the influence of oxygen does not give an explanation in these cases. Furthermore in the case of PTPA blends oxygen seems to be necessary.

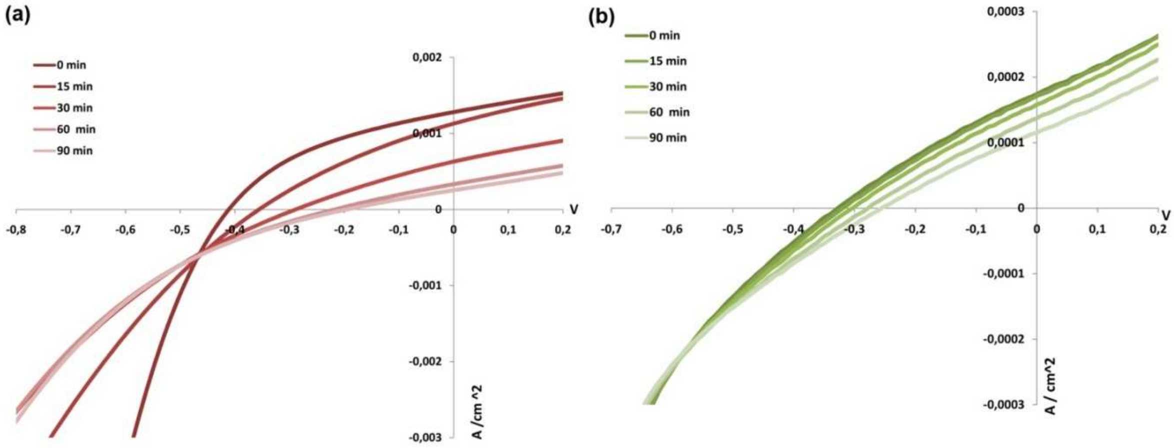

Figure 47: Longtime exposure of devices at 1 sun and 1.5 AM. TiO_2/P3HT blend, measured in inert atmosphere (with PEDOT layer; active area: 0.063 cm^2) (a), PTPA/TiO_2 blend, measured under ambient condition (with PEDOT layer; active area: 0.072 cm^2) (b).

On the contrary the TiO_2/PTPA blends show an increased efficiency when measured under ambient conditions (Table 7). Furthermore the decay of the power conversion efficiency was less dramatic upon continuous white light illumination (Table 8 and Figure 47, b). Hence for the PTPA/TiO_2 system the above described positive influence of oxygen on hybrid systems might be seen. *Kempa* et al. already demonstrated the long-term and air stability of PTPA in field effect transistors.[165] This confirms the results found here.

Device assembly	**0 min**	**15 min**	**30 min**	**60 min**	**90 min**
Eff. (%)* P3HT/PA	0.102	0.056	0.027	0.011	0.007
Eff. (%)* PTPA	0.010	0.010	0.009	0.007	0.006

Table 8: Efficiency progression during long-term illumination. (PA): Measured in protecting atmosphere. * Efficiencies are averages taken from 6 pixels of one device.

4.3.1.3 Further Improvement of P3HT/TiO_2 Blend Devices

It is known that by using chlorobenzene as solvent instead of THF the overall power conversion efficiency for P3HT systems e.g. in combination with fullerene materials can be doubled. Also in hybrid heterojunction bulk systems the overall efficiency can be largely influenced by the choice of solvent. In this case xylene was found to be most effective.[36] In the here reported hybrid systems the power conversion efficiency could be doubled from 0.11 % to 0.22 % by changing the solvent from THF to chlorobenzene (Table 7 and Table 9). The choice of solvent has a strong influence on the structure of the polymer film formed by evaporation of the solvent. *Kwang* et al. also showed the strong influence of the solvent on the device performance when prepared from TiO_2 in a P3HT matrix. They obtained 0.18 % for cells casted from chlorobenzene solutions and 0.033 % from THF solutions.[36]

Device assembly*	**FF / %**	**Voc / V**	**Isc / A/cm^2**	**Eff / %**
P3HT/PA	31	-0.33	$1.5*10^{-3}$	**0.22**
P3HT/Annealed* PA**	29	-0.29	$4.8*10^{-4}$	0.04
P3HT/Annealed* **	30	-0.36	$4.5*10^{-4}$	0.05
P3HT	31	-0.35	$1.3*10^{-3}$	0.13

Table 9: Measurements of solar cell devices under 1 sun and 1.5 AM. The blend materials were drop casted from chlorobenzene solution. (PA): measured in protecting atmosphere * All results are averages taken from 8 cells containing 6 pixel each * Annealing was done at 160 °C for 10 min.

In fullerene-P3HT systems annealing and choice of solvent have a major influence on the film morphology. Slow Drying leads to phase separation and affects crystallization.[166] Casting films from solvents with a lower vapor pressure like xylene and chlorobenzene are more appropriate than solvents like THF and chloroform. As seen in Table 9 and Table 7 the I_{SC} for blends drop coated from chlorobenzene increased one order of magnitude compared to devices prepared from THF solution (from $2*10^{-4}$ to about $2*10^{-3}$). The degree of crystallinity of P3HT is of importance for its hole conducting ability. Therefore, additional time for crystallization given during evaporation of the solvent will be beneficial. Here the advantage of using PTPA in optoelectronic devices becomes evident. Since PTPA is an amorphous hole conductor[165] the use of a high boiling solvent or an extra annealing step is redundant. Surprisingly further thermal annealing of the investigated P3HT films does not improve solar cell performance. A common treatment for P3HT films at 160 °C for 10 min leads to a dramatical drop of the power conversion efficiency. Maybe due to the small molecular weight of the used P3HT, an increase of chain alignment leading to a higher crystallinity does not occur. Other than that, the annealing possibly leads to a higher concentration of oxygen in the film because the heat treatment was performed under ambient condition. Furthermore the TiO_2 rod network might not be flexible enough to initiate a change in phase separation like it is found in fullerene P3HT systems.

Higher efficiencies for TiO_2/P3HT blend solar cell devices are reported by *Wu* et al.. Efficiencies of 0.65 % were reached by adding PMMA into the TiO_2 nanorod/P3HT blend.[167] It was claimed that the additional PMMA smoothes the film and reduces the occurrence of pores and defects. Another approach for these kinds of hybrid composites was published by *Williams* et al., where nanostructured TiO_2-P3HT composites were formed via an imprinting technique. Without an additional dye efficiencies of about 0.33 % were obtained, while after addition of a Ru-dye over 0.6 % power conversion efficiency was reached.[57] An explanation for the higher efficiencies compared to this study might be the different P3HT polymer used. Indeed, the P3HT used here has a molecular weight of only 4 000 g/mol. P3HTs with small molecular weight are known to have lower hole mobility than high molecular weight polymers and therefore lower power conversion efficiencies. Wu et al. found a power conversion efficiency of 0.2 % for low molecular weight (about 10 000 g/mol) that perfectly matches with the result of 0.22 % obtained in this study with a P3HT of even smaller molecular weight (4 000 g/mol).[168] With an increased molecular weight of 66000 g/mol Wu et al. almost reached 1 % efficiency.

4.3.2 FUNCTIONAL COPOLYMER TEMPLATED HYBRID SOLAR CELLS

A prototypical hybrid solar cell consists of an electron semiconducting metal oxide (electron conducting material) and a hole conducting organic material as the active material, where the exciton formation, charge separation and charge transport takes place. Therefore a high surface area between the hole and electron conducting materials and the right separation of the percolation way towards the electrodes (limited by the diffusion length of excitons) is needed to avoid recombination of the created holes and electrodes. This can be fulfilled in a bulk heterojunction that consists of a penetrating network of the donor (hole transporting material) and the acceptor (electron transporting material) phases with a reproducible morphology. The successful combination of structure formation and dual functionality, using a semiconducting block copolymer to template a metaloxide like TiO_2 and ZnO was accomplished.

4.3.2.1 Functional Templates for Hybrid Solar Cells prepared from TTiP[149]

A solid state dye sensitized hybrid solar cell was build from active material described in chapter 4.2.2. A one-pot mixture of PEO-*b*-PTPA, dye, TTiP in DMF and HNO_3 leads to several self-assembled percolated nano network structures which were tested in devices. The hole conducting polymer PTPA showed no intrinsic absorption in the visible spectrum and in consequence transparent films were obtained after spin coating. For solar cell application the absorption of light is indispensable. Therefore a standard dye (Ru Z907) was introduced that is commonly used in combination with TiO_2.[116] Block copolymer, precursor (TTiP) and Z907 (Ru-dye) were added into a single solution of DMF, isopropanol and HNO_3 prior to heating. The UV-VIS measurement (Figure 48, left) showed that the dye is stable in this environment even after heating to 100 °C for 1 hour also seen in the colour code at different concentration (Figure 48, right).

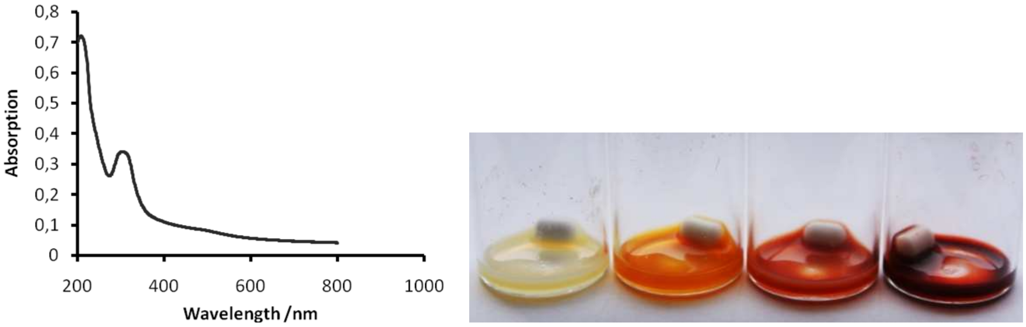

Figure 48: UV-VIS measurement of dye in polymer/TiO_2 matrix (left). Sol-gel mixtures from the left to the right: without Ru-dye, with 0.001 g, 0.005 g and the pure dye dissolved in DMF (after heating to 100 °C for 1 h) (right).

The assembling of the devices is seen in Figure 49 and was set up as followed: FTO (~350 nm) and gold (50 nm) were used as electrode materials. A barrier layer (BL, ~100 nm) spin coated on top of the FTO, followed by the active matrix and PEDOT:PSS (~30-50 nm). *Ravirajan* et al. Found that PEDOT:PSS improves the efficiency since it can be used as a protecting layer, to prevent the active matrix from damage by the evaporation of gold as top electrode on the device. In addition it should overcome the low effective work function of gold.[169] To increase the conductivity silver was put at the contacts of the measurement needles.

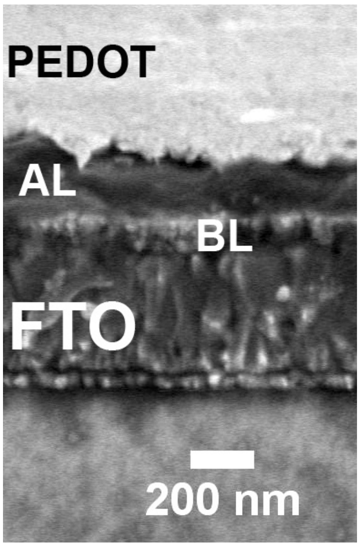

Figure 49: SEM picture of device cross section prepared by a spin coated active layer of the sphere like morphology [M84].

For solar cell measurement an irradiance of 1 sun (100 mW/cm^2) with a 1.5 AM spectral characteristic was used. In Table 10 the results are summarized for proof of principle devices build out of the most promising morphologies. A promising morphology is an ordered structure that lies in the lengthscale of the exciton diffusion length and shows possibilities for charges to find percolation pathways through the hybrid film.

Morphology	Amount of working pixels*	Average η of working pixels	Best pixel	Thickness (AL)
Spheres [M84]	42	0.025%	**0.151%**	5 nm
Wire [M102]	35	0.010%	0.037%	5 nm
Foam [M83]	30	0.004%	0.053%	2 nm

Table 10: Efficiency dependence on morphology. From each morphology 8 devices had been built. Each device featuring 6 pixels which could be addressed individually.* 48 Pixel are possible for each batch.

The best efficiency was found for the sphere-like morphology. As shown in Figure 50 a I-V curve was plotted with a FF of 0.77 and I_{Sc} 1.8*10^{-4} A/cm^2 and V_{oc} = -1 V.

It seems that compared to the other morphologies for this morphology the optimal percolation for holes and electrons is realized. In literature[170] the gyroid structures formed by block copolymers in a self-assembled fashion are very often described as the favoured structures for percolating networks, since they offer a reliable pathway between electrodes, allowing the existence of small defects. It could be shown that the present hexagonal structure is a promising alternative towards these synthetically challenging gyroid structures. As seen in Figure 31 the polymer spheres surrounded by TiO_2 are creating a network itself, since the TiO_2 shell is not perfect and the polymer cores are allowed to touch each other. But it is also seen that the TiO_2 phase consists of very small grains between 5 and 10 nm. While smaller particles exhibit a higher surface area and therefore allow for a higher dye loading, they also create a large number of grain boundaries that are potential traps for electrons. *Cao* et al.[171] varied particles from 9 to 23 nm and found better conversion efficiencies for the bigger particle. An overall improvement of the efficiency could be reached tuning the TiO_2 particle size.

Surprisingly the concentration of TiO_2 is much higher in the foam like structure than in the sphere like structure but the performance is worse. This could be due to the effect that with increasing amount of titania the quality of the film typically decreases, it was not homogeneous and showed many cracks. The decreasing amount of working pixel (Table 8) gives an evidence to suggest short cuts that appear because of the cracks in the film.

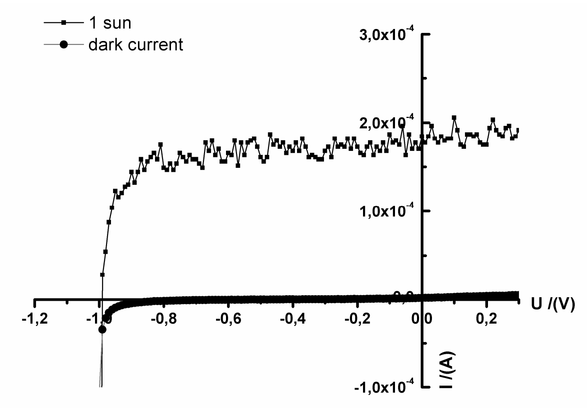

Figure 50: I-V curve for a solar cell prepared of sphere like morphology [M84] measured at 1 sun (100 mW/cm^2) and 1.5 AM. $\eta = 0.15$ %, $V_{oc} = -1.0$ V, $I_{sc} = 0.2$ mA/cm^2, active area = 0.055 cm^2.

Furthermore the percolation pathways are long and highly branched in the foam like structure because of the small size of the primary TiO_2 particles. Therefore the chance of recombination is higher as well as the distance towards the electrodes is extended, increasing internal resistance. The wormlike structure might not give sufficient contact between the nanocrystalline TiO_2 particles and the barrier layer, since the titanium particles are at least partly surrounded by polymer. The sphere like morphology seems to be an optimized balance and therefore gives the best efficiency in the presented devices.

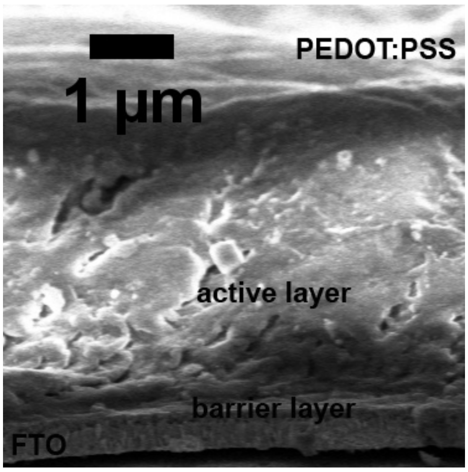

Figure 51: SEM picture of a cross section of a device prepared by a drop coated active layer.

With X-ray reflectivity the film thickness was measured to be about 5 nm for the sphere- and wire-like structure and about 2 nm for the foam-like structure (Table 10). The film thickness explains why the prepared cells were only weakly coloured. A low dye concentration entails a weak absorbance of the sun light and therefore no chance for proper photoconversion efficiency. Therefore an increased film thickness was hoped to improve the efficiency. As seen in Table 11 different film thicknesses of the most promising morphology [M84] were prepared. With slower spin coating the thickness could be increased dramatically to about 790 nm, but at the same time the obtained films had a roughness of about 100 nm and seemed to be very inhomogeneous. This decrease in film quality might explain the poor efficiency.

sphere morphlogy	Average η of working pixel (work/poss.)	Best pixel	Film Thickness
sc 1000 rpm	0.025 % (42/48)	0.151 %	5 nm*
sc 500 rpm	0.013 % (33/48)	0.05 %	~790 nm*
drop coating	0.020 % (30/30)	0.05 %	1 – 2 µm**
plate coating	0.020 % (18/18)	0.06 %	~ 200 nm**

Table 11: Film thickness dependence of efficiencies for solar cells prepared from sphere-like morphology. (sc): spin coating. *measured with X-ray reflectivity. **measured with alpha stepper.

But also for drop and plate coated films the efficiency could not exceed 0.02 %. Even so drop coated films produced nice films of well defined spheres as seen in Figure 52. A reason for the poor performance could be dedicated to the longer percolation way provided in thicker layers. For film thicknesses of 1 to 2 µm (Figure 51) the degree of crystallinity and number of grain boundaries in the TiO_2 phase should greatly influence the charge mobility in the device. Obviously the plate coated 200 nm thick devices show that the limitation is quite strong. Therefore the mobility of the hole conducting polymer PTPA could also play a limiting role. But as seen in chapter 4.3.2.2 with an alternative TiO_2 precursor, film thicknesses of over 1 µm showed an improved efficiency. Since the hole conducting polymer used in the EGMT precursor devices were the same as used here the proposed assumption of the bad charge mobility in the TiO_2 phase seems to be confirmed.

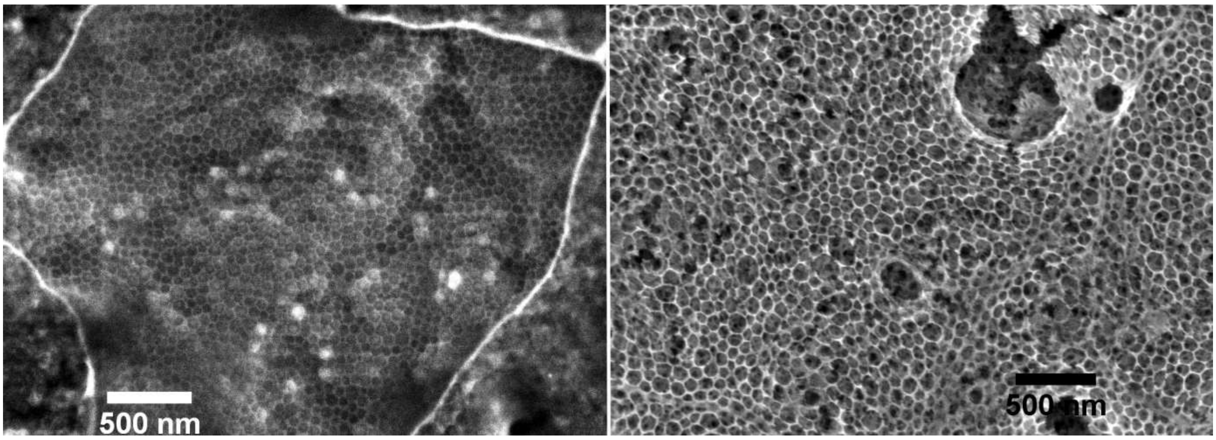

Figure 52: Sphere-like morphology [M84] in drop coated films for solar cell measurements. Pristine film (left) after calcinations at 450 °C for 2 h revealing the TiO_2 skeleton (right).

4.3.2.2 Functional Templates for Hybrid Solar Cells prepared from EGMT

To overcome the problem of low mobility of the TiO_2 phase that had been raised with the TTiP/polymer systems in thick films discussed previously, a crystalline precursor EGMT is used. Again different self-assembled morphologies with orthogonal functionality were tested in photovoltaic devices. Foam [M190, M175] and sphere-like [M172] morphologies (Figure 34) were used with a Ru-dye as absorbing material in an inverse set up (FTO and Au as electrodes). As it has been discussed in chapter 4.3.2.1, sphere- and foam-like structures are able to form percolated systems. All films were drop coated on a barrier layer of crystalline TiO_2 that was spin coated on the transparent electrode FTO. An active layer thickness of 1 to 2 µm was obtained via drop coating of the sol-gel mixture. A cross section of these devices is shown in Figure 53 (left).

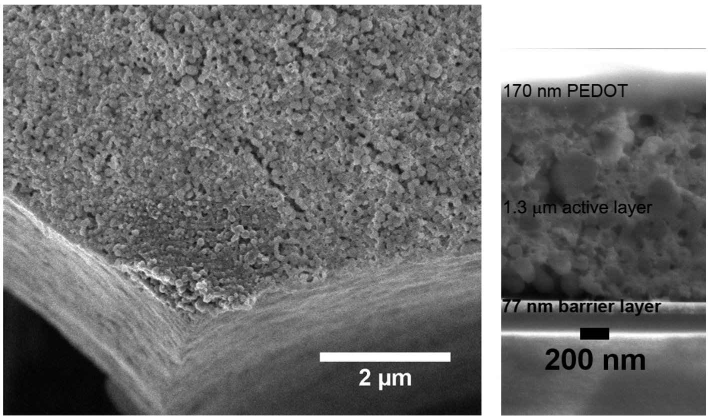

Figure 53: SEM picture of a film prepared from a mixture of 0.4 g of acid, 0.02 g of EGMT and 0.01 g of polymer in 1 g DMF [M155] (right). SEM picture of a cross section of a solar cell device with an active layer of the previous described mixture (left).

Comparing these morphologies by incorporating them as active materials in solar cell devices a clear difference can be found as seen in Table 12Table 12: Average values of solar cell devices prepared from different morphologies and measured at 1 sun at 1.5 AM.

Devices were measured under 1 sun (100 mW/cm^2) and 1.5 AM. The dense morphology [M190] as expected is showing the lowest efficiencies since the percolation way of the polymer phase seems not been developed well through the densely packed TiO_2 particles. While for composites made of [M172] and [M175] an increased I_{sc} was obtained indicating the reduction of charge recombination due to less grain boundaries. An increase of even two magnitudes showed devices prepared from morphologies [M155] (Table 12).

Power conversion efficiencies for the less dense structures of compositions [M172] and [M175] more than doubled, compared to devices prepared from [M190]. But as seen in Table 12 the open circuit voltage for [M175] is low compared to the other morphologies.

Device	**FF /%**	**Voc /V**	**Isc /A/cm^2**	**P.c.Eff. /%**
[M190]	29	-0.40	$5.0*10^{-5}$	0.006
[M172]	27	-0.29	$2.3*10^{-4}$	0.023
[M175]	27	-0.54	$2.4*10^{-4}$	0.034
[M155]	29	-0.39	$0.5*10^{-3}$	0.110

Table 12: Average values of solar cell devices prepared from different morphologies and measured at 1 sun at 1.5 AM.

While the fill factor is more or constant for all devices, a much higher efficiency was found for the morphology shown in Figure 54 (right) [M155]. Devices with an average power conversion efficiency of about a 0.1 % and a maximum value of 0.4 % (FF: 0.51; V_{oc}: -0.69 V; I_{sc}: 1.0 mA/cm^2) could be prepared (at 100 mW/cm², 1.5 AM). This indicates that the mixed sphere/rod morphology [M155] is most favoured to form a percolated network.

It was successfully shown that thicker films showed increased power conversion efficiency. When thin films were prepared by spin coating no photocurrent at all could be measured as indicated in Figure 54, green line. For these layers a short circuit was found resulting in a linear I-V relationship. The short circuits might indicate that no proper uniform film is formed upon spin coating. In contrast thick layers sometimes exhibit a s-shape I-V curve (Figure 54, blue curve). This abnormal behaviour can be caused by several reasons. Either a delamination of the films exists or impurities in the sample infect the I-V measurement. Furthermore a too fast evaporation of the gold electrodes can cause gaps between the electrode and active material that explains this behaviour. If the film formation of drop coated samples does not face the difficulties of delamination or impurities, a normal diode characteristic is found (Figure 54, red line).

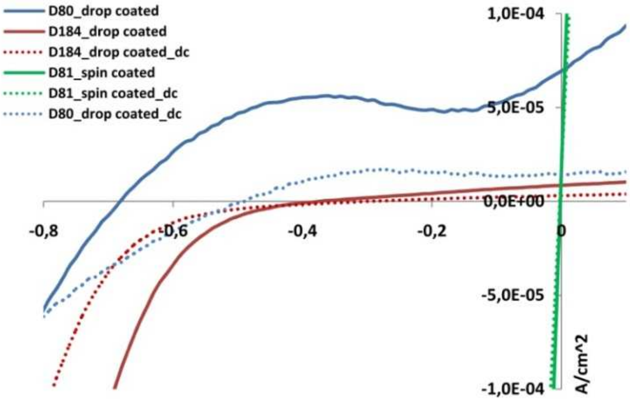

Figure 54: Solar cell measurements of devices prepared from sphere/rod-like morphology [M155], measured at 1 sun, 1.5 AM (solid line) and without illumination (dotted line).

Since the light absorbing dye is distributed in the whole coating, a thicker film should lead to a higher absorption and therefore to a higher photocurrent. However, in thicker films the presumable percolation ways get longer and thus the probability of charge recombination increases. Nevertheless the structures have to have sufficient alternatives for the charge to find its way through the material, but not being too highly branched. Therefore it is questionable whether the active layer of 1 to 2 µm thickness (Figure 53 (right)) is still showing a percolated network. This was investigated by conductive scanning force microscopy (c-SFM) at a cross section of devices prepared from morphology [M155] that was fractured along one of the gold electrodes. The sample was mounted vertically to allow a scan along the cross section of the device (Scheme 6). For a better resolution in

SFM measurements, the edge of the fracture was polished with a focused ion beam (FIB, FEI Nova 600 Dual Beam). In the SEM images (Figure 55, a) of the polished area the polymer embedded in the inorganic matrix can be seen (dark areas) as well as in the height image of the SFM measurement (Figure 55, b).

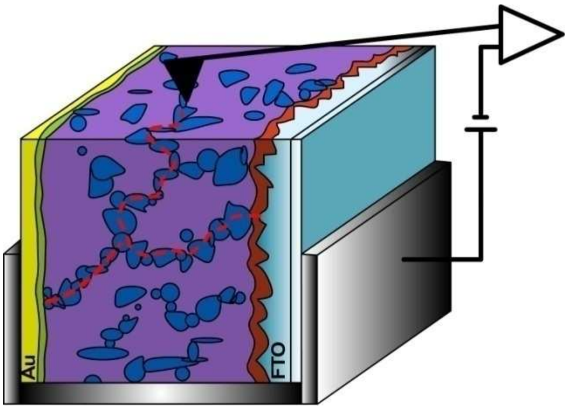

Scheme 6: Conductive-SFM measurement set up.

The structure of the sample investigated by c-SFM was performed on the polished area (MFP3D with ORCA current amplifier, Asylum Research). The whole sample (including the active layer and the top electrode) is set on a constant bias voltage and the resulting electrical current through the grounded SFM tip is recorded by a current amplifier (Scheme 6). In Figure 55 c and d the recorded current (absolute values) on the FIB polished area under positive (U_S = 1 V) and negative (U_S = -2 V) bias is shown. The function of the barrier layer as an electron conductor in the middle of the sample can be clearly observed from the change in the current from an average of 200 fA in the positive bias case (Figure 55 (c)) to 0.33 nA under negative sample bias (Figure 55 (d)). In the active layer on the left hand side of the sample patches of 50 – 200 nm in diameter can be observed. The average current on top of these patches is 2.4 pA and 9.3 pA under positive and negative bias, respectively, whereas the surrounding area carries a current of about 1 pA in both cases. No correlation of the current with the distance to either of the electrodes was found for both bias measurements. Thus, the electrical conduction is not limited by the length of the connection to the electrode, which indicates a well percolated network of conducting structures inside the active layer as outlined in Scheme 6. The measurement in forward bias of the barrier layer (Figure 55 (d)) shows a smaller current for the patches of the active layer than the barrier layer itself. A possible explanation might be dedicated to defects in the contact between the active layer and the barrier layer could influence the decreased current intensity. Therefore an improved contact between the layers might improve the power conversion efficiency of the solar cell by an increased current flow.

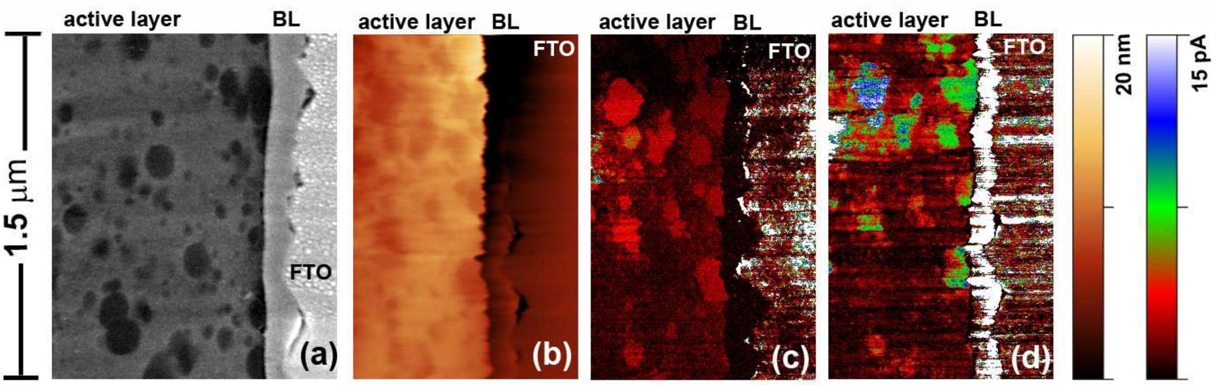

Figure 55: SEM image of a cross section of a solar cell device prepared from [M155] polished with a FIB (a). SFM height image of polished cross section measured in contact mode (b). Conductive SFM pictures of a cross section corresponding to the height image (c), (d); under positive bias (c), under negative bias (d).

Very convenient is the fact of air stability of all devices, since just measurements under ambient condition resulted in a power conversion efficiency. Furthermore oxygen seems to be essential for these kinds of composites, without oxygen no power conversion efficiency at all was obtained. Therefore further effort to improve the active material is worthwhile. The crystallinity of the TiO_2 is one part to be optimized. The precursor EGMT is known to be already crystalline, but unfortunately so far no reliable XRD patterns could be measured to see the degree of crystallinity of the resulting hybrid material used in the devices after the complete manufacturing steps. An increase of efficiencies in the here reported systems could be obtained by an improvement of the crystallinity or increase of crystal size, reducing the grain boundaries that lower the conductivity for electrons to pass towards the FTO electrode. Further improvement is possible with the exchange of the standard Ru-dye Z907 used. Z907 is easy available but offers an absorption spectrum that stays behind many other dyes that make much better use of the solar spectrum in hybrid solar cells and are therefore having a great influence on the overall power conversion efficiency. Furthermore the delocalization of the Ru-dye can cause recombination of the charge carriers that result in low short current density of the devices. In the reported system the dye can be located anywhere in the active layer material, not just at the interface between TiO_2 and hole conducting polymer that would be most favourable. A last issue might be given by delamination problems of the active film in between the active material and the barrier layer. As seen in Figure 53 (right) of the SEM cross section there is a dark area between the barrier and the active layer that can be dedicated towards delamination.

With discussed improvements the system introduced offers a fast and convenient method to prepare photovoltaic devices since they do not require any difficult sealing technique due to their air stability and no post processing treatments.

4.3.2.3 Functional Templates for ZnO Hybrid Solar Cells

In this work the successful transferability of the introduced systems was shown by exchanging TiO_2 with ZnO as electron conducting specie. ZnO is proven to give promising results in ZnO/MDMO:PPV hybrid solar cell devices published by *Beek* et al. .[172] The work is limited to the proof of concept while no further efforts have been put into improving the solar cell efficiency of these devices.

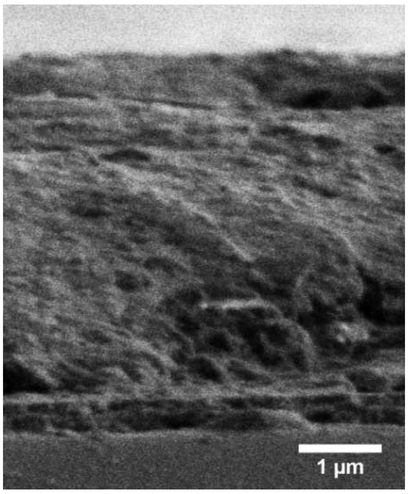

Figure 56: SEM picture of a cross section of a ZnO/PEO-PTPA device. With an active layer of about 3 - 4 µm.

The active material made of the functional, hole conducting PEO-*b*-PTPA (P2), Ru-dye Z907 and ZnO – precursor was prepared as described in chapter 4.2.4. The composition of the interconnecting sphere morphology [M132] was chosen to be most promising and therefore tested in solar cell devices as drop coated films resulting in a layer thickness of about 3 to 4 µm (Figure 56). The active layer was sandwiched between a FTO and gold electrode, while a barrier layer of TiO_2 was put between FTO and the active layer to prevent short circuits (FTO/BL/ZnO:Ru-dye:PEO-*b*-PTPA/Au). In Figure 57, a SEM picture is seen of the drop coated film used in the photovoltaic cell. The SEM picture on the right is just for monitoring the ZnO structure obtained within this drop coated film by burning away the polymer (450 °C, 2 h). On the one hand side it is seen in the calcined sample that there is a percolated ZnO network formed but on the other hand the polymer filled sample is very rough with a very inhomogeneous surface structure that might be a reason for the low power conversion efficiencies.

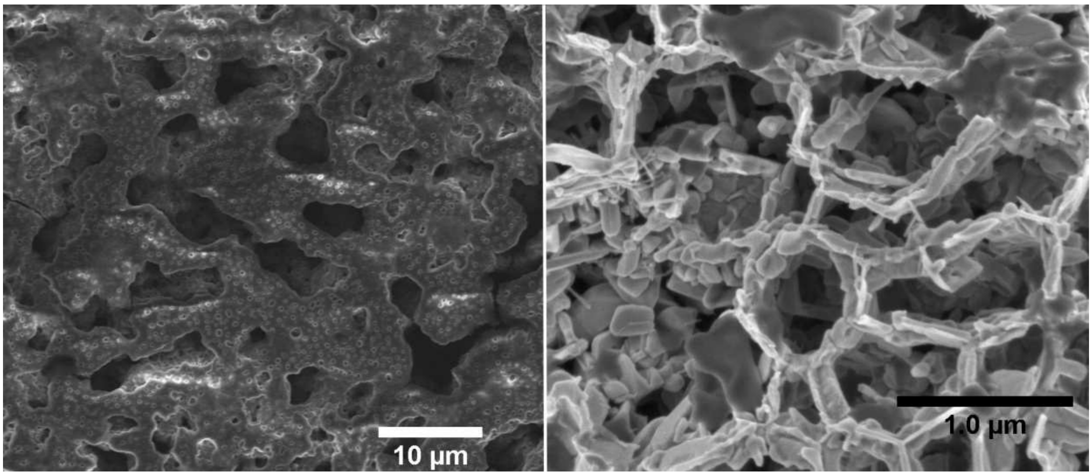

Figure 57: SEM pictures of ZnO moprhology [M132] tested in solar cell application. Drop coated film as used in the devices (left), after burning away the polymer to reveal the ZnO skeleton (right).

The average power conversion efficiencies obtained for that kind of systems were about 0.005 % at ambient condition, measured at 100 mW/cm^2 and 1.5 AM. In Figure 58 the solar cell measurement for the best pixel is shown with η = 0.011 % (I_{sc} = 4.1*10-5 A/cm2; V_{oc} = - 0.7 V; FF = 36 %). As previously reported for TiO_2/PTPA hybrid systems a certain oxygen doping seems to be required for an efficient device. The red curve in Figure 58 is the I-V curve for the cell measured under ambient condition while the blue curve presents the measurement done in argon atmosphere and for the latter no solar current could be obtained. However the dark current is also influenced by the oxygen level (red dotted curve) it displays a certain offset compared to the dark current measured in protecting atmosphere (blue dotted line). Furthermore an annealing procedure was applied on the samples at 150 °C under ambient condition for 15 min. But this routine just decreased the overall efficiency drastically (green line). Though the kink of the pristine device measured at 1 sun could be removed by annealing, that could be due to better contact between the layers. The influence of electrode and active layer contact was described by *Gupta* et al. to induce a s-shaped I-V curve.[173] The off-set of the dark current (green dotted line) can be just explained by an imperfect calibration.

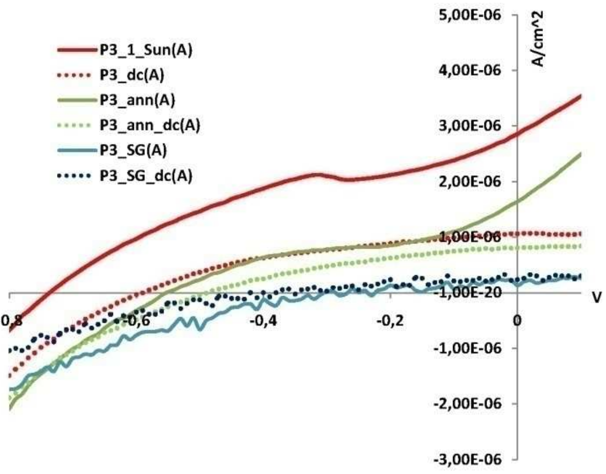

Figure 58: Solar cell mesurement at 1 sun (100 mW/cm^2) and 1.5 AM at ambient condition if not indicated. Measured in dark (dc), after annealing 150 °C for 15 min (ann), measured in argon (SG).

These functional templated ZnO hybrid solar cells are facing the same difficulties as the TiO_2 cells. The degree of crystallinity is not assured by the reported synthetic strategy as well as the location of the Ru-dye. Furthermore more efficient photoactive specie should have a major impact of an increase in efficiency.

4.3.2.4 Functional Templates in Combination of Blended Systems

The approach of using the EGMT one-pot system supported by the functional PEO-*b*-PTPA template (introduced in chapter 4.2.3) was combined with the blending technique. To be thinking about an increase of the charge mobility in the TiO_2 phase by introducing pre-synthesized crystalline TiO_2 rods (introduced in chapter 4.3.1).

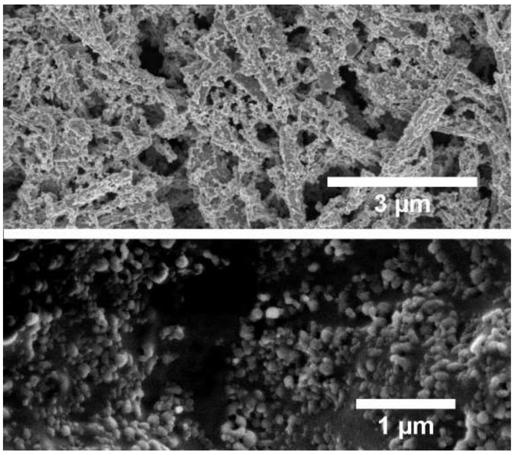

Figure 59: SEM pictures of mixed structure of EGMT - template morphology [M175] and TiO_2 rods (lower picture) after calcination at 450 °C for 2 h (upper picture).

EGMT-morphologies were prepared by mixing the EGMT precursor with the right amount of acid, solvent and PEO-*b*-PTPA (P2) block copolymer and additional crystalline TiO_2 nanorods leading to films seen in Figure 59 and Figure 60. A constant amount of TiO_2 rods were mixed with three different morphologies of the EGMT/PEO-*b*-PTPA system. Burning away the polymer exposes a TiO_2 network of rods braided by a fine TiO_2 foam. These films were used as active materials in the same inverse assembly introduced previously. To obtain thick films the mixture was drop coated. Solar cells were measured under ambient condition at 1 sun and 1.5 AM. Results of the combined system are compared with the pure template system (4.3.2.2) as seen in Table 13.

Morphology	**FF**	**Voc / V**	**Isc / A/cm^2**	**Eff. / %**
[M190]/rods	0.29	-0.20	$1.6*10^{-5}$	0.005
[M190]	0.29	-0.40	$5.0*10^{-5}$	**0.006**
[M172]/rods	0.26	-0.31	$2.7*10^{-4}$	0.023
[M172]	0.27	-0.29	$2.3*10^{-4}$	0.023
[M175]/rods	0.29	-0.20	$1.9*10^{-4}$	0.011
[M175]	0.27	-0.30	$2.9*10^{-4}$	**0.019**

Table 13: Solar cell measurements at 1 sun and 1.5 AM, under ambient condition.

For all cells no improvement could be obtained by the addition of crystalline TiO_2 rods. Even a decrease of the power conversion efficiency, open circuit voltage and short circuit current was found for morphologies [M175] and [M190]. In the best case the power conversion efficiency stayed the same for morphology [M172]. A reason for the decrease in efficiency could be dedicated to the irregular distribution of the rods in the film. Agglomerates of rods are found at some parts of the film as seen in Figure 60, c.

Since the combination of the one-pot and the blend approach did not result in an improved efficiency at all, no further investigation on this system was done.

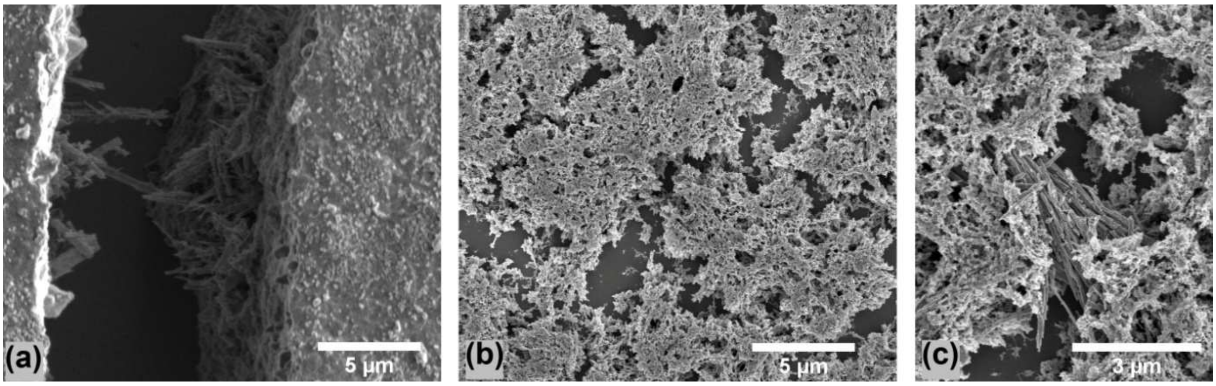

Figure 60: SEM pictures of a film prepared of morphology [M172] mixture and additional TiO_2 rods. The film as prepared (a), the film after calcinations at 450 °C for 2 h (b and c).

5 SUMMARY/CONCLUSION/OUTLOOK

A new amphiphilic block copolymer (PEO-*b*-PTP) was synthesized and used to structure hybrid materials. The self-assembling mechanism of the amphiphilic block copolymer was employed in a template process of a sol-gel system leading to nanostructured morphologies. In search of network structures a phase diagram was mapped indicating morphologies in dependence of weight fractions of the used components. The reproducibility of the investigated morphologies was shown, resulting in hybrid materials whose appearance is determined by the structure of the lyotropic aggregates formed during the synthesis. Further on the transferability of the phase diagram onto other systems became apparent by exchanging the block copolymer (chapter 4.2.1) or the precursor (TTiP and EGMT) still leading to similar structures in similar weight fractions of the components. However the in situ crystallization of the TiO_2 phase in both systems, EGMT/polymer and TTiP/polymer, is not yet solved satisfyingly. But nevertheless the system was successfully implemented in solar cell devices.

At first systematic investigations on “simple” hybrid solar cell systems were described using a blend approach of an inorganic material TiO_2 and different hole conducting polymers (chapter 4.3.1). Comparing PTPA and P3HT blends the advantage of the latter clearly lies in the higher overall power conversion efficiency. Focusing on the long term stability PTPA shows better performance. Furthermore the PTPA blends are air stable and do not require special solvents or annealing treatment since they are amorphous polymers. This leads to convenient preparation methods. As long as the low charge carrier mobility is not increased and the need for an efficient and expensive dye is not solved the P3HT seems to be the hole conducting polymer of choice. Even though the preparation is more challenging due to solvent and heat annealing steps, air and long-term instability, P3HT systems are well studied and offer promising results in optoelectronic application.

Indeed blend structures show self-assembled structures but not as defined as it is possible with the aid of amphiphilic block copolymers. Therefore a new approach to prepare hybrid solar cells with a controlled morphology was successfully established. Network morphologies obtained in a one-pot synthesis from a sol-gel containing the templating block copolymer (PEO-*b*-PTPA) and the inorganic precursor were used as active materials in solar cell devices. Even though P3HT shows higher power conversion efficiencies in combination with TiO_2, PTPA was used in the reported one-pot system. Since the advantages of PTPA, the air stability and amorphous structure are of major importance for the self-assembled functional template approach (chapter 4.3.2.1, 4.3.2.2 and 4.3.2.3). With TTiP as TiO_2 precursor very thin films already showed power conversion efficiencies comparable to other systems found in literature.[37, 40, 174] Unfortunately the increase of the layer thickness did not result in the expected exponential power conversion efficiency increase, according to Lambert-Beer.

Exchanging the precursor, thick layers with an increased efficiency were possible, giving rise to the assumption that the crystallinity of the TiO_2 network is higher. In both systems the morphology was proven to play a decisive role to form an efficient heterojunction. With c-SFM it was successfully shown that with the new precursor system morphologies of even 2 µm thick layers are forming percolating networks. With discussed improvements the system introduced offers a fast and convenient method to prepare photovoltaic devices since they do not require any difficult sealing technique due to their air stability and no post processing treatments.

Even though a system that forms a favourable morphology in a self-assembled fashion is quite effective, there are still open issues left for optimization. Almost all prepared films of self-assembled materials will show defects due to shrinkage, which in-deed do not have an impedimental influence on functionality, but to be understood and controlled to avoid that they are not dominating performance. Many intrinsic and extrinsic factors can be used to control the morphology. On the contrary it is difficult to understand all influences and to control all of these factors to guide towards a certain, reproducible structure. These factors are the degree of crystallinity of e.g the metal oxides, relative miscibility and external factors, such as solvent choice, overall concentration and blend composition as well as deposition -, evaporation - and annealing techniques.[175]

For organic and hybrid solar cell devices still the same challenges are waiting to be solved that are proposed since years. Recently some have been improved a lot in a short period of time: Light harvesting, photocurrent generation, charge transport, understanding of device function and performance limits and long term stability. The strict screening of combinations and the experimental conditions during the last decades lead to rapidly increasing efficiencies. In some cases, the simple approach like blending materials instead of complicated templating proved to be more effective, especially with regard to reproducibility. With advanced measurement methods like TEM tomography[176], conductive[177] and Kelvin probe SFM the investigation of the morphologies targeting percolating networks is possible. Further exploration of hybrid and organic solar cell devices therefore can be prosperous if defined preparation conditions are used and Round-Robin tests are established.

A further improvement of organic solar cells can be obtained with materials that offer a better compromise between the absorption properties and the charge carrier mobility.[178] On the one hand the development of a PEO-*b*-P3HT block copolymer could find its way in the one-pot approach. Due to the higher absorption and charge carrier mobility of P3HT compared to PEO-*b*-PTPA the overall efficiency could be increased. On the other hand the degree of crystallinity that is essential for P3HT could lead to difficulties in controlling the structure of the block copolymer. Further on there are still new device architectures that can be tested for photovoltaic purposes, e.g. the addition of quantum dots in DSSCs[179]. Additionally, the further understanding of these systems will improve organic and hybrid solar cells in a very convenient fashion with the aid of self-assembly. For flexible plastic devices, a high surface coverage of ordered systems is needed to be produced in roll on printing techniques. To obtain this in a reasonable and non-time-consuming manner, self-assembled systems are most suitable.

6 LITERATURE

1. Kamat, P. V., Meeting the Clean Energy Demand: Nanostructure Architectures for Solar Energy Conversion. *J. Phys. Chem. C.* **2007,** 111, 2834.

2. Saheen, S. E.; Ginley, D. S.; Jabbour, G. E., Organic Based Photovoltaics: Toward Low-Cost Power Generation. *MRS Bulletin* **2005,** 30, 10-19.

3. Brabec, C. J., Organic photovoltaics: technology and market. *Solar Energy Materials and Solar Cells* **2004,** 83, (2-3), 273-292.

4. Yoonmook, K.; Nam-Gyu, P.; Donghwan, K., Hybrid solar cells with vertically aligned CdTe nanorods and a conjugated polymer. *Applied Physics Letters* **2005,** 86, (11), 113101.

5. Schmidt-Mende, L.; Bach, U.; Humphry-Baker, R.; Horiuchi, T.; Miura, H.; Ito, S.; Uchida, S.; Grätzel, M., Organic Dye for Highly Efficient Solid-State Dye-Sensitized Solar Cells. *Advanced Materials* **2005,** 17, (7), 813-815.

6. Benanti, T. L.; Venkataraman, D., Organic Solar Cells: An overview focusing on the active layer morphology. *Photosy. Res.* **2006,** 87, 73-81.

7. Sun, S.; Fan, Z.; Wang, Y.; Haliburton, J., Organic Solar Cell Optimization. *J. Mater. Sci.* **2005,** 40, 1429-1443.

8. Kippelen, B.; Bredas, J.-L., Organic photovoltaics. *Energy & Environmental Science* **2009,** 2, (3), 251-261.

9. Kroeze, J. E.; Hirata, N.; Schmidt-Mende, L.; Orizu, C.; Ogier, S. D.; Carr, K.; Grätzel, M.; Durrant, J. R., Parameters Influencing Charge Separation in Solid-State Dye-Sensitized Solar Cells Using Novel Hole Conductors. *Advanced Functional Materials* **2006,** 16, (14), 1832-1838.

10. Rui, Z.; Chang-Yun, J.; Bin, L.; Ramakrishna, S., Highly Efficient Nanoporous TiO2-Polythiophene Hybrid Solar Cells Based on Interfacial Modification Using a Metal-Free Organic Dye. *Advanced Materials* **2009,** 21, (9), 994-1000.

11. Gregg, B. A.; Pichot, F.; Ferrere, S.; Fields, L. F., Interfacial Recombination Processes in Dye-Sensitized Solar Cells and Methods To Passivate the Interfaces. *J. Phys. Chem. B* **2001,** 105, 1422-1429.

12. Dhritiman, G.; Monojit, B.; Narayan, K. S., Correlating reduced fill factor in polymer solar cells to contact effects. *Applied Physics Letters* **2008,** 92, (9), 093301.

13. Kim, M.-S.; Kim, B.-G.; Kim, J., Effective Variables To Control the Fill Factor of Organic Photovoltaic Cells. *ACS Applied Materials & Interfaces* **2009,** 1, (6), 1264-1269.

14. Lindner, S. M.; Hüttner, S.; Chiche, A.; Thelakkat, M.; Krausch, G., Charge Separation at Self-Assembled Nanostructured Bulk Interface in Block Copolymers. *Angew. Chem. Int. Ed.* **2006,** 45, 3364-3368.

15. McNeill, C. R.; Abrusci, A.; Zaumseil, J.; Wilson, R.; McKiernan, M. J.; Burroughes, J. H.; Halls, J. J. M.; Greenham, N. C.; Friend, R. H., Dual electron donor/electron acceptor character of a conjugated polymer in efficient photovoltaic diodes. *Applied Physics Letters* **2007,** 90, (19), 193506.

16. Kietzke, T.; Horhold, H.-H.; Neher, D., Efficient Polymer Solar Cells Based on M3EH:PPV. *Chemistry of Materials* **2005,** 17, (26), 6532-6537.

17. Marc, M. K.; Jorgen, S.; Kornel, T. H.; Herman, F. M. S.; Sjoerd, C. V.; Jan, M. K.; Xiaoniu, Y.; Joachim, L., Efficient polymer:polymer bulk heterojunction solar cells. *Applied Physics Letters* **2006,** 88, (8), 083504.

18. Kietzke, T.; Neher, D.; Landfester, K.; Montenegro, R.; Guntner, R.; Scherf, U., Novel approaches to polymer blends based on polymer nanoparticles. *Nat Mater* **2003,** 2, (6), 408-412.

19. Li, G.; Shrotriya, V.; Huang, J.; Yao, Y.; Moriarty, T.; Emery, K.; Yang, Y., High-efficiency solution processable polymer photovoltaic cells by self-organization of polymer blends. *Nat Mater* **2005,** 4, (11), 864-868.

20. Park, S. H.; Roy, A.; Beaupre, S.; Cho, S.; Coates, N.; Moon, J. S.; Moses, D.; Leclerc, M.; Lee, K.; Heeger, A. J., Bulk heterojunction solar cells with internal quantum efficiency approaching 100%. *Nat Photon* **2009,** 3, (5), 297-302.

21. Kim, J. Y.; Kim, S. H.; Lee, H. H.; Lee, K.; Ma, W.; Gong, X.; Heeger, A. J., New Architecture for High-Efficiency Polymer Photovoltaic Cells Using Solution-Based Titanium Oxide as an Optical Spacer. *Advanced Materials* **2006,** 18, (5), 572-576.

22. Hoppe, H.; Sariciftci, N. S., Morphology of polymer/fullerene bulk heterojunction solar cells. *Journal of Materials Chemistry* **2006,** 16, (1), 45-61.

23. Peet, J.; Senatore, M. L.; Heeger, A. J.; Bazan, G. C., The Role of Processing in the Fabrication and Optimization of Plastic Solar Cells. *Advanced Materials* **2009,** 21, (14-15), 1521-1527.

24. Stalmach, U.; de Boer, B.; Videlot, C.; van Hutten, P. F.; Hadziioannou, G., Semiconducting Diblock Copolymers Synthesized by Means of Controlled Radical Polymerization Techniques. *Journal of the American Chemical Society* **2000,** 122, (23), 5464-5472.

25. Nogueira, A. F.; Longo, C.; De Paoli, M. A., Polymers in dye sensitized solar cells: overview and perspectives. *Coordination Chemistry Reviews* **2004,** 248, (13-14), 1455-1468.

26. Gratzel, M., Photoelectrochemical cells. *Nature* **2001,** 414, (6861), 338-344.

27. Motonari, A.; Yusuke, M.; Jun, T.; Jinting, J.; Masaru, S.; Fumin, W., Highly Efficient Dye-Sensitized Solar Cells with a Titania Thin-Film Electrode Composed of a Network Structure of Single-Crystal-like TiO2 Nanowires Made by the Oriented Mechanism. *Journal of the American Chemical Society* **2004,** 126, (45), 14943-14949.

28. Wei, M.; Konishi, Y.; Zhou, H.; Yanagida, M.; Sugihara, H.; Arakawa, H., Highly efficient dye-sensitized solar cells composed of mesoporous titanium dioxide. *Journal of Materials Chemistry* **2006,** 16, (13), 1287-1293.

29. Crossland, E. J. W.; Kamperman, M.; Nedelcu, M.; Ducati, C.; Wiesner, U.; Smilgies, D.-M.; Toombes, G. E. S.; Hillmyer, M. A.; Ludwigs, S.; Steiner, U.; Snaith, H. J., A bicontinuous Double Gyroid Hybrid Solar Cell. *Nano Lett.* **2008**, 10.1021/nl803174.

30. Crossland, E. J. W.; Nedelcu, M.; Ducati, C.; Ludwigs, S.; Hillmyer, M. A.; Steiner, U.; Snaith, H. J., Block Copolymer Morphologies in Dye-Sensitized Solar Cells: Probing the Photovoltaic Structure&Function Relation. *Nano Lett.* **2008**, 10.1021/nl800942c.

31. Ravirajan, P.; Bradley, D. D. C.; Nelson, J.; Haque, S. A.; Durrant, J. R.; Smit, H. J. P.; Kroon, J. M., Efficient charge collection in hybrid polymer/TiO2 solar cells using poly(ethylenedioxythiophene)/polystyrene sulphonate as hole collector. *Applied Physics Letters* **2005,** 86, (14), 143101.

32. Wei, Q.; Hirota, K.; Tajima, K.; Hashimoto, K., Design and Synthesis of TiO2 Nanorod Assemblies and Their Application for Photovoltaic Devices. *Chem. Mater.* **2006,** 18, (21), 5080-5087.

33. Oey, C. C.; Djurisic, A. B.; Wang, H.; Man, K. K. Y.; Chan, W. K.; Xie, M. H.; Leung, Y. H.; Pandey, A.; Nunzi, J.-M.; Chui, P. C., Polymer–TiO2 solar cells: TiO2 interconnected network for improved cell performance. *Nanotechnology* **2006,** 17, 706-713.

34. Gebeyehu, D.; Brabec, C. J.; Sariciftci, N. S., Solid-state organic/inorganic hybrid solar cells based on conjugated polymers and dye-sensitized TiO2 electrodes. *Thin Solid Films* **2002,** 403-404, 271-274.

35. Coakly, K. M.; McGehee, M. D., Photovoltaic cells made from conjugated polymers infiltrated into mesoporous titania. *Appl. Phys. Lett.* **2003,** 83, 3380.

36. Kwong, C. Y.; Choy, W. C. H.; Djurisic, A. B.; Chui, P. C.; Cheng, K. W.; Chan, W. K., Poly(3-hexylthiophene):TiO2 nanocomposites for solar cell applications. *Nanotechnology* **2004,** 15, (9), 1156.

37. Kuo, C. Y.; Tang, W. C.; Gau, C.; Guo, T. F.; Jeng, D. Z., Ordered bulk heterojunction solar cells with vertically aligned TiO[sub 2] nanorods embedded in a conjugated polymer. *Applied Physics Letters* **2008,** 93, (3), 033307.

38. Greene, L. E.; Law, M.; Yuhas, B. D.; Yang, P., ZnO-TiO2 Core-Shell Nanorod/P3HT Solar Cells. *J. Phys. Chem. C* **2007,** 111, (50), 18451-18456.

39. Nedelcu, M.; Lee, J.; Crossland, E. J. W.; Warren, S. C.; Orilall, M. C.; Guldin, S.; Huttner, S.; Ducati, C.; Eder, D.; Wiesner, U.; Steiner, U.; Snaith, H. J., Block copolymer directed synthesis of mesoporous TiO2 for dye-sensitized solar cells. *Soft Matter* **2009,** 5, (1), 134-139.

40. Chang, Y.-M.; Su, W.-F.; Wang, L., Photoactive Polythiophene:Titania Hybrids with Excellent Miscibility for Use in Polymer Photovoltaic Cells. *Macromolecular Rapid Communications* **2008,** 29, (15), 1303-1308.

41. Huynh, W. U.; Dittmer, J. J.; Alivisatos, A. P., Hybrid Nanorod-Polymer Solar Cells. *Science* **2002,** 295, (5564), 2425-2427.

42. Beek, W. J. E.; Wienk, M. M.; Janssen, R. A. J., Efficient Hybrid Solar Cells from Zinc Oxide Nanoparticles and a Conjugated Polymer. *Advanced Materials* **2004,** 16, (12), 1009-1013.

43. Baoquan, S.; Henry, J. S.; Anoop, S. D.; Sebastian, W.; Neil, C. G., Vertically segregated hybrid blends for photovoltaic devices with improved efficiency. *Journal of Applied Physics* **2005,** 97, (1), 014914.

44. Peiro, A. M.; Ravirajan, P.; Govender, K.; Boyle, D. S.; O'Brien, P.; Bradley, D. D. C.; Nelson, J.; Durrant, J. R., Hybrid polymer/metaloxide solarcells based on ZnO columnar structures. *J. Mater. Chem.* **2006,** 16, 2088-2096.

45. Beek, W. J. E.; Wienk, M. M.; Janssen, R. A. J., Hybrid Solar Cells from Regioregular Polythiophene and ZnO Nanoparticles. *Advanced Functional Materials* **2006,** 16, (8), 1112-1116.

46. Haberkorn, N.; Theato, P.; Lechmann, M. C.; Gutmann, J. S.; Sohn, B.-H.; Char, K., Templated Organic and Hybrid Materials for Optoelectronic Application. *Macrom. Rapid Commun.* **2009,** 30, DOI: 10.1002/marc.200900213.

47. Wang, M.; Lian, Y.; Wang, X., PPV/PVA/ZnO nanocomposite prepared by complex precursor method and its photovoltaic application. *Current Applied Physics* **2009,** 9, (1), 189-194.

48. Blom, P. W. M.; Mihailetchi, V. D.; Koster, L. J. A.; Markov, D. E., Device Physics of Polymer:Fullerene Bulk Heterojunction Solar Cells. *Advanced Materials* **2007,** 19, (12), 1551-1566.

49. Stefan Spange, S. G., Nanostructured Organic-Inorganic Composite Materials by Twin Polymerization of Hybrid Monomers. *Advanced Materials* **2009,** 21, (20), 2111-2116.

50. Veenstra, S. C.; Loos, J.; Kroon, J. M., Nanoscale structure of solar cells based on pure conjugated polymer blends. *Progress in Photovoltaics: Research and Applications* **2007,** 15, (8), 727-740.

51. Zhang, J. Z.; Wang, Z.-L.; Liu, J.; Chen, S.; Gang, L.-Y., *Self-Assembled Nanostructures*. Kulwar Academic Publisher: New York, Boston, Dordrecht, London, Moscow, 2004.

52. Abetz, V.; Simon, P. F. W., Phase Behaviour andMorphologies of Block Copolymers. *Adv Polym Sci* **2005,** 189, 125-212.

53. Park, C.; Yoon, J.; Thomas, E. L., Enabling nanotechnology with self assembled block copolymer patterns. *Polymer* **2003,** 44, (22), 6725-6760.

54. Volker, A.; Thorsten, G., Formation of superlattices via blending of block copolymers. *Macromolecular Rapid Communications* **2000,** 21, (1), 16-34.

55. Riess, G., Micellization of block copolymers. *Progress in Polymer Science* **2003,** 28, (7), 1107-1170.

56. Gohy, J.-F., Block Copolymer Micelles. *Adv Polym Sci* **2005,** 190, 65-136.

57. Williams, S. S.; Hampton, M. J.; Gowrishankar, V.; Ding, I. K.; Templeton, J. L.; Samulski, E. T.; DeSimone, J. M.; McGehee, M. D., Nanostructured Titania:Polymer Photovoltaic Devices

Made Using PFPE-Based Nanomolding Techniques. *Chemistry of Materials* **2008,** 20, (16), 5229-5234.

58. Her, H.-J.; Kim, J.-M.; Kang, C. J.; Kim, Y.-S., Hybrid photovoltaic cell with well-ordered nanoporous titania-P3HT by nanoimprinting lithography. *Journal of Physics and Chemistry of Solids* **2008,** 69, (5-6), 1301-1304.

59. Kim, S.-S.; Jo, J.; Chun, C.; Hong, J.-C.; Kim, D.-Y., Hybrid solar cells with ordered TiO2 nanostructures and MEH-PPV. *Journal of Photochemistry and Photobiology A: Chemistry* **2007,** 188, (2-3), 364-370.

60. Lazzari, M.; López-Quintela, M. A., Block Copolymers as a Tool for Nanomaterial Fabrication. *Advanced Materials* **2003,** 15, (19), 1583-1594.

61. Soler-Illia, G. J. d. A. A.; Scolan, E.; Louis, A.; Albouy, P.-A.; Sanchez, C., Design of meso-structured titanium oxo based hybrid organic-inorganic networks. *New J. Chem.* **2001,** 25, 156.

62. Förster, S.; Plantenberg, T., From Self-Organizing Polymers to Nanohybrid and Biomaterials. *Angewandte Chemie International Edition* **2002,** 41, (5), 688-714.

63. Stephan Förster, M. A., Amphiphilic Block Copolymers in Structure-Controlled Nanomaterial Hybrids. *Advanced Materials* **1998,** 10, (3), 195-217.

64. Huo, Q.; Margolese, D. I.; Ciesla, U.; Demuth, D. G.; Feng, P.; Gier, T. E.; Sieger, P.; Firouzi, A.; Chmelka, B. F., Organization of Organic Molecules with Inorganic Molecular Species into Nanocomposite Biphase Arrays. *Chemistry of Materials* **1994,** 6, (8), 1176-1191.

65. Kresge, C. T.; Leonowicz, M. E.; Roth, W. J.; Vartuli, J. C.; Beck, J. S., Ordered mesoporous molecular sieves synthesized by a liquid-crystal template mechanism. *Nature* **1992,** 359, (6397), 710-712.

66. Yanqin, L.; Aurora, R.; Marco, M.; Luigi, C.; Liberato, M.; Roberto, C.; Giuseppe, G., White organic light-emitting devices with CdSe/ZnS quantum dots as a red emitter. *Journal of Applied Physics* **2005,** 97, (11), 113501.

67. Jialong, Z.; Jingying, Z.; Chaoyang, J.; Jolanta, B.; Thomas, B.; Alf, M., Electroluminescence from isolated CdSe/ZnS quantum dots in multilayered light-emitting diodes. *Journal of Applied Physics* **2004,** 96, (6), 3206-3210.

68. Artemyev, M. V.; Sperling, V.; Woggon, U., Electroluminescence in thin solid films of closely packed CdS nanocrystals. *Journal of Applied Physics* **1997,** 81, (10), 6975-6977.

69. Yang, C.-H.; Bhongale, J.; Liao, Y.-M.; Hsu, C.-S., Fabrication of hybrid chromophoric amphiphile-silica nanocomposite-based light emitting devices with enhanced performance. *J. Mater. Chem.* **2007,** 17, 243.

70. Nicole, L.; Boissiere, C.; Grosso, D.; Quach, A.; Sanchez, C., Mesostructured hybrid organic-inorganic thin films. *J. Mater. Chem.* **2005,** 15, 3598.

71. Brinker, C. J.; Lu, Y.; Sellinger, A.; Fan, H., Evaporation-Induced Self-Assembly: Nanostructures Made Easy. *Advanced Materials* **1999,** 11, (7), 579-585.

72. Grosso, D.; Cagnol, F.; Soler-Illia, G. J. d. A. A.; Crepaldi, E. L.; Amenitsch, H.; Brunet-Bruneau, A.; Bourgeois, A.; Sanchez, C., Fundamentals of Mesostructuring Through Evaporation-Induced Self-Assembly. *Advanced Functional Materials* **2004,** 14, (4), 309.

73. Gopal, M.; Moberly Chan, W. J.; Jonghe de, L. C., Room temperature synthesis of crystalline metal

oxides. *J. Mater. Sci.* **1997,** 32, 6001.

74. Huynh, W. U.; Dittmer, J. J.; Libby, W. C.; Whiting, G. L.; Alivisatos, A. P., Controlling the Morphology of Nanocrystal-Polymer Composites for Solar Cells. *Advanced Functional Materials* **2003,** 13, (1), 73-79.

75. Coakley, K. M.; McGehee, M. D., Photovoltaic cells made from conjugated polymers infiltrated into mesoporous titania. *Applied Physics Letters* **2003,** 83, (16), 3380-3382.

76. Kartini, I.; Meredith, P.; Diniz da Costa, J. C.; Lu, G. Q., A Novel Route to the Synthesis of Mesoporous Titania with Full Anatase Nanocrystalline Domains. *J. Sol Gel Science a. Techn.* **2004,** 31, 185.

77. Sun, Z.; Kim, D. H.; Wolkenhauer, M.; Bumbu, G. G.; Knoll, W.; Gutmann, J. S., Synthesis and Photoluminescence of Titania Nanoparticle Arrays Templated by Block-Copolymer Thin Films. *ChemPhysChem* **2006,** 7, 370.

78. Wang, H.; Oey, C. C.; Djurisic, A. B.; Xie, M. H.; Leung, Y. H.; Pandey, A.; Nunzi, J.-M.; Man, K. K. Y.; Chan, W. K.; Chui, P. C., Titania bicontinuous network sturctures for solar call application. *Applied Physics Letters* **2005,** 87, 023507.

79. Williams, S. S.; Hampton, M. J.; Gowrishankar, V.; Ding, I.-K.; Templeton, J. L.; Samulski, E. T.; DeSimone, J. M.; McGehee, M. D., Nanostructured Titania-Polymer Photovoltaic Devices Made Using PFPE-Based Nanomolding Techniques. *Chemistry of Materials* **2008,** 20, 5229.

80. K.M. Coakley, Y. L. M. D. M. K. L. F. G. D. S., Infiltrating Semiconducting Polymers into Self-Assembled Mesoporous Titania Films for Photovoltaic Applications. *Advanced Functional Materials* **2003,** 13, (4), 301-306.

81. Soler-Illia, G. J. d. A. A.; Crepaldi, E. L.; Grosso, D.; Sanchez, C., Block copolymer-templated mesoporous oxides. *Current Opinion in Colloid and Interface Science* **2003,** 8, 109.

82. Cheng, Y.-J.; Gutmann, J. S., Morphology Phase Diagram of Ultrathin Anatase TiO2 Films Templated by a Single PS-b-PEO Block Copolymer. *J. Am. Chem. Society* **2006,** 128, 4658.

83. Memesa, M.; Gutmann, J. S., Integrated blocking layers for hybrid organic solar cells. *Energy & Environmental Science* **2009**.

84. Templin, M.; Franck, A.; Du Chesne, A.; Leist, H.; Zhang, Y.; Ulrich, R.; Schadler, V.; Wiesner, U., Organically Modified Aluminosilicate Mesostructures from Block Copolymer Phases. *Science* **1997,** 278, (5344), 1795-1798.

85. Nedelcu, M.; Lee, J.; Crossland, E. J. W.; Warren, S. C.; Oriall, M. C.; Guldin, S.; Hüttner, S.; Ducati, C.; Eder, D.; Wiesner, U.; Steiner, U.; Snaith, H. J., Block copolymer directed synthesis of mesoporous TiO2 for dye-sensitized solar cells. *Soft Matter* **2009,** 5, 134.

86. Crossland, E. J. W.; Kamperman, M.; Nedelcu, M.; Ducati, C.; Wiesner, U.; Smilgies, D. M.; Toombes, G. E. S.; Hillmyer, M. A.; Ludwigs, S.; Steiner, U.; Snaith, H. J., A Bicontinuous Double Gyroid Hybrid Solar Cell. *Nano Letters* **2009,** 0, (0).

87. Crossland, E. J. W.; Nedelcu, M.; Ducati, C.; Ludwigs, S.; Hillmyer, M. A.; Steiner, U.; Snaith, H. J., Block Copolymer Morphologies in Dye-Sensitized Solar Cells: Probing the Photovoltaic Structure−Function Relation. *Nano Letters* **2009,** 0, (0).

88. A.W. Fahmi, H. G. B. M. S., Fabrication of Metallized Nanowires from Self-Assembled Diblock Copolymer Templates. *Advanced Materials* **2003,** 15, (14), 1201-1204.

89. Pietsch, T.; Gindy, N.; Fahmi, A., Preparation and control of functional nano-objects: Spheres, rods and rings based on hybrid materials. *Polymer* **2008,** 49, (4), 914-921.

90. Fahmi, A. W.; Stamm, M., Spatially Correlated Metallic Nanostructures on Self-Assembled Diblock Copolymer Templates. *Langmuir* **2005,** 21, (3), 1062-1066.

91. Stein, A.; Schroden, R. C., Colloidal crystal templating of three-dimensionally ordered macroporous solids: materials for photonics and beyond. *Current Opinion in Colloid and Interface Science* **2001,** 5, 553.

92. Holland, B. T.; Blanford, C. F.; Do, T.; Stein, A., Synthesis of Highly Ordered, Three-Dimensional, Macroporous Structures of Amorphous or Crystalline Inorganic Oxides, Phosphates, and Hybrid Composites. *Chemistry of Materials* **1999,** 11, (3), 795.

93. Berhanu, S.; McLachlan, M. A.; McComb, D. W.; Jones, T. S., Colloidal Crystals as Nanostructured Templates for Organic Solar Cells. *Proc of SPIE* **2008,** 7052, 70521H.

94. Kim, S.-S.; Jo, J. J.; Chun, C.; Hong, J.-C.; Kim, D.-Y., Hybrid solar cells with ordered TiO2 nanostructures and MEH-PPV. *J. Photochem. Photob. A* **2007,** 188, 364.

95. Mor, G. K.; Shankar, K.; Paulose, M.; Varghese, O. K.; Grimes, C. A., Use of Highly-Ordered TiO2 Nanotube Arrays in Dye-Sensitized Solar Cells. *Nano Letters* **2006,** 6, (2), 215-218.

96. Shankar, K.; Bandara, J.; Paulose, M.; Wietasch, H.; Varghese, O. K.; Mor, G. K.; LaTempa, T. J.; Thelakkat, M.; Grimes, C. A., Highly Efficient Solar Cells using TiO2 Nanotube Arrays Sensitized with a Donor-Antenna Dye. *Nano Letters* **2008,** 8, (6), 1654-1659.

97. Zhu, K.; Neale, N. R.; Miedaner, A.; Frank, A. J., Enhanced Charge-Collection Efficiencies and Light Scattering in Dye-Sensitized Solar Cells Using Oriented TiO2 Nanotubes Arrays. *Nano Letters* **2007,** 7, (1), 69-74.

98. Shankar, K.; Mor, G. K.; Prakasam, H. E.; Varghese, O. K.; Grimes, C. A., Self-Assembled Hybrid Polymer−TiO2 Nanotube Array Heterojunction Solar Cells. *Langmuir* **2007,** 23, (24), 12445-12449.

99. Zhang, Y.; Wang, C.; Rothberg, L.; Ng, M.-K., Surface-initiated growth of conjugated polymers for functionalization of electronically active nanoporous networks: synthesis, structure and optical properties. *J. Material Chemistry* **2006,** 16, 3721.

100. Kang, Y.; Kim, D., Well-aligned CdS nanorod/conjugated polymer solar cells. *Solar Energy Materials and Solar Cells* **2006,** 90, (2), 166-174.

101. Law, M.; Greene, L. E.; Johnson, J. C.; Saykally, R.; Yang, P., Nanowire dye-sensitized solar cells. *Nature Materials* **2005,** 4, 455.

102. Unalan, H. E.; Hiralal, P.; Kuo, D.; Parekh, B.; Amaratunga, G.; Chhowalla, M., Flexible organic photovoltaics from zinc oxide nanowires grown on transparent and conducting single walled carbon nanotubes. *J. Material Chemistry* **2008,** 18, 5909.

103. Rattanavoravipa, T.; Sagawa, T.; Yoshikawa, S., Photovoltaic performance of hybrid solar cell with TiO2 nanotubes arrays fabricated through liquid deposition using ZnO template. *Solar Energy Materials and Solar Cells* **2008,** 92, (11), 1445-1449.

104. Yang, K.; Zhu, J.; Zhu, J.; Huang, S.; Zhu, X.; Ma, G., Sonochemical synthesis and microstructure investigation of rod-like nanocrystalline rutile titania. *Materials Letters* **2003,** 57, (30), 4639-4642.

105. Gur, I.; Former, N. A.; Chen, C.-P.; Kanaras, A. G.; Alivisatos, A. P., Hybrid Solar Cells with Prescribed Nanoscale Morphologies Based on Hyberbranched Semiconductor Nanocrystals. *Nano Letters* **2007,** 7, (2), 409.

106. Schlamp, M. C.; Xiaogang, P.; Alivisatos, A. P., Improved efficiencies in light emitting diodes made with CdSe(CdS) core/shell type nanocrystals and a semiconducting polymer. *Journal of Applied Physics* **1997,** 82, (11), 5837-5842.

107. Kim, D. H.; Kim, S. H.; Lavery, K.; Russell, T. P., Inorganic Nanodots from Thin Films of Block Copolymers. *Nano Letters* **2004,** 4, (10), 1841-1844.

108. Kim, F. H.; Jia, X.; Lin, Z.; Guarini, K. W.; Russell, T. P., Growth of Silicon Oxide in Thin Film Block Copolymer Scaffolds. *Adv. Mater.* **2004,** 16, (8), 702.

109. Lopes, W. A.; Jaeger, H. M., Hierarchical self-assembly of metal nanostructures on diblock copolymer scaffolds. *Nature* **2001,** 414, (6865), 735-738.

110. Chen, C.; Zhang, H.; Shen, L.; Hillmyer, M. A.; Guo, S., Facile Loading of metal ions in the nanopores of polymer thin films and in situ generation of metal sulfide nanoparticle arrays. *Nanotechnology* **2008,** 19, 365304.

111. Lo, K.-H.; Tseng, W.-H.; Ho, R.-M., In-Situ Formation of CdS Nanoarrays by Pore-Filling Nanoporous Templates from Degradable Block Copolymers. *Macromolecules* **2007,** 40, (8), 2621-2624.

112. Park, S.; Wang, J.-Y.; Kim, B.; Russell, T. P., From Nanorings to Nanodots by Patterning with Block Copolymers. *Nano Letters* **2008,** 8, (6), 1667.

113. Bockstaller, M. R.; Lapetnikov, Y.; Margel, S.; Thomas, E. L., Size-Selective Organization of Enthalpic Compatibilized Nanocrystals in Ternary Block Copolymer/Particle Mixtures. *Journal of the American Chemical Society* **2003,** 125, (18), 5276-5277.

114. Lin, Y.; Boker, A.; He, J.; Sill, K.; Xiang, H.; Abetz, C.; Li, X.; Wang, J.; Emrick, T.; Long, S.; Wang, Q.; Balazs, A.; Russell, T. P., Self-directed self-assembly of nanoparticle/copolymer mixtures. *Nature* **2005,** 434, (7029), 55-59.

115. Ochsmann, J. W.; Lenz, S.; Emmerling, S.; Kappes, R.; Nett, S. K.; Lechmann, M. C.; Roth, S. V.; Gutmann, J. S., PS-b-PEO block copolymer thin films as structured reservoirs for nanoscale precipitation reactions. *J Polym Science B* **2009,** accepted.

116. Wang, P.; Zakeeruddin, S. M.; Moser, J. E.; Nazeeruddin, M. K.; Sekiguchi, T.; Gratzel, M., A stable quasi-solid-state dye-sensitized solar cell with an amphiphilic ruthenium sensitizer and polymer gel electrolyte. *Nat Mater* **2003,** 2, (6), 402-407.

117. Behl, M.; Hattemer, E.; Brehmer, M.; Zentel, R., Tailored Semiconducting Polymers: Living Radical Polymerization and NLO-Functionalization of Triphenylamines. *Macrom. Chem. Phys.* **2002,** 203, (3), 503-510.

118. Jesberger, M.; Barner, L.; Stenzel, M. H.; Malmström, E.; Davis, T. P.; Barner-Kowollik, C., Hyperbranched polymers as scaffolds for multifunctional reversible addition-fragmentation chain-transfer agents: A route to polystyrene-core-polyesters and polystyrene-block-poly(butyl acrylate)-core-polyesters. *J. Polym. Sci. A* **2003,** 41, (23), 3847-3861.

119. Xu, X.; Jia, Z.; Sun, R.; Huang, J., Synthesis of well-defined, brush-type, amphiphilic [poly(styrene-2-hydroxyethyl methacrylate)-graft-poly(-caprolactone)]-poly(ethylene oxide)-[poly(styrene-2-hydroxyethyl methacrylate)-graft-poly(-caprolactone)] and its aggregation behavior inaqueous media. *J. Polym. Sci. A* **2006,** 44, (15), 4396-4408.

120. Kubiak, P.; Geserick, J.; Hüsing, N.; Wohlfahrt-Mehrens, M., Electrochemical performance of mesoporous TiO2 anatase. *Journal of Power Sources* **2008,** 175, (1), 510-516.

121. Jeffries-El, M.; Sauve, G.; McCullough, R. D., In-Situ End-Group Functionalization of Regioregular Poly(3-alkylthiophene) Using the Grignard Metathesis Polymerization Method *Adv. Mater.* **2004,** 16, (12), 1017-1019.

122. Grant, C. D.; Schwartzberg, A. M.; Smestad, G. P.; Kowalik, J.; Tolbert, L. M.; Zhang, J. Z., Optical and electrochemical characterization of poly(3-undecyl-2,2'-bithiophene) in thin film solid state TiO2 photovoltaic solar cells. *Synthetic Metals* **2003,** 132, (2), 197-204.

123. Yu, H.; Zhang, S.; Zhao, H.; Will, G.; Liu, P., An efficient and low-cost TiO2 compact layer for performance improvement of dye-sensitized solar cells. *Electrochimica Acta* **2009,** 54, (4), 1319-1324.

124. Bundgaard, E.; Krebs, F. C., Low band gap polymers for organic photovoltaics. *Solar Energy Materials and Solar Cells* **2007,** 91, (11), 954-985.

125. Stenzel, M. H.; Davis, T. P., Star polymer synthesis using trithiocarbonate functional. *J. Polym. Sci. A* **2002,** 40, 4498.

126. Thomas, E. L.; Lescanec, R. L.; Frank, F. C.; Higgins, J. S.; Klug, A.; Hamley, I. W., Phase Morphology in Block Copolymer Systems. *Philosophical Transactions: Physical Sciences and Engineering* **1994,** 348, 149.

127. Tian, F.; Yu, Y.; Wang, C.; Yang, S., Consecutive Morphological Transitions in Nanoaggregates Assembled from Amphiphilic Random Copolymer via Water-Driven Micellization and Light-Triggered Dissociation. *Macromolecules* **2008,** 41, (10), 3385-3388.

128. Thelakkat, M.; Hagen, J.; Haarer, D.; Schmidt, H. W., Poly(triarylamine)s- synthesis and application in electroluminescent devices and photovoltaics. *Synthetic Metals* **1999,** 102, (1-3), 1125-1128.

129. Liu, Y.; Liu, M. S.; Jen, A. K. Y., Synthesis and characterization of a novel and highly efficient light-emitting polymer. *Acta Polym.* **1999,** 50, (2-3), 105-108.

130. Bredas, J. L.; Silby, R.; Boudreaux, D. S.; Chance, R. R., Chain-length dependence of electronic and electrochemical properties of conjugated systems: polyacetylene, polyphenylene, polythiophene, and polypyrrole. *J. Am. Chem. Soc.* **1983,** 105, (22), 6555-6559.

131. Karthikeyan, C. S.; Peter, K.; Wietasch, H.; Thelakkat, M., Highly efficient solid-state dye-sensitized TiO2 solar cells via control of retardation of recombination using novel donor-antenna dyes. *Solar Energy Materials and Solar Cells* **2007,** 91, (5), 432-439.

132. Cheng, Y.-J.; Müller-Buschbaum, P.; Gutmann, J. S., Ultrathin Anatase TiO2 Films with Stable Vesicle Morphology Templated by PMMA-b-PEO. *Small* **2007,** 3, (8), 1379-1382.

133. Park, N. G.; van de Lagemaat, J.; Frank, A. J., Comparison of Dye-Sensitized Rutile- and Anatase-Based TiO2 Solar Cells. *The Journal of Physical Chemistry B* **2000,** 104, (38), 8989-8994.

134. Müller, U., *Anorganische Strukturchemie*. 3rd ed.; B. G. Teubner: Stuttgart, 1996; p 336.

135. Yin, H.; Wada, Y.; Kitamura, T.; Kambe, S.; Murasawa, S.; Mori, H.; Sakata, T.; Yanagida, S., Hydrothermal synthesis of nanosized anatase and rutile TiO2 using amorphous phase TiO2. *Journal of Materials Chemistry* **2001,** 11, (6), 1694-1703.

136. Cheng, H.; Ma, J.; Zhao, Z.; Qi, L., Hydrothermal Preparation of Uniform Nanosize Rutile and Anatase Particles. *Chemistry of Materials* **2002,** 7, (4), 663-671.

137. Guo, W.; Lin, Z.; Wang, X.; Song, G., Sonochemical synthesis of nanocrystalline TiO2 by hydrolysis of titanium alkoxides. *Microelectronic Engineering* **2003,** 66, (1-4), 95-101.

138. Yang, S.; Liu, J.; Guo, Y.; Zhao, J.; Xu, H.; Wang, Z., Preparation of rutile titania nanocrystals by liquid method at room temperature. *Mater. Chem. and Phys.* **2002,** 77, 501-506.

139. Yanagisawa, K.; Ovenstone, J., Crystallization of Anatase from Amorphous Titania Using the Hydrothermal Technique: Effects of Starting Material and Temperature. *The Journal of Physical Chemistry B* **1999,** 103, (37), 7781-7787.

140. So, W. W.; Park, S. B.; Kim, K. J.; Moon, S. J., Phase Transformation Behavior at Low Temperature in Hydrothermal Treatment of Stable and Unstable Titania Sol. *Journal of Colloid and Interface Science* **1997,** 191, (2), 398-406.

141. Cozzoli, P. D.; Kornowski, A.; Weller, H., Low-Temperature Synthesis of Soluble and Processable Organic-Capped Anatase TiO2 Nanorods. *J. Am. Chem. Soc.* **2003,** 125, (47), 14539-14548.

142. Gutierrez, J.; Tercjak, A.; Garcia, I.; Peponi, L.; Mondragon, I., Hybrid titanium dioxide/PS-b-PEO block copolymer nanocomposites based on sol–gel synthesis. *Nanotechnology* **2008,** 19, 155607.

143. Chou, T. M.; Prayoonthong, P.; Aitouchen, A.; Libera, M., Nanoscale artifacts in RuO4-stained poly(styrene). *Polymer* **2002,** 43, (7), 2085-2088.

144. Cheng, Y. J.; Gutmann, J. S., Morphology Phase Diagram of Ultrathin Anatase TiO2 Films Templated by a Single PS-b-PEO Block Copolymer. *J. Am. Chem. Soc.* **2006,** 128, (14), 4658-4674.

145. Lin, E. K.; Gast, A. P., Semicrystalline Diblock Copolymer Platelets in Dilute Solution. *Macromolecules* **1996,** 29, (12), 4432-4441.

146. Lenz, S.; Bonini, M.; Nett, S. K.; Memesa, M.; Lechmann, M. C.; Emerling, S.; Kappes, R.; Timmann, A.; Roth, S. V.; Gutmann, J. S., Global scattering functions: A tool for Grazing

Incidence Small Angle XRay Scattering (GISAXS) data analysis of low correlated lateral structures. *The European Physical Journal - Applied Physics* **2009,** revised.

147. Qiquan, Q.; James T. McLeskey, Jr., Water-soluble polythiophene/nanocrystalline TiO[sub 2] solar cells. *Applied Physics Letters* **2005,** 86, (15), 153501.

148. Vishal, S.; Gang, L.; Yan, Y.; Chih-Wei, C.; Yang, Y., Transition metal oxides as the buffer layer for polymer photovoltaic cells. *Applied Physics Letters* **2006,** 88, (7), 073508.

149. Lechmann, M. C.; Kessler, D.; Gutmann, J. S., Functional Templates for Hybrid Materials with Orthogonal Functionality. *Langmuir* **2009,** 25, (17), 10202-10208.

150. Sensfuss, S.; Al-Ibrahim, M.; Konkin, A.; Nazmutdinova, G.; Zhokhovets, U.; Gobsch, G.; Egbe, D. A. M.; Klemm, E.; Roth, H.-K., Characterisation of potential donor acceptor pairs for poylmer solar cells by ESR, optical and electrochemical investigations. *Proc. of SPIE* **2003,** 5215, 129-140.

151. Ravirajan, P.; Peiro, A. M.; Nazeeruddin, M. K.; Graetzel, M.; Bradley, D. D. C.; Durrant, J. R.; Nelson, J., Hybrid Polymer/Zinc Oxide Photovoltaic Devices with Vertically Oriented ZnO Nanorods and an Amphiphilic Molecular Interface Layer. *The Journal of Physical Chemistry B* **2006,** 110, (15), 7635-7639.

152. Kyaw, A. K. K.; Sun, X. W.; Jiang, C. Y.; Lo, G. Q.; Zhao, D. W.; Kwong, D. L., An inverted organic solar cell employing a sol-gel derived ZnO electron selective layer and thermal evaporated MoO[sub 3] hole selective layer. *Applied Physics Letters* **2008,** 93, (22), 221107.

153. Karthikeyan, C. S.; Thelakkat, M., Key aspects of individual layers in solid-state dye-sensitized solar cells and novel concepts to improve their performance. *Inorganica Chimica Acta* **2008,** 361, 635-655.

154. Kumar, S.; Scholes, G. D., Colloidal nanocrystal solar cells. *Michrochim Acta* **2008,** 160, 315.

155. Huang, Q.; Gao, L., A Simple Route for the Synthesis of Rutile TiO2 Nanorods. *Chem. Lett.* **2003,** 32, 638-639.

156. Yu, H.-Z.; Liu, J.-C.; Peng, J.-B., Photovoltaic Cells with TiO2 Nanocrystals and Conjugated Polymer Composites. *Chin. Phys. Lett.* **2008,** 25, (8), 3013-3016.

157. Goh, C.; Scully, S. R.; McGehee, M. D., Effects of molecular interface modification in hybrid organic-inorganic photovoltaic cells. *Journal of Applied Physics* **2007,** 101, (11), 114503.

158. Lin, Y.-Y.; Chu, T.-H.; Li, S.-S.; Chuang, C.-H.; Chang, C.-H.; Su, W.-F.; Chang, C.-P.; Chu, M.-W.; Chen, C.-W., Interfacial Nanostructuring on the Performance of Polymer/TiO2 Nanorod Bulk Heterojunction Solar Cells. *Journal of the American Chemical Society* **2009,** 131, (10), 3644-3649.

159. Kessler, D.; Lechmann, M. C.; Noh, S.; Berger, R.; Lee, C.; Gutmann, J. S.; Theato, P., Surface Coatings Based on Polysilsesquioxanes: Solution-Processible Smooth Hole-Injection Layers for Optoelectronic Applications. *Macromolecular Rapid Communications* **2009,** 30, (14), 1238-1242.

160. Allard, S.; Forster, M.; Souharce, B.; Thiem, H.; Scherf, U., Organic Semiconductors for Solution-Processable Field-Effect Transistors (OFETs). *Angew. Chem. Int. Ed.* **2008,** 47, (22), 4070-4098.

161. Lira-Cantu, M.; Norrman, K.; Andreasen, J. W.; Krebs, F. C., Oxygen Release and Exchange in Niobium Oxide MEHPPV Hybrid Solar Cells. *Chemistry of Materials* **2006,** 18, (24), 5684-5690.

162. Zhenan, B.; Ananth, D.; Andrew, J. L., Soluble and processable regioregular poly(3-hexylthiophene) for thin film field-effect transistor applications with high mobility. *Applied Physics Letters* **1996,** 69, (26), 4108-4110.

163. Sirringhaus, H.; Tessler, N.; Friend, R. H., Integrated Optoelectronic Devices Based on Conjugated Polymers. *Science* **1998,** 280, (5370), 1741-1744.

164. Wang, M.; Wang, X., P3HT/TiO2 bulk-heterojunction solar cell sensitized by a perylene derivative. *Solar Energy Materials and Solar Cells* **2007,** 91, (19), 1782-1787.

165. Kempa, H.; Reuter, K.; Bartzsch, M.; Hahn, U.; Huebler, A. C.; Zielke, D.; Forster, M.; Scherf, U. In *Stability study of all-polymer field-effect transistors*, Polymers and Adhesives in Microelectronics and Photonics, Polytronic, 2005. Polytronic 2005. 5th International Conference on, 2005; 2005; pp 67-71.

166. Li-Min, C.; Ziruo, H.; Gang, L.; Yang, Y., Recent Progress in Polymer Solar Cells: Manipulation of Polymer:Fullerene Morphology and the Formation of Efficient Inverted Polymer Solar Cells. *Advanced Materials* **2009,** 21, (14-15), 1434-1449.

167. Wu, M.-C.; Liao, H.-C.; Lo, H.-H.; Chen, S.; Lin, Y.-Y.; Yen, W.-C.; Zeng, T.-W.; Chen, C.-W.; Chen, Y.-F.; Su, W.-F., Nanostructured polymer blends (P3HT/PMMA): Inorganic titania hybrid photovoltaic devices. *Solar Energy Materials and Solar Cells* **2009,** 93, (6-7), 961-965.

168. Wu, M.-C.; Chang, C.-H.; Lo, H.-H.; Lin, Y.-S.; Lin, Y.-Y.; Wen, W.-C.; Yen, W.-C.; Su, W.-C.; Chen, Y.-F.; Chen, C.-W., Nanoscale morphology and performance of molecular-weight-dependent poly(3-hexylthiophene)/TiO2 nanorod hybrid solar cells. *J. Mater. Chem.* **2008,** 18, 4097.

169. Ravirajan, P.; Haque, S. A.; Durrant, J. R.; Bradley, D. D. C.; Nelson, J., The Effect of Polymer Optoelectronic Properties on the Performance of Multilayer Hybrid Polymer/TiO2 Solar Cells. *Advanced Functional Materials* **2005,** 15, (4), 609-618.

170. Crossland, E. J. W.; Kamperman, M.; Nedelcu, M.; Ducati, C.; Wiesner, U.; Smilgies, D. M.; Toombes, G. E. S.; Hillmyer, M. A.; Ludwigs, S.; Steiner, U.; Snaith, H. J., A Bicontinuous Double Gyroid Hybrid Solar Cell. *Nano Letters* 0, (0).

171. Chou, T. P.; Zhang, Q.; Russo, B.; Fryxell, G. E.; Cao, G., Titania Particle Size Effect on the Overall Performance of Dye-Sensitized Solar Cells. *J. Phys. Chem. C* **2007,** 111, 6296-6302.

172. Beek, W. J. E.; Wienk, M. M.; Janssen, R. A. J., Hybrid polymer solar cells based on zinc oxide. *Journal of Materials Chemistry* **2005,** 15, (29), 2985-2988.

173. Gupta, D.; Mukhopadhyay, S.; Narayan, K. S., Fill factor in organic solar cells. *Solar Energy Materials and Solar Cells* **2008,** DOI: 10.1016/j.solmat.2008.06.001.

174. McLeskey, J. T.; Qiao, Q., Hybrid Solar Cells from Water-Soluble Polymers. *Intern. J. Photoenergy* **2006**, 1.

175. Barry C. Thompson, Jean M. J. F., Polymer-Fullerene Composite Solar Cells. *Angewandte Chemie International Edition* **2008,** 47, (1), 58-77.

176. Bavel, S. S. v.; Sourty, E.; With, G. d.; Loos, J., Three-Dimensional Nanoscale Organization of Bulk Heterojunction Polymer Solar Cells. *Nano Letters* **2009,** 9, (2), 507-513.

177. Memesa, M.; Weber, S.; Lenz, S.; Perlich, J.; Berger, R.; Muller-Buschbaum, P.; Gutmann, J. S., Integrated blocking layers for hybrid organic solar cells. *Energy & Environmental Science* **2009**, 10.1039/b902754h.

178. Heremans, P.; Cheyns, D.; Rand, B. P., Strategies for Increasing the Efficiency of Heterojunction Organic Solar Cells: Material Selection and Device Architecture. *Accounts of Chemical Research* **2009,** 42, (11), 1740-1747.

179. Nozik, A. J., Quantum dot solar cells. *Physica E: Low-dimensional Systems and Nanostructures* **2002,** 14, (1-2), 115-120.

COLLABORATION

The following materials and methods were conducted in collaboration:

- Synthesis of EGMT Precursor System
- Synthesis of TiO_2 rods
- Synthesis of PTPA
- CV measurement
- Conductive SFM
- GISAXS analysis
- Synthesis of Ru-dye, BSPAC RAFT agent and PEO

PUBLICATIONS

1. **M. C. Lechmann**, D. Kessler, J. S. Gutamnn „Functional Templates for Hybrid Materials with Orthogonal Functionality” *Langmuir* **(2009),** 25, 10202-10208

2. **M. C. Lechmann**, D. Koll, D. Kessler, P. Theato, W. Tremel, J. S. Gutmann “Hybrid Blends for Solar Cell Application” *Energies* **(2009)** revised

3. **M. C. Lechmann**, S. A. L. Weber, J. Geserick, N. Hüsing, R. Berger, J. S. Gutmann „Self-Assembled Hybrid Systems for Solar Cells“ *Nano Letters* **(2010)** submitted

4. N. Haberkorn, **M. C. Lechmann**, J. S. Gutmann, P. Theato, B. H. Sohn, K. „Templated Organic and Hybrid Materials for Optoelectronic Application” *Char, Macrom. Rapid Comm.* **(2009)**, 30, 1146

5. D. Kessler, **M. C. Lechmann**, S. Noh, R. Berger, C. Lee, J. S., Gutmann, P. Theato „ Surface Coatings Based on Polysiloxanesesquioxane” *Macrom. Rapid Comm*. **(2009),** 30, 1238

6. Z. Sun, Y-J. Cheng, **M. C. Lechmann**, J. Li, J. Li, J. Wu, A. Grimsdale, K. Müllen, H.-J. Butt, J. S. Gutmann „Exciton Diffusion Controlled Quantum Efficiency in Hybrid Dye Sensitized Solar Cells” *Phys. Chem. Chem. Phys*. **(2009)** 11, 1604–1609

7. J. Ochsmann, S. Lenz, S. G. J. Emmerling, R. S. Kappes, S. K. Nett, **M. C. Lechmann**, S. V. Roth, J. S. Gutmann “PS-*b*-PEO block copolymer thin films as structured reservoirs for nanoscale precipitation reactions” *Journal of Polymer Science, Part B: Polymer Physics* **(2009)** accepted

8. S. Lenz, M. Bonini, S. K. Nett, M. Memesa, **M. C. Lechmann,** S. Emmerling, R. Kappes, A. Timmann, S. V. Roth, J. S. Gutmann, “Global scattering functions: A tool for Grazing Incidence Small Angle XRay Scattering (GISAXS) data analysis of low correlated lateral structures” *The European Physical Journal - Applied Physics* **(2009)** revised.

APPENDIX

Phyton program for evaluation of the I-V solar cell measurements:

“Solarfrickler“

```
from numpy import*  #numpy um mit arrays zu arbeiten und zu rechnen
from pylab import*  #alles aus pylab importieren um grafiken anzuzeigen

Source = array([])  #festlegen der variablen die in einem array wiedergegeben werden
Strom = array([])
dcStrom = array([])

Zellennummer = (raw_input("Zellennummer:"))
Pixel = (raw_input("Pixel:"))
pfad = "d:\\Doktorarbeit\\Solarzellenmessung\\MCL D"+Zellennummer+"\\"
filename=pfad+"Result"+Pixel+".csv"
fobj = open(filename,"r")     #importieren der datei

for line in fobj.readlines()[1:132]:       #eine for schleife um zeilen einzulesen von 1 bis 132
    Zuordnung = line.split(",")            #anschliessend wird zeile gesplitet und die spalten als arrays in float(komma)zahlen ausgegeben
    Source = append(Source, float(Zuordnung[1]))
    Strom = append(Strom, float(Zuordnung[2]))
fobj.close()
#print Source,Strom

Area = float(raw_input("Area(cm^2):"))  #Pixelflaeche eingeben
Aproqcm = Strom/Area    #Strom wiedergeben pro Pixelflaeche
#print Aproqcm

Isc=Aproqcm[100]    #In Zeile 100 ist V immer 0 und deshalb immer dort schnittpunkt mit y-achse
print "Isc=",Isc,"A/cm^2"

Stromnull = Strom.searchsorted(0)   #geht nur fuer sorted lines, findet 0-wert
Voc=Source[Stromnull]   #aus Source angeben wo Strom=Null (Strom index=Source index)
print "Voc=",Voc,"V"

Flaeche=Source*Aproqcm
#print Flaeche
GrossFlaeche=Flaeche.min()  #wo die Flaeche minimal ist (da negatives vorzeichen)
#print GrossFlaeche
FF=GrossFlaeche/(Isc*Voc)
print "FF=",FF

Solarmess=float(raw_input("Solarmess(A):"))  #1000W/m^2 liefert 1 sun, 100000*Solarref um Einheiten anzupassen
Solarref=0.143
Sonne=(1000*Solarmess)/(10000*Solarref)
#print "Sonne(W/m^2):",Sonne

Effizienz=((FF*Isc*Voc*-1)/Sonne)*100
print "Effizienz=",Effizienz,"%"

dcpfad = "d:\\Doktorarbeit\\Solarzellenmessung\\MCL D"+Zellennummer+"\\dark current\\"
dcfilename=dcpfad+"Result"+Pixel+".csv"
dcfobj = open(dcfilename,"r")
for line in dcfobj.readlines()[1:132]:
    Zuordnung = line.split(",")
    dcStrom = append(dcStrom, float(Zuordnung[2]))
dcfobj.close()
```

```
dcAproqcm = dcStrom/Area
#print dcAproqcm
plot(Source,Aproqcm, Source,dcAproqcm)
font = {'fontname'   : 'Courier',
        'color'      : 'black',
        'fontweight' : 'bold',
        'fontsize'   : 12}

xlabel("source / V",font)                    # x-Achse beschriften
ylabel("measure / A/qcm",font)

title(filename)
grid(True)
legend(("solar current","dark current"),loc=4, shadow=True)
text(-0.9,-0.025,"Voc:"+str(Voc)+"   Isc:"+str(Isc)+"   FF:"+str(FF)+"   Eff:"+str(Effizienz),font)
show()
outputname=pfad+"MCL D"+(raw_input("Zelle:"))+"Pixel"+(raw_input("Pixel:"))+".png"
```

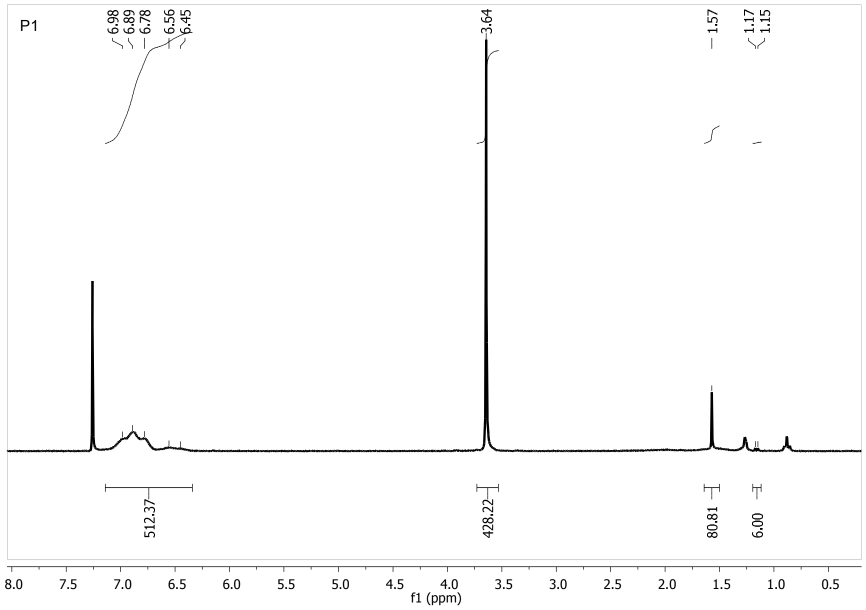

Figure 61: NMR spectrum of P1.

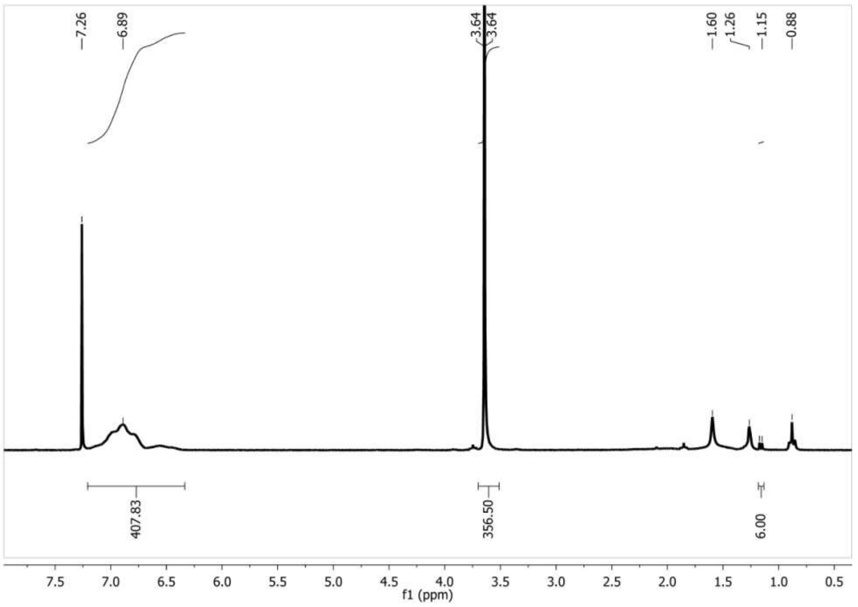

Figure 62: NMR spectrum of P2.

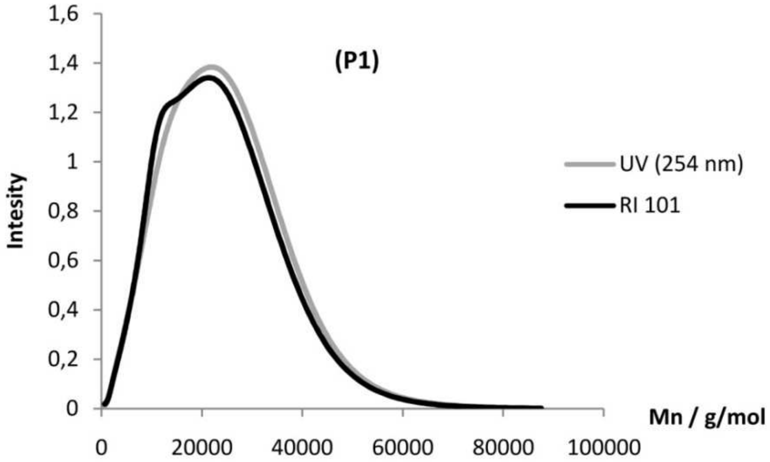

Figure 63: GPC of P1.

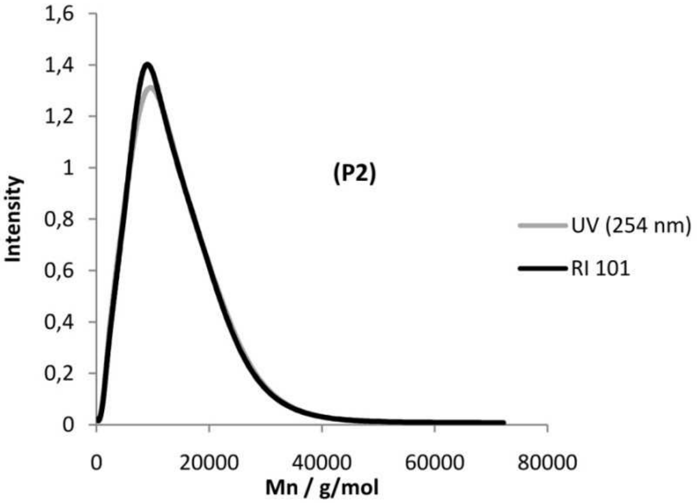

Figure 64: GPC of P2.

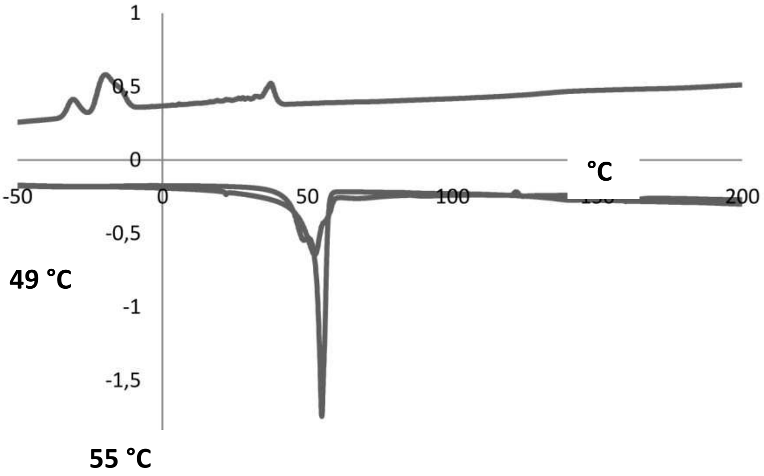

Figure 65: DSC for P1

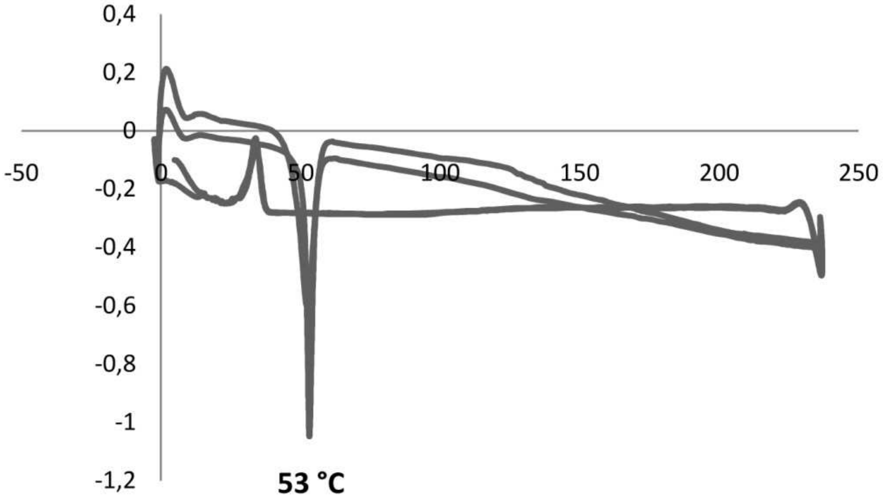

Figure 66: DSC for P2

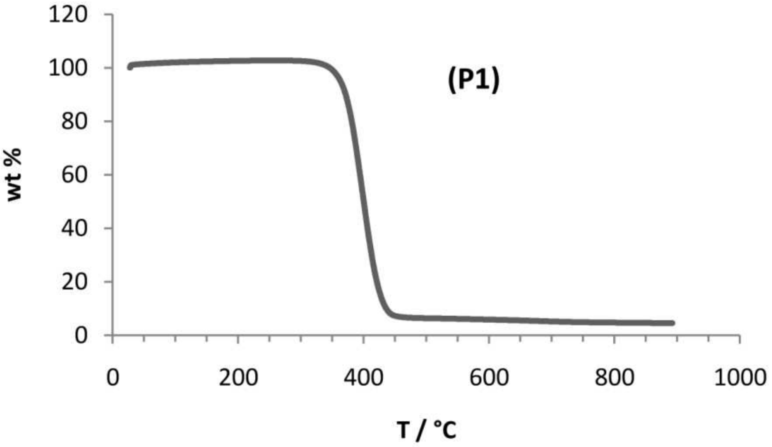

Figure 67: TGA of PEO-b-PTPA (P1).

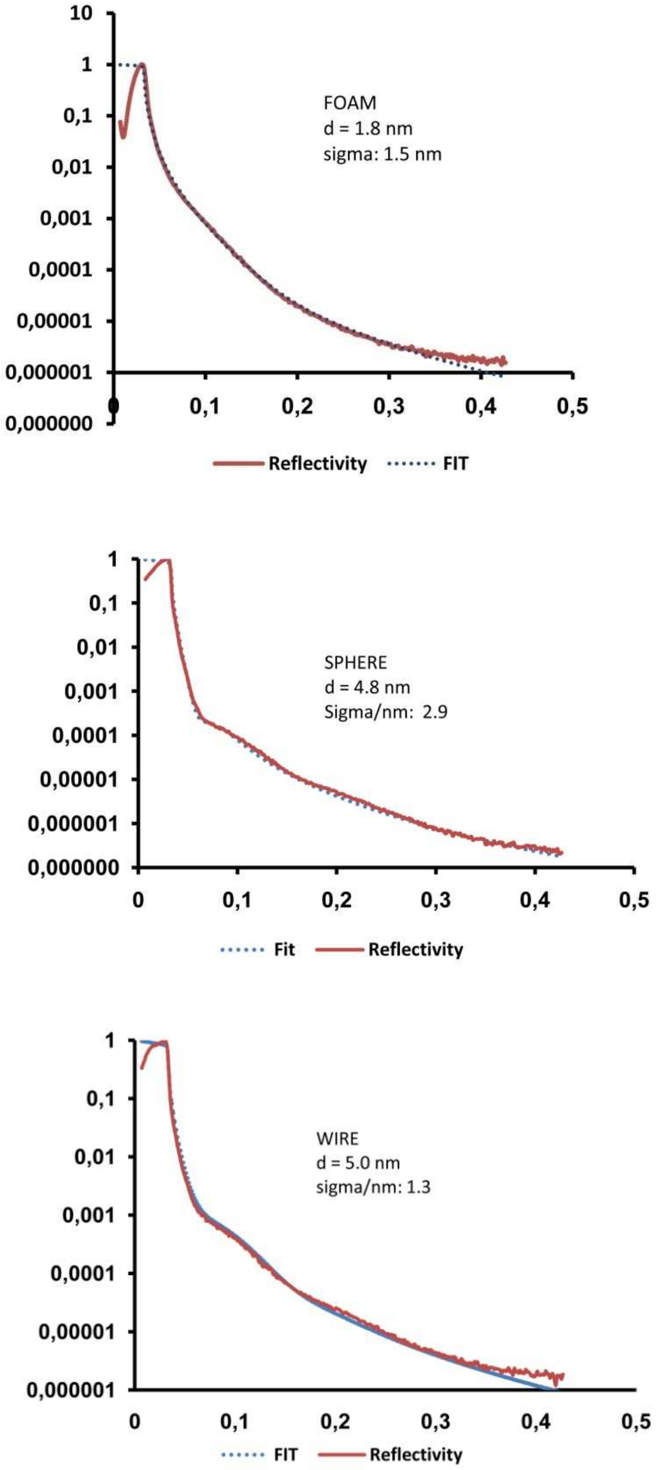

Figure 68: SAXS measurement for determining film thicknesses.